Accounting for the Effects of Power System Controllers and Stability on Power Dispatch and Electricity Market Prices

by

Sameh K. M. Kodsi

A thesis
presented to the University of Waterloo
in fulfillment of the
thesis requirement for the degree of
Doctor of Philosophy
in
Electrical and Computer Engineering

Waterloo, Ontario, Canada, 2005

I hereby declare that I am the sole author of this thesis. This is a true copy of the thesis, including any required final revisions, as accepted by my examiners.

I understand that my thesis may be made electronically available to the public.

ABSTRACT

Recently, the widespread use of power system controllers, such as PSS and FACTS controllers, has led to the analysis of their effect on the overall stability of power systems. Many studies have been conducted to allocate FACTS controllers so that they achieve optimal power flow conditions in the context of Optimal Power Flow (OPF) analysis. However, these studies usually do not examine the effect of these controllers on the voltage and angle stability of the entire system, considering that the types of these controllers and their control signals, such as reactive power, current, or voltage, have significant effect on the entire system stability.

Due to the recent transition from government controlled to deregulated electricity markets, the relationship between power system controllers and electricity markets has added a new dimension, as the effect of these controllers on the overall power system stability has to be seen from an economic point of view. Studying the effect of adding and tuning these controllers on the pricing of electricity within the context of electricity markets is a significant and novel research area. Specifically, the link among stability, FACTS controllers and electricity pricing should be appropriately studied and modelled.

Consequently, in this thesis, the focus is on proposing and describing of a novel OPF technique which includes a new stability constraint. This technique is compared with respect to existent OPF techniques, demonstrating that it provides an appropriate modelling of system controllers, and thus a better understanding of their effects on system stability and energy pricing. The proposed OPF technique offers a new methodology for pricing the dynamic services provided by the system's controllers. Moreover, the new OPF technique can be used to develop a novel tuning methodology for PSS and FACTS controllers to optimize power dispatch and price levels, as guaranteeing an adequate level of system security. All tests and

comparisons are illustrated using 3-bus and 14-bus benchmark systems.

ACKNOWLEDGEMENTS

I would like to express my profound gratitude, and thanks to my supervisor, Prof. Claudio A. Cañizares for his constant financial support, invaluable advice and continuous encouragement throughout my Ph.D. program.

Also, I am grateful for the support of Mithulananthan Nadarajah, and Hong Chen during the initial period of my stay at the University of Waterloo. I will always remember Fedrico Milano, my colleague, for his help with PSAT software and other related issues. I also extend my thanks to my office-mates Hassan Ghasemi, Hamid Zareipour, Warren King, Valery Knyazkin, Jose Rafael Avalos-Munoz, Ismael El-Samahy, Alejandro Marano-Marcolini, and Gregor Verbic.

It is impossible to find the right words to thank my beloved wife for her love and encouragement. Without it, this thesis would not be completed. This work is dedicated to my wife.

" The God of heaven, he will prosper us;
therefore we his servants will arise and build. "
(NE 2:20)

Contents

List of Figures

List of Tables

List of Terms

Acronyms:

AVR	:	Automatic Voltage Regulator
CC	:	Congestion Cost
CP	:	Controller Pricing
CPF	:	Continuation Power Flow
DAE	:	Differential-Algebraic Equations
DISCO	:	Distribution Company
DLM	:	Dynamic Loading Margin
ELD	:	Economic Load Dispatch
ESCO	:	Energy Services Company
FACTS	:	Flexible AC Transmission Systems
GENCO	:	Generation Company
HBI	:	Hopf Bifurcation Index
IEEE	:	Institute of Electrical and Electronics Engineers
IPM	:	Interior Point Method
ISO	:	Independent System Operator
LMP	:	Locational Marginal Price
MCP	:	Market Clearing Price
MTC	:	Maximum Transfer Capability
OPF	:	Optimal Power Flow
PSS	:	Power System Stabilizer
SLM	:	Static Loading Margin
SSC-OPF	:	Small-Perturbation-Stability-Constrained Optimal Power Flow
SVC	:	Static Var Compensator

TCR	:	Thyristor Controlled Reactor
TCSC	:	Thyristor Controlled Series Compensator
TRANSCO	:	Transmission Company
TSC	:	Thyristor Switched Capacitor
UWPFLOW	:	University of Waterloo Power Flow
VSC-OPF	:	Voltage-Stability-Constrained Optimal Power Flow
WSCC	:	Western System Coordination Council

Chapter 1

INTRODUCTION

1.1 Research Motivation and Literature Review

During the last two decades, nonlinear issues in power system stability have been the subject of several studies [1, 2, 3, 4, 5, 6, 7, 8, 9]. In general, power system stability problems can be classified into three categories: angle, voltage, and frequency stability problems [10]. Due to torque imbalance of synchronous machines, angle stability problems occur. Voltage stability problems result from reactive power imbalance. Lastly, the coordination of the control and protection equipment and the generation reserve are responsible for frequency stability issues. Large or small disturbances can cause stability problems. For example, first swing stability problems occur as a result of large disturbances in the system; these problems can be monitored by time domain simulation tools. Oscillatory instability, on the other hand, may be associated with large or small disturbances; this phenomenon can be studied by using eigenvalue analysis tools.

Voltage stability problems can not be isolated from angle stability problems.

The capability of the system to maintain a steady voltages at all buses in the system after being subjected to a certain disturbance may be broken not only because of the insufficient reserve of reactive power, but also due to angle instability [10]. Typically, voltage stability problems are associated with system bifurcations, i.e. saddle-node or limit induced bifurcations, that lead to voltage collapse [11]. The lack of sufficient damping torque leads to oscillatory instabilities, which may be associated with Hopf bifurcations, as it has been discussed in a variety of power system models [12, 13, 14, 15, 16], and in practice [17, 18, 19].

The probability of a bifurcation problem occurring depends on the loading level of the system. For heavy loaded systems, when the operating point approaches the maximum loading point on the P-V curve, the region of attraction is very small [20]; consequently, perturbations cannot be withstanded by the system. Many of today's networks are operating close to their stability limits due to economical reasons; this, in turn, has led to system collapse problems [17, 18]. From this point of view, additional controllers should be added to enhance the overall stability of systems [9].

1.1.1 Effect of Power System Controllers on System Stability

Since a Power System Stabilizer (PSS) provides additional system damping, this controller has become an accepted solution for oscillatory instability problems and thus improves system stability [21]. Shunt and series compensation can also increase the Maximum Transfer Capability (MTC) of power networks and hence enhance system stability [11]. Improvements of the current and voltage handling capabilities of power electronic devices have led to the development of Flexible Alternating

Current Transmission Systems (FACTS), resulting in the use of FACTS controllers for efficient shunt and series compensation. As a result, FACTS controllers based on thyristor controlled reactor (TCR), such as Static Var Compensator (SVC) and Thyristor Controlled Series Compensator (TCSC), have been adopted by several utilities to enhance their system stability [22].

To improve the transfer capacity of power systems with FACTS controllers, the focus has been on controlling the power flows in the network without generation rescheduling or topological changes. By using controllable components such as controllable series and shunt capacitors, line flows can be modified in such a way that thermal limits are not violated, losses are minimized, and stability margins are increased [23, 24]. Thus, angle and voltage stability problems may be solved by adding FACTS controllers to the system; in particular, FACTS controllers can be used to enhance damping by choosing the best location and suitable control signals [9].

To enhance voltage stability by increasing loadability margins, the use of FACTS controllers has been examined. Other studies have concentrated on the use of FACTS controllers to control system oscillations. However, these studies have not considered the relatively high cost associated with the inclusion of these system controllers vis-a-vis the "savings" to the system attained by the stability improvements. Thus, there is a need for evaluating and pricing the stability services provided by these controllers.

1.1.2 Power System Stability and Energy Pricing

The deregulation and privatization process in the electricity industry has affected the overall operation of power systems. In this environment, an Independent System

Operator (ISO) is responsible for ensuring a certain level of stability, security, and reliability of the system. Consequently, system security, where the social benefit for all the market participants is maximized, is a major ISO concern. In this context, there is a need to include suitable security constraints within the market pricing mechanism, so that the correct market signals can be sent to all market participants while operating the system within reasonable security margins.

Since optimization-based tools, particularly, optimal power flows (OPF), are the main scheduling mechanism used by ISOs, various algorithms have been proposed to include stability constraints in the OPF. In [25] and [26], the authors propose the use of the minimum singular value of the power flow Jacobian as an index to detect proximity to voltage instability, which is then used as a stability constraint to propose a voltage-stability-constrained OPF (VSC-OPF) in [27]. In [28], a different strategy is proposed based on the use of a multi-objective OPF technique to maximize both social benefit and the distance to a voltage instability point. The problem with the inclusion of only voltage security constraints is that, in some power systems, oscillatory instabilities (interarea or plant and local oscillation modes) are the key limiting factor for maintaining system security (e.g. WSCC, now WECC, August 1996 blackout) [29]. All these papers are based on power flow models, without accounting for the system dynamics. In [30], however, a stability-constrained OPF is proposed for some of the generator dynamic equations, but it does not account for the other significant variables in stability studies such as voltage regulators. Hence, there is a need to develop a new stability-constraint OPF in order to predict both voltage and oscillatory instabilities, and thus use this tool to generate appropriate market signals and energy pricing.

1.1.3 Tuning Power System Controllers and Pricing Their Stability Services

In recently restructured power systems, the regulation of voltage and frequency is part of the services provided by the ISO to maintain a stable and reliable operation of systems. The regulation of voltage and frequency and other services are categorized as ancillary services in FERC Order No. 888 [31]. Hence, the enhancement of angle and voltage stability of a system can be categorized as ancillary services. PSS and FACTS controllers (e.g. Static Var Compensator or SVC and Thyristor Controlled Series Compensator or TCSC) are acceptable solutions for voltage and oscillatory instability problems, since these controllers increase loading margins and provide additional system damping [32, 33, 34]. Furthermore, PSS and FACTS control actions can be also technically classified as an ancillary service. The valuation of the services provided by FACTS controllers, based on their effect on system loadability, has been discussed in [35]. However, the dynamic services provided by these controllers are an issue, because one of the key features of these controllers is their dynamic response characteristics. Therefore, this thesis presents the use of a novel stability-constrained OPF to value the services provided by these controllers, thus proposing a pricing technique somewhat different than other ancillary service pricing techniques previously proposed in the literature (e.g. [36]). However, these controllers (e.g. PSS and TCSC) should be first "optimally" tuned to optimize the market operating conditions, i.e. power dispatch and price levels, and adequate system security.

The tuning of the PSS and the TCSC has been discussed in [37, 38], in terms of targeting better coordination to enhance oscillation damping using an optimization-based tuning algorithm. In [39], the optimal tuning of PSS and FACTS controllers is

accomplished by a simple parameter-constrained nonlinear optimization algorithm to minimize an implicit objective function that accounts for the oscillatory instability. Another approach presented in [40, 41] involves formulating an eigenvalue-based objective function to enhance system damping during the tuning process. Similarly, in [42], the authors suggest a PSS design that is derived from a multi-objective optimization algorithm to enhance the system damping. All these approaches concentrate on system damping enhancement and the effect of the interaction between the PSS and the TCSC on oscillatory instability; however, the effect of controller tuning on market signals within the context of deregulated operating environment has not yet been discussed in the current literature. In this thesis, the effect of the tuning process of system controllers by using a newly developed stability-constrained OPF, that appropriately represents security levels in the operation of electricity markets and their associated power systems, is investigated .

1.2 Research Objectives

In this research, the effect of power system controllers on system stability in the context of restructured electricity markets is investigated, to address the following three main issues:

1. The development of a stability-constrained OPF which predicts oscillatory and voltage instabilities.

2. The development of a new methodology in order to value the dynamic stability services of system controllers, in particular PSS and FACTS.

3. The development of a novel technique to properly tune the system controllers, based on dynamic stability enhancement and adequate market conditions.

Hence, the main goal of this thesis is to present and discuss a new Small-Perturbation-Stability-Constrained OPF (SSC-OPF) to properly tune the system controllers and value their dynamic services.

1.3 Outline of the Thesis

This thesis is organized into six chapters and two appendices. Chapter 2 provides the theoretical background of power system stability and electricity markets, and models of power system components and controllers used in this thesis. In addition, the analysis techniques, analytical tools, and test systems used in this thesis are introduced.

The new SSC-OPF, based on the inclusion of a stability index in the OPF algorithm, besides the mathematical procedures used to solve this particular optimization problem, are discussed in Chapter 3. The application of the proposed SSC-OPF on two different test systems is also described. Also, a comparison of the novel SSC-OPF with the standard OPF auction, and the previously discussed VSC-OPF is included.

Chapter 4 introduces the new methodology to value the dynamic stability services of the system controllers, and its application to PSS and FACTS controllers on two different benchmark systems.

A novel technique to tune PSS and TCSC, and the application of this technique on a test case is detailed in Chapter 5. Lastly, conclusions and suggestions for future research are presented in Chapter 6.

The static, dynamic and market data of the test systems, are given in Appendices A and B.

Chapter 2

Models, Background and Tools

2.1 Introduction

In Chapter 1, the need to develop a new technique which combines power system stability and deregulated electricity is argued. In this chapter detailed background is provided on these two areas. The definition and types of power system stability, the deregulation process of the electricity industry, and the structures of the electricity markets are discussed here. The analysis techniques and tools used in this thesis are also described in terms of various stability and deregulations aspects.

Mathematical models for stability analysis (steady-state or small signal stability), including those for generators, loads and FACTS controllers, are illustrated in this chapter as well. Specifically, PSS, SVC, and TCSC controllers, and the power system components used in this thesis are presented. The test systems utilized for this thesis are also briefly discussed here.

2.2 Power System Models

2.2.1 Synchronous Generator Model

Mathematical models of a synchronous machine vary from elementary classical models to more detailed ones. In detailed models, transient and subtransient behaviours are considered [11, 43]. In this thesis, the classical generator transient model, as shown in Figure 2.1, is used to represent the machines in various test systems [44, 45, 46].

In this model, the following equations link the mechanical variables with the electrical variables, and result in the block diagram representation in Figure 2.2:

$$\begin{aligned} (D \ + \ \tau_j S)\, \omega \ &= T_m \ - \ (\Psi_q \ I_q + \Psi_d \ I_d) \\ S\delta \ &= \omega \ - \ 1 \end{aligned} \tag{2.1}$$

where D and τ_j represent the damping constant and the inertia time constant, respectively; T_m is the input mechanical torque; ω and δ represent the rotational speed and rotor angle, respectively; Ψ_d and Ψ_q correspond to the flux linkage in the direct and quadrature axes; and I_d and I_q are the armature current in the direct and quadrature axes, respectively.

For eigenvalue studies (small signal stability analysis), it is necessary to include the effects of the excitation controller, which indirectly controls the reactive output of a generator. A simple Automatic Voltage Regulator (AVR) model is used here to represent the excitation control of the generators, as depicted in Figure 2.3 [44, 45].

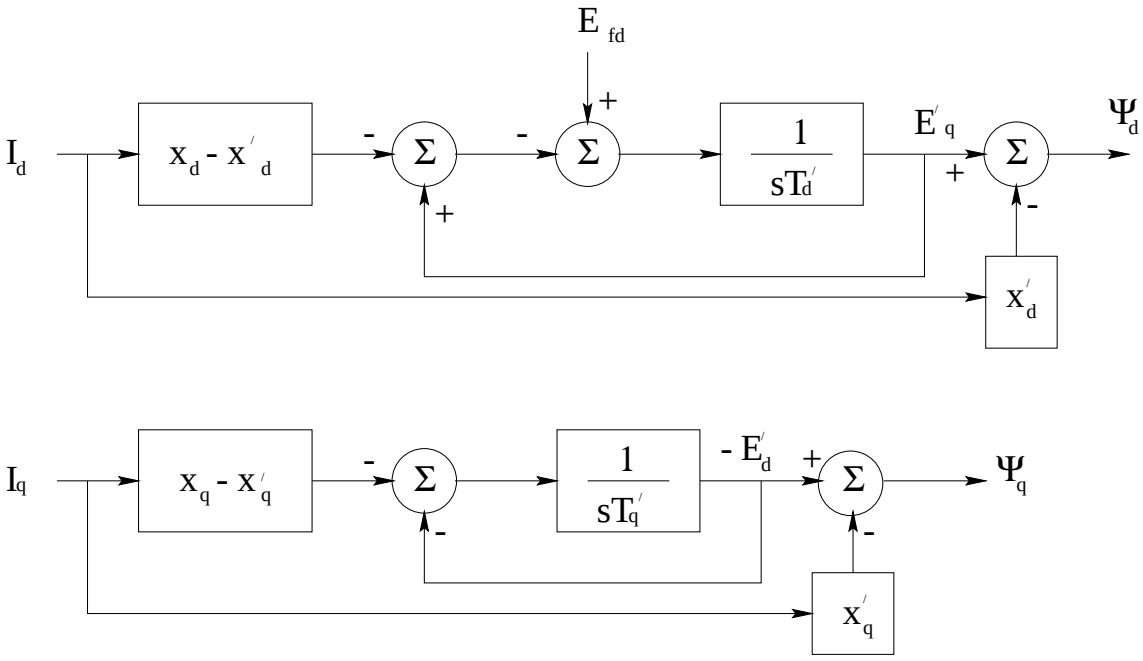

Figure 2.1: The transfer function of the transient machine model, where x_d is the direct axis reactance, x'_d is d-axis transient reactance, x_q is the quadrature axis reactance, x'_q is q-axis transient reactance, and T'_d and T'_q are the direct and quadrature axes transient time constants.

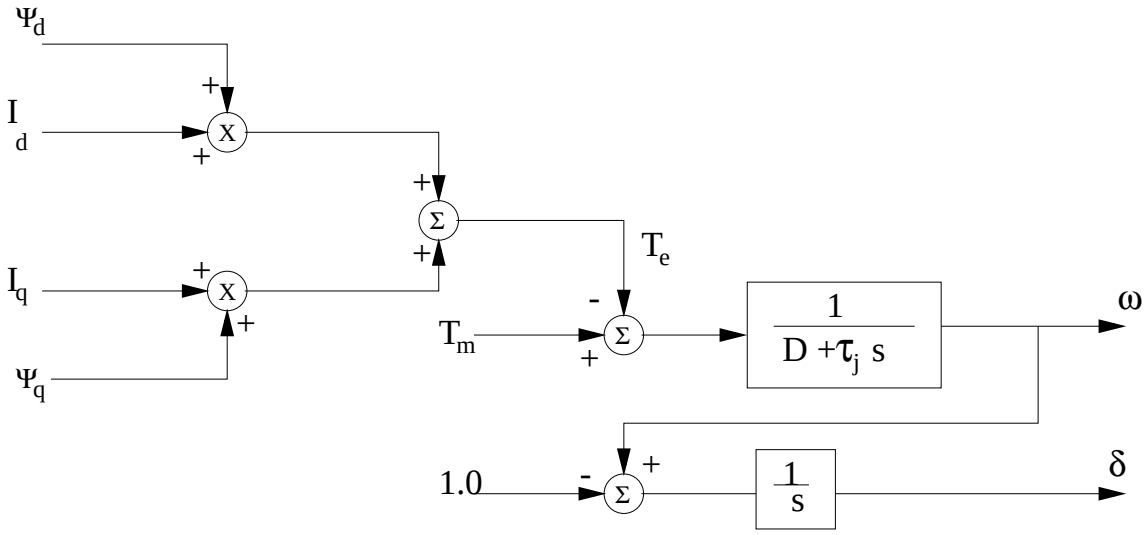

Figure 2.2: Computation of torque and speed in the transient machine model.

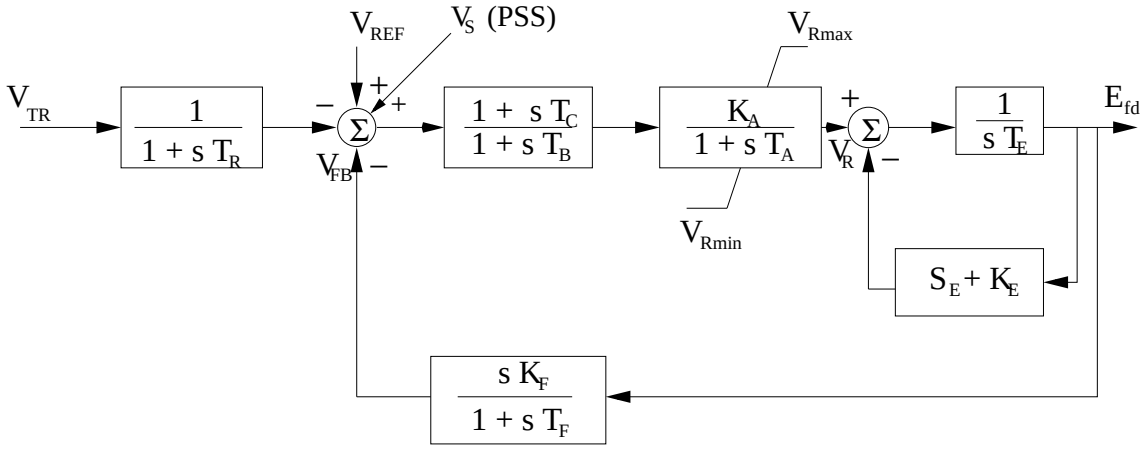

Figure 2.3: AVR and exciter model for synchronous generator, where S_E is the saturation effect, all Ks are constant gains, and all Ts are time constants.

2.2.2 Load Models

The modelling of loads in stability studies is a complex problem due to the unclear nature of aggregated loads (e.g. a mix of fluorescent, compact fluorescent, and incandescent lamps, refrigerators, heaters, motors, etc.). Load models are typically classified into two broad categories: static and dynamic. In this research work, the loads are modeled using constant power static load models [47]. In this model, the real and reactive powers have no relation to the voltage magnitude. It is also referred to as a constant MVA load model.

In power flow studies and to obtain the P-V curves in the test systems, loads are typically represented as constant PQ loads with a constant power factor, and are increased according to

$$\begin{aligned} P_L &= P_{Lo}(1+\lambda) \\ Q_L &= Q_{Lo}(1+\lambda) \end{aligned} \tag{2.2}$$

where P_{Lo} and Q_{Lo} are the initial real and reactive power, respectively, and λ is a p.u. loading factor, representing the slow varying parameter typically used in voltage stability studies.

2.2.3 Power System Stabilizer (PSS) Model

A PSS model is viewed as an additional control block to enhance system stability [44]. This block is added to the (AVR), and uses stabilizing feedback signals such as shaft speed, terminal frequency and/or power to change the input signal of the AVR. A PSS contains three blocks as shown in Figure 2.4. The first block is the stabilizer gain block with the constant gain K_{PSS}, which determines the amount of damping. The second is the Washout Filter, which serves as a high-pass filter, with

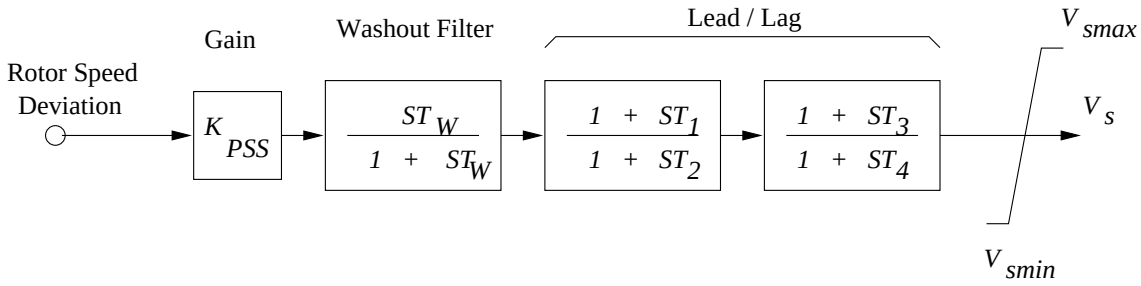

Figure 2.4: Transfer function of the PSS model, where K_{pss} is a constant gain, and all Ts are time constants.

a time constant that allows the signal associated with oscillations in rotor speed to pass unchanged, and does not allow the steady state changes to modify the terminal voltages. The last block, the Phase-Compensation, provides the desired phase-lead characteristic to compensate for the phase lag between the AVR input and the generator electrical (air-gap) torque. In practice, two or more first-order blocks can be used to achieve the desired phase compensation.

2.2.4 FACTS Controllers Models

FACTS controllers are a family of power electronics controllers for enhancing power system performance [48]. Some are widely used, and others are under development. In particular, SVC and TCSC are FACTS controllers that are employed in this thesis [23, 49, 50, 51, 52, 53, 54]. Here, a brief description of each model follows.

SVC

The role of a SVC is to inject a controlled capacitive or inductive current to maintain or control a specific variable, particularly bus voltage [48]. Well-known configurations of an SVC are the Fixed Capacitor (FC) with a Thyristor Controlled Reactor

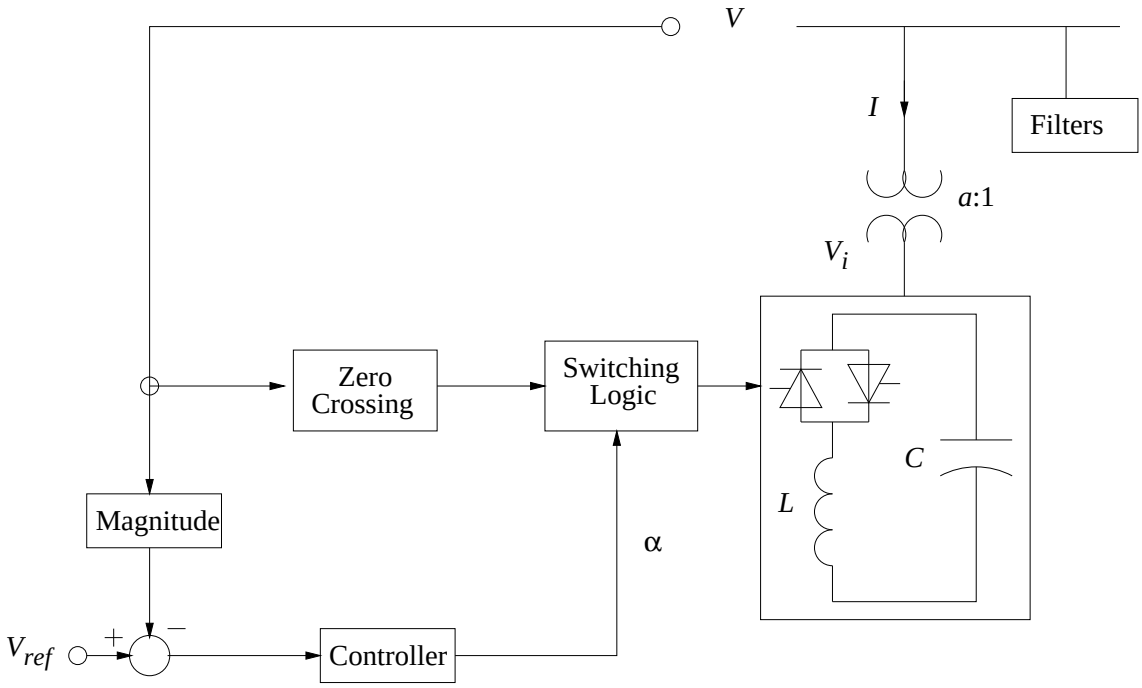

Figure 2.5: Basic SVC structure with voltage control.

(TCR), and a Thyristor Switched Capacitor (TSC) in particular with the TCR. Figures 2.5 and 2.7 illustrate the structure of an SVC with voltage control and its steady state control characteristic, respectively, for a FC-TCR type SVC [55].

Typically, the SVC is modelled by a variable reactance with maximum inductive and capacitive limits (see Figure 2.7), which directly correspond to the limits in the firing angles of the thyristors. In addition to the main job of the SVC controller, which is mainly the control of the SVC bus voltage, the reactance of the SVC controller may be used to damp system oscillations using an additional control signal denoted in Figure 2.7 by “SVC-sig”.

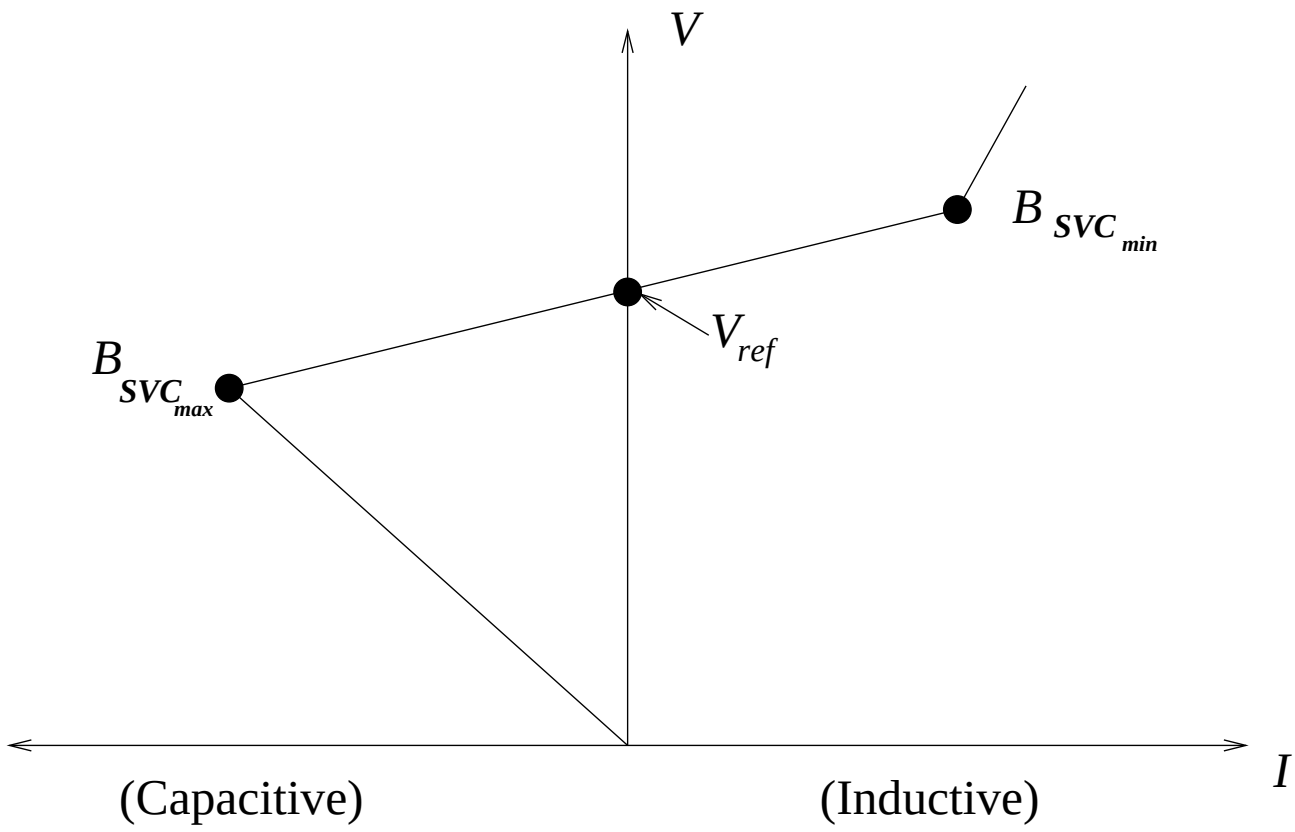

Figure 2.6: Typical steady-state voltage control characteristic of an SVC.

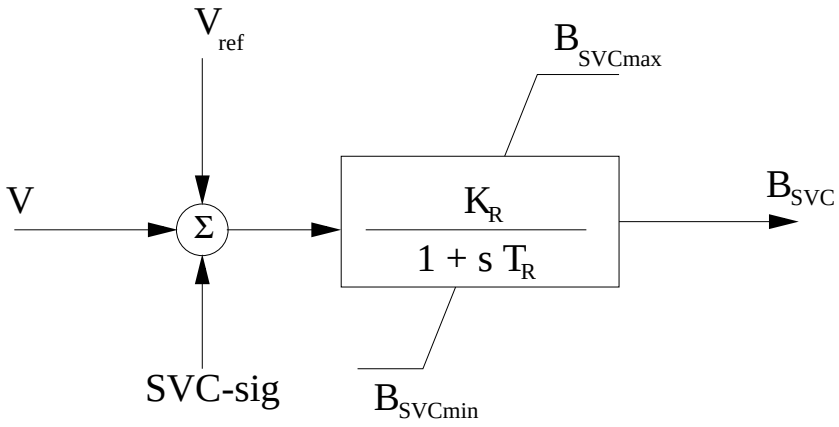

Figure 2.7: Transfer function of an SVC, where K_R stands for a constant gain, T_R stands for a time constant and B_{SVC} stands for the SVC susceptance.

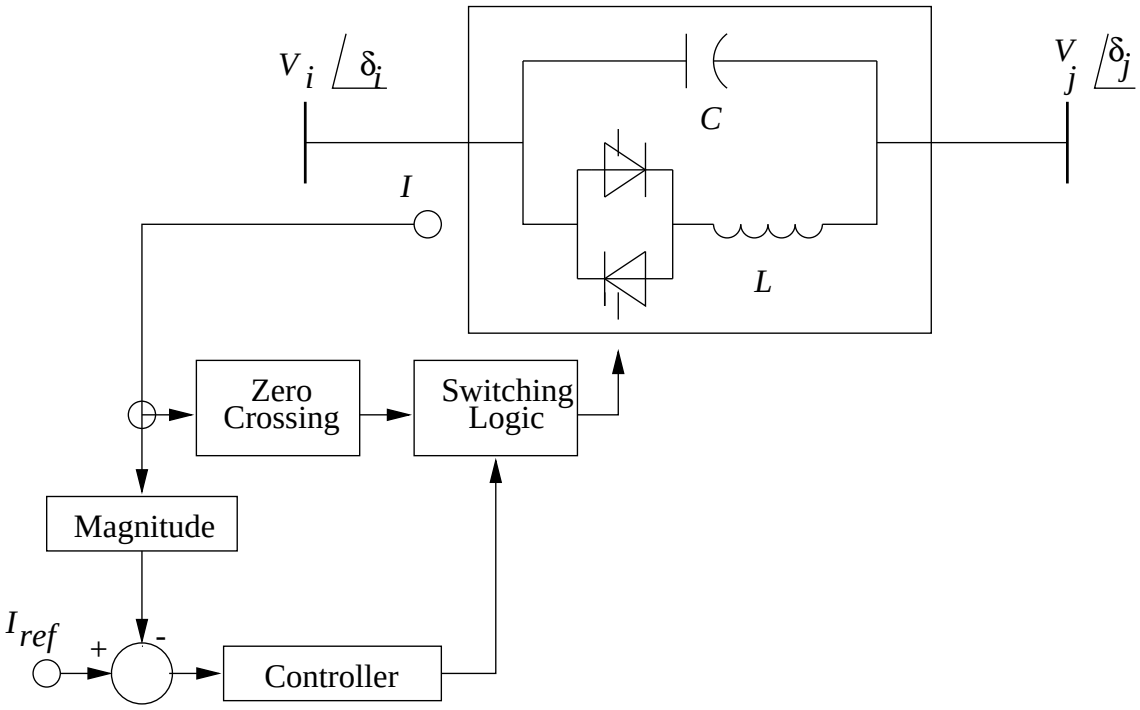

Figure 2.8: Basic TCSC structure with current control.

TCSC

A TCSC controller is a TCR in parallel with a bank of capacitors. A typical one-line diagram of a TCSC structure based on current control is illustrated in Figure 2.8; the usual steady-state V-I characteristic of this controller is portrayed in Figure 2.9 [22, 55].

In a TCSC, two operational blocks can be clearly identified: an external control and an internal control [22]. The function of the former is to operate the controller to fulfill specified compensation objectives; this control directly depends on measured systems variables to define the reference for the internal control, which is defined by the value of the controller reactance. The function of the latter is to provide the right gate drive signals for the thyristor valve to produce the appropri-

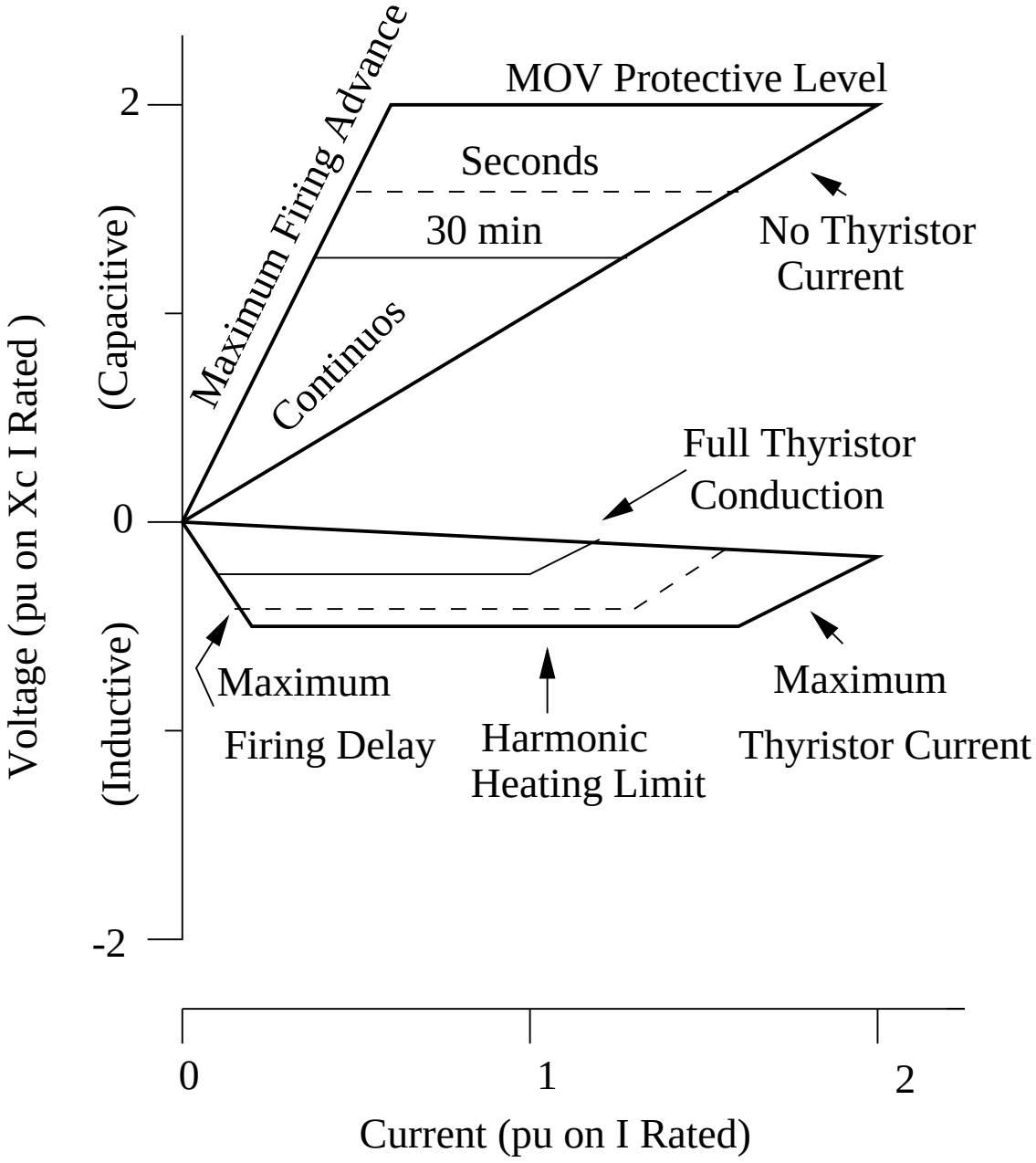

Figure 2.9: TCSC V-I steady-state characteristics.

ate compensating reactance. As a result, the functional operation of the controller is defined by the external control [22, 56].

The external control is defined by the control objectives. The typical steady state function of a TCSC is reactance control; however, additional functions for stability improvement, such as damping controls, may be included in this control. Another steady state control that has been discussed in the literature is power flow control, which is achieved either automatically with a "slow" PI controller, or manually, through direct operator intervention [57].

The block diagram of the TCSC model and external control structure used of this research is depicted in Figure 2.10 [34]. In this figure, X_m is defined by the stability control modulation reactance value which is determined by the stability or dynamic control loop, and X_{eo} stands for the TCSC steady state reactance or set point, whose value is provided by the steady state control loop. The sum of these two values results in X'_m, the net reactance order from the external control block. Since the natural response of the device internal control is characterized by the delayed action, this signal is put through a first-order lag that yields the equivalent capacitive reactance X_e of the TCSC [58]. The steady state control loop can have either a large time constant, or be adjusted manually; thus, for large disturbance transients X_{eo} is assumed to be constant. In this work, X_{eo} is fixed during large disturbance events by disabling the steady state control after a large disturbance. The equivalent reactance of the TCSC is a function of the firing angle α, based on the assumption of a sinusoidal steady-state controller current. Therefore, the operating limits are defined by the limits of the firing angle α. The range of the equivalent reactance is $X_{emin} \leq X_e \leq X_{emax}$ with $X_{emax} = X_e\ (\alpha_{min})$, and $X_{emin} = X_e\ (180^o) = X_c$, where X_c is the reactance of TCSC capacitor.

The structure of the stability controller is shown in Figure 2.11 [34], and it

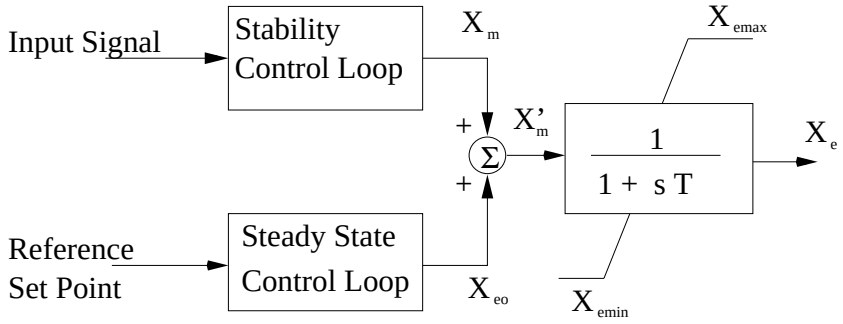

Figure 2.10: TCSC model for stability studies.

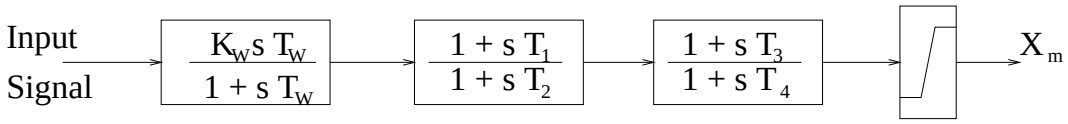

Figure 2.11: Transfer function of the TCSC stability control loop, where K_W represents a constant gain, and all Ts stand for time constants.

consists of a Washout Filter with a constant gain K_{TCSC}, a Dynamic Compensator, and a Limiter. The Washout Filter is used to avoid a controller response to the dc offset of the input signal. The Dynamic Compensator consists of two (or more) lead-lag blocks to provide the necessary phase-lead characteristics. Finally, the Limiter is employed to improve the controller response to large deviations in the input signal.

2.3 Power System Stability

Power system stability is defined as the capability of a system to maintain an operating equilibrium point after being subjected to a disturbance for given initial operating conditions [10]. To understand the different aspects and characteristics of power system stability, the following issues need to be considered [10, 11]:

1. Besides the highly non-linear nature of a power system, this system is continuously subjected to changing in operating conditions (e.g. loads, generation, etc.). Hence, the stability of the system depends on the initial operating conditions.

2. Power systems are usually subjected to a wide range of disturbances. These are classified as small disturbances (e.g. load changes) or large disturbances (e.g. fault conditions). For example, short circuits and transmission line outages can lead to structural changes from the reaction of the protection devices to isolate the faulty elements.

Based on the previous discussion, power system stability is categorized based on the following considerations [10, 11]:

1. The nature of the resulting instability mode indicated by the observed instability on certain system variables.

2. The size of the disturbance which consequently influences the tool used to assess the system stability.

3. The time margin needed to assess system stability.

Thus, power system stability can be classified as follows:

2.3.1 Angle Stability

It is defined as the capability of the synchronous generators in the system to maintain its synchronism after being subjected to a disturbance. Maintaining this synchronism depends on the synchronizing torque and the damping torque. The lack

of sufficient synchronizing torque leads to aperiodic or non oscillatory instability, whereas the lack of damping torque leads to oscillatory instability [10, 11, 59, 44]. Angle stability is hence categorized as follows [10]:

Small-disturbance Angle Stability

This category refers to the system's ability to maintain angle stability under small disturbances. Lack of sufficient damping torque leads to oscillatory instabilities, which may be associated with Hopf bifurcations, as it has been discussed in a variety of power system models [12, 13, 14, 15, 16] as well as in practice [17, 18, 19]. Linearization techniques of the system equations are used to assess the system's stability for such small disturbances. The time frame of these stability studies is in the order of 10-20 seconds following the disturbances.

Large-disturbance Angle Stability (Transient Stability)

Transient stability is associated with sever disturbances. In this case, instabilities are related to a aperiodic angular separations due to insufficient synchronizing torque, which result in first swing instabilities, such as single area swing modes or interarea swing modes [11]. The time frame of these stability studies is in the order of 3-5 seconds following the disturbances.

2.3.2 Voltage Stability

The capability of a power system to maintain steady voltages at all its buses after a disturbance from an initial operating condition defines the voltage stability phenomenon [10, 32, 60, 61]. The time frame for voltage stability has a wide range

from a few seconds to several minutes. Thus, the voltage stability assessment varies between a short term assessment which involves the dynamics of fast acting load components for a study period in the order of several seconds to a large term assessment which involves relatively slower acting system components (e.g. tap-changing transformers) for a period of several minutes. The voltage stability criteria is also categorized into two types, large disturbance and small disturbance voltage stability [10, 61].

Typically, two types of bifurcations, i.e. saddle-node bifurcations or limit-induced bifurcations, lead to voltage collapse [11]. Saddle-node bifurcations, are associated with a singularity of the system Jacobian and/or state matrix that results in the disappearance of steady-state solutions. Limit-induced bifurcations, on the other hand, correspond to the disappearance of steady-state solutions when the system controls limits are reached (e.g. generator reactive power limits), leads to limit-induced bifurcations.

Large-disturbance Voltage Stability

Here, the concern is to maintain a steady bus voltages following a large disturbance such as system faults. This ability is determined by the system and load characteristics, and the interactions between the different voltage control devices in the system, and it is typically studied using time-domain and steady-state dynamic analysis tools.

Small-disturbance Voltage Stability

This category considers small perturbations such as an incremental change in system load. It is the load characteristics and voltage control devices that determine

the system capability to maintain its steady-state bus voltages. This problem is usually studied using power-flow-based tools.

2.3.3 Frequency Stability

It refers to the ability of the system to maintain a steady frequency, following a system drastic change resulting in a significant imbalance between generated and demand power [10].

Due to the difference in the process time frame for different system devices, the frequency stability phenomenon is classified as short-term or as long-term frequency stability. The short-term is affected by load shedding, generator controls, and protection devices, and covers the first several seconds following the disturbance. Long-term assessment is determined by other factors such as the prime mover energy supply, covering several minutes following the disturbance [10, 62]

2.4 Power System Stability Tools

When a system's operating point is defined, the ability of the system to maintain a stable operating condition under small and large perturbations should be studied. For small perturbations, the available Static Load Margin (SLM), which is the maximum loading level beyond which power flow solutions cannot be obtained for the system, and that are usually associated with saddle-node and limit-induced bifurcations, must be determined. This is accomplished by calculating full P-V curves for various operating conditions and system topologies. On these P-V curves, Dynamic Load Margins (DLM), which are typically the loading levels at which the system presents oscillatory instabilities associated with Hopf bifurcations, and tends

to be less than SLM, should also be determined. A mix of continuation power flow, eigenvalue analysis tools, and a Hopf bifurcation index are used here to determine these P-V curves and associated SLM and DLM values.

2.4.1 Continuation Power Flow (CPF)

Typically, CPF methods are employed to determine the P-V curves, and thus maximum loading points (maximum loadability or steady state stability limits) of power systems. Although they are computationally demanding [11, 63], these techniques provide useful information regarding system behaviour with respect to certain parameter variations, especially load changes.

The CPF technique is based on an iterative process, involving predictor and corrector steps, as illustrated in Figure 2.12. Thus, from a known initial point A, a tangent predictor step is used to estimate a solution point B for a given load direction defined by the parameter λ. A corrector step is then used to determine the exact solution C using a power flow with an additional equation to find the proper value of λ. A parameterization step may be used to avoid convergence problems if the Jacobian becomes ill-conditioned around the maximum loading point.

All P-V curves here were obtained using the University of Waterloo Power Flow (UWPFLOW) package [64]. A variety of output files permit further analysis such as tangent vectors, left and right eigenvectors at the bifurcation point, power flow solutions at different loading levels, and voltage stability indices.

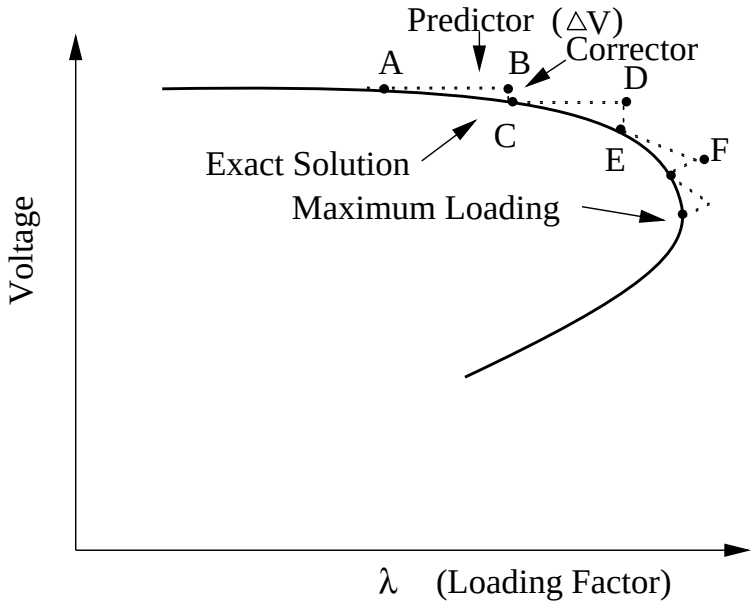

Figure 2.12: Continuation Power Flow technique (CPF) to obtain a P-V curve.

2.4.2 Eigenvalue Analysis

From the equations of the various system components and control models discussed in Section 2.1, a power system can be represented by the following set of differential and algebraic equations (DAE) [45]:

$$\begin{bmatrix} \dot{x} \\ 0 \end{bmatrix} = \begin{bmatrix} f(x,y,p) \\ g(x,y,p) \end{bmatrix} = F(x,y,p) \tag{2.3}$$

where

- $x = [\delta_G^T\ \omega^T\ E'^T_q\ E'^T_d\ E_{fd}^T\ V_R^T\ R_f^T\ x_{cont}^T]^T \in \Re^n$ is a vector of state variables that represents the dynamic states of generators, loads, and other system controllers. Thus, δ_G represents the generator torque angles; ω is the rotor speed variations; E'_q stands for the quadrature components of the generator internal voltages; E'_d represents the direct components of the generator internal voltages; E_{fd} is the exciter output voltages; V_R represents the voltage

regulator output voltages; R_f stands for the rate of feed-back of the exciter output voltages; and x_{cont} represents all the dynamic variables of PSS and FACTS controllers, such as the PSS voltage signal or the TCSC controlled variable reactance.

- $y = [\delta^T \ V^T \ Q_G^T]^T \in \Re^m$ is a vector of steady-state algebraic variables that typically result from neglecting fast dynamics (e.g. load voltage phasor magnitudes and angles). Thus, δ is the bus voltage phasor angles, V represents the bus voltage phasor magnitudes, and Q_G denotes the bus generated reactive powers.

- $p = [P_G^T \ P_L^T \ Q_L^T \ V_{o_G}^T \ P_{o_{TCSC}}^T K]^T \in \Re^k$ is a set of controllable and uncontrollable parameters such as Automatic Voltage Regulator (AVR) settings or load levels. Therefore, P_G represents the generator power levels; P_L and Q_L are the load active and reactive power levels, respectively; V_{o_G} signifies the reference voltage settings of the generators; $P_{o_{TCSC}}$ represents the active power settings of the TCSC; and K indicates the PSS and TCSC controller's PI gains.

- The vector field $f(\cdot) = [f_G^T(\cdot) \ f_{AVR}^T(\cdot) \ f_{cont}^T(\cdot)]^T : \Re^n \times \Re^m \times \Re^k \mapsto \Re^n$ is the system non-linear differential (state) equations [45]. Here, $f_G(\cdot)$ are the generator state equations (generator 4^{th} order transient model), $f_{AVR}(\cdot)$ represent the voltage regulator state equations (IEEE Type 1), and $f_{cont}(\cdot)$ represents for the state equations of the PSS and TCSC.

- The vector field $g(\cdot) = [g_G^T(\cdot) \ g_L^T(\cdot)]^T : \Re^n \times \Re^m \times \Re^k \mapsto \Re^m$ represents the system algebraic constraints (power flow equations $g_L(\cdot)$ and generators' stator algebraic equations $g_G(\cdot)$) [45].

- $F(\cdot) = [f^T(\cdot) \ g^T(\cdot)]^T$.

In a small-perturbation stability analysis, (2.3) is linearized around an equilibrium or operating point (x_o, y_o) for the given values of the parameters p_o. Thus,

$$\begin{bmatrix} \Delta\dot{x} \\ 0 \end{bmatrix} = \underbrace{\begin{bmatrix} J_1 & J_2 \\ J_3 & J_4 \end{bmatrix}}_{J} \begin{bmatrix} \Delta x \\ \Delta y \end{bmatrix} \tag{2.4}$$

where J is the system Jacobian, and $J_1 = \partial f/\partial x|_0$, $J_2 = \partial f/\partial y|_0$, $J_3 = \partial g/\partial x|_0$, and $J_4 = \partial g/\partial y|_0$. If it is assumed that J_4 is nonsingular, which is a requirement for equations (2.3) to appropriately represent the system [65], the system eigenvalues can be readily computed by eliminating the vector of the algebraic variable Δy in (2.4), as follows:

$$\Delta\dot{x} = (J_1 - J_2\ J_4^{-1}\ J_3)\Delta x = A\ \Delta x \tag{2.5}$$

Once the reduced system state matrix A is determined at an equilibrium point on the P-V curve, the system state matrix eigenvalues and eigenvectors are defined by

$$\begin{aligned} Av &= \mu v \\ A^T w &= \mu w \end{aligned} \tag{2.6}$$

where μ is the eigenvalue, and v and w are the corresponding right and left eigenvectors, respectively.

2.4.3 Hopf Bifurcation Index

Based on (2.3) and (2.4), a complex pair of eigenvalues of J can be represented as:

$$\begin{bmatrix} J_1 & J_2 \\ J_3 & J_4 \end{bmatrix} \begin{bmatrix} v_{1_R} \pm j v_{1_I} \\ v_{2_R} \pm j v_{2_I} \end{bmatrix} = [\alpha \pm j\beta] \begin{bmatrix} v_{1_R} \pm j v_{1_I} \\ 0 \end{bmatrix} \tag{2.7}$$

By separating the real and imaginary parts and rearranging these equations:

$$\begin{bmatrix} J_1 - \alpha I & J_2 & \beta I & 0 \\ J_3 & J_4 & 0 & 0 \\ -\beta I & 0 & J_1 - \alpha I & J_2 \\ 0 & 0 & J_3 & J_4 \end{bmatrix} \begin{bmatrix} v_{1_R} \\ v_{2_R} \\ v_{1_I} \\ v_{2_I} \end{bmatrix} = 0$$

$$\left(\begin{bmatrix} J_1 & J_2 & \beta I & 0 \\ J_3 & J_4 & 0 & 0 \\ -\beta I & 0 & J_1 & J_2 \\ 0 & 0 & J_3 & J_4 \end{bmatrix} - \alpha \begin{bmatrix} B & 0 \\ 0 & B \end{bmatrix} \right) \begin{bmatrix} v_{1_R} \\ v_{2_R} \\ v_{1_I} \\ v_{2_I} \end{bmatrix} = 0$$

$$\left(\underbrace{\begin{bmatrix} J & \beta B \\ -\beta B & J \end{bmatrix}}_{J_m} - \alpha \begin{bmatrix} B & 0 \\ 0 & B \end{bmatrix} \right) \begin{bmatrix} v_{1_R} \\ v_{2_R} \\ v_{1_I} \\ v_{2_I} \end{bmatrix} = 0 \tag{2.8}$$

where $B = \begin{bmatrix} I & 0 \\ 0 & 0 \end{bmatrix}$. Since at a Hopf bifurcation $\alpha = 0$, the matrix J_m becomes singular; the same holds at a saddle-node bifurcation point. Therefore, the minimum singular value of the modified full Jacobian matrix J_m is adopted as an index to indicate the proximity to a Hopf or a saddle-node bifurcation. Consequently, the following stability index is proposed in [9, 29]:

$$HBI = \sigma_{min}(J_m) \tag{2.9}$$

This index, as shown in [29], has a fairly linear behaviour with respect to the changing on system loading, with no significant discontinuities due to the control

limits for a series of practical examples. Also, this particular behaviour is observed in the current thesis for the test systems used. Nevertheless, even in the presence of possible discontinuities, these are not a significant factor for the proposed OPF technique, where this index is used as a security constraint as explained in Chapter 3. This is due to the fact that the main concern is the value of this index "near" a bifurcation point, where it is demonstrated in [29, 66] that the index is smooth and quasi-linear, since it is only at this point where this security constraint becomes binding.

2.5 Energy Deregulation and Markets

In the past, the electric power industry has been vertically integrated, meaning that a central "authority" monitored and controlled all the activities in generation, transmission, and distribution. For the last decade or so, the electric power industry has been undergoing a process of transition and restructuring, in particular the separation of transmission from generation activities. Furthermore, competition has been introduced in generation activities either through the creation of power pools, provision for direct bilateral transactions, or bidding on spot markets [67, 68]. In this environment, a system operator has been appointed with the responsibility of ensuring a balance between production and consumption for the whole system, guaranteeing open and fair access to the transmission system. This system operator must never be involved in the market competition, and is usually called the Independent System Operator (ISO).

2.5.1 Different Entities in Deregulated Electricity Markets

The restructuring process has brought several new entities to the market. Variations exist across many market structures around the world, but typically these entities are:

Generation Companies (GENCOs)

They are the producers and the sellers of electricity, and they are classified by different markets according to their rated capacity, or in the way the generators are contracted to operate in the market.

Transmission Companies (TRANSCOs)

They are the owners and the operators of the transmission system. TRANSCOs' prime responsibility is to transport the electricity from the generators to the customers, ensuring the availability of the transmission system to all the entities in the system.

Distribution Companies (DISCOs)

They are the owners and the operators of the local distribution companies. DISCOs buy wholesale electricity either through the spot-markets or through direct contracts with GENCOs, and supply the electricity to the end-use customers.

Energy Services Companies (ESCOs)

These may be large industrial customers, customer pools or private companies, and their main goal is to purchase power at the least cost for their customers from

GENCOs. They participate in the market like DISCOs, except that they do not own or operate the local distribution companies.

Customers

They are the consumers of electricity. Depending on the market structure, the customers have several options for buying electricity. They can choose to buy electricity from the spot-market by bidding for purchase, or buy directly from a GENCO, a DISCO or an ESCO.

Independent System Operator (ISO)

The ISO is responsible for ensuring the reliability and security of the entire system. As an independent authority, the ISO does not trade in the electricity market, and it usually does not own generating resources. In order to maintain the system security and reliability, the ISO procures various services such as the supply of emergency reserves or reactive power form other entities in the system. The specific role of the ISO depends on the particular market structure, in some markets the ISO is directly involved in settling market transactions (e.g. Ontario), whereas in other markets the market transactions are handled by a different entity (e.g. "old" California) [67, 68].

2.5.2 Market Clearing Process

In most markets, both GENCOs and ESCOs bid in the market. A market clearing price (MCP) is obtained, as illustrated in Figure 2.13, by stacking the supply bids in order of increasing prices and the demand bids in order of decreasing prices.

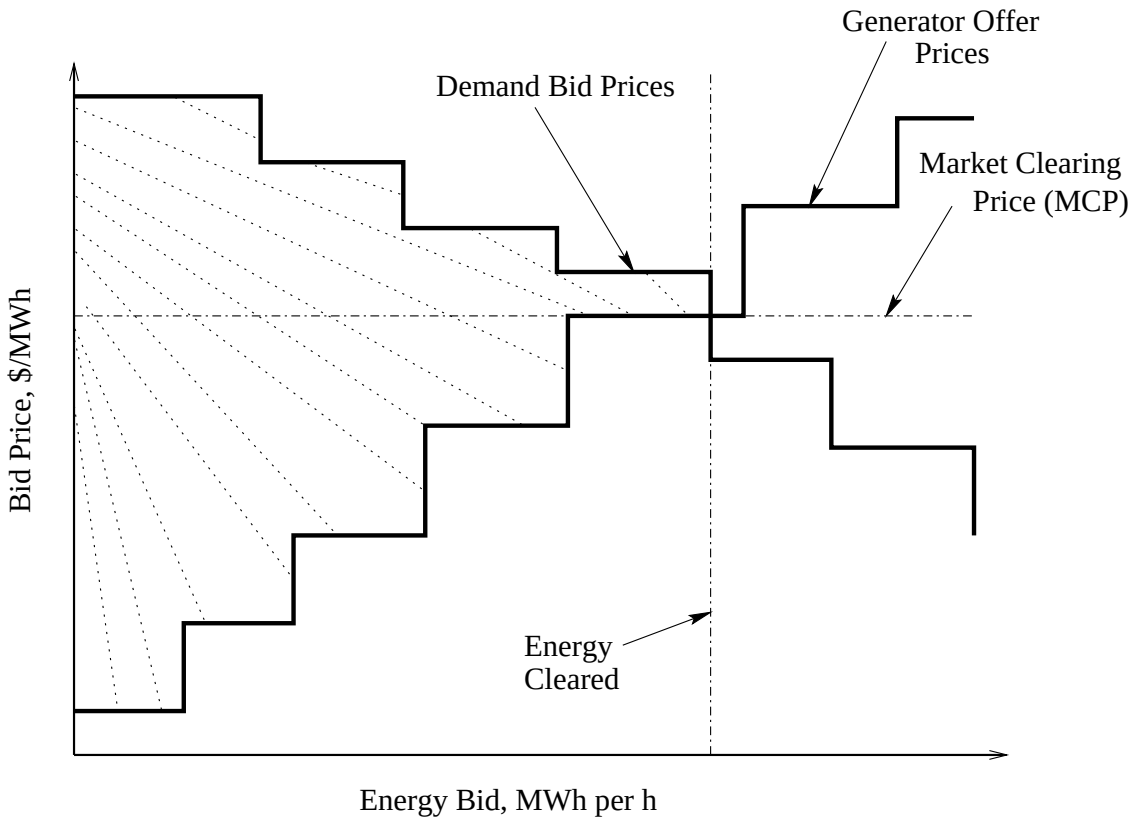

Figure 2.13: Double-auction markets.

The MCP and the amount of energy cleared for trading are obtained from the intersecting point of these curves. This market clearing process is referred to as double auction power pools [67, 68].

In practice, however, the load in most markets does not actively bid, i.e. the load is inelastic. In this case, the system price is cleared by matching the supply curve with a forecast of undispatchable load (e.g. Ontario). Typically, only GENCOs submit bids that are stacked in increasing order of prices, as shown in Figure 2.14. The highest priced bid to intersect with the system demand forecast determines the MCP. Typically, such a market model is known as a single auction power pool.

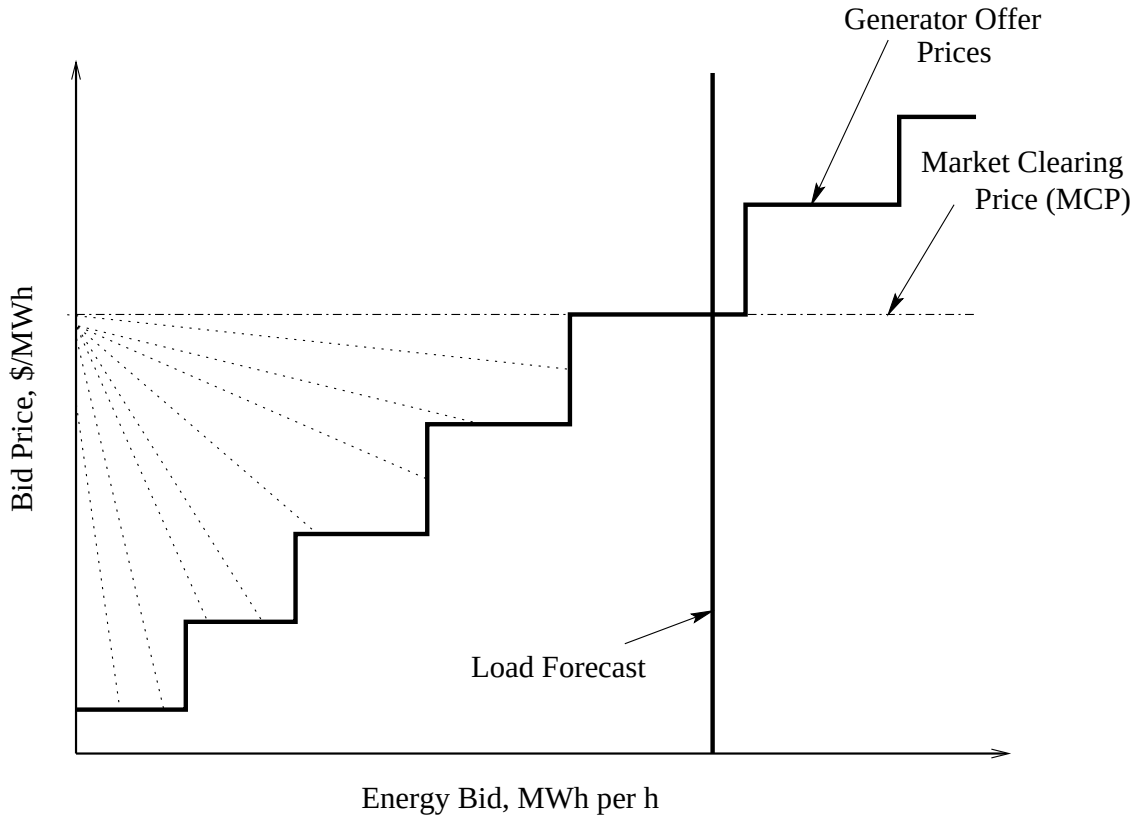

Figure 2.14: Single-auction markets.

2.6 Market Tools

One of the objectives of this thesis is to study stability issues within the framework of deregulated markets. Hence, a number of analysis programs and simulation software are available to aid in the decision-making process, and to make power system operation more reliable and economical. These programs are usually based on OPF algorithms. In the following sections, the OPF is discussed in details, since this is one of the principal optimization tools used in competitive market environments nowadays.

2.6.1 Optimum Power Flow (OPF) Dispatch

The OPF-based auction is defined as a non-linear constrained optimization problem, and consists of a scalar objective function (S_b), and a set of equality and inequality constraints. The following optimization problem represents a typical OPF-based auction model [28, 69]:

$$\begin{aligned}
\text{Min.} \quad & S_b(x,p,\lambda) = -(C_d^T P_d - C_s^T P_s) \\
\text{s.t.} \quad & F_{PF}(\delta, V, Q_G, P_s, P_d) = 0 \\
& 0 \le P_s \le P_{s_{\max}} \\
& 0 \le P_d \le P_{d_{\max}} \\
& \mid P_{ij}(\delta, V) \mid \le P_{ij_{\max}} \\
& \mid P_{ji}(\delta, V) \mid \le P_{ji_{\max}} \\
& I_{ij}(\delta, V) \le I_{ij_{\max}} \\
& I_{ji}(\delta, V) \le I_{ji_{\max}} \\
& Q_{G_{\min}} \le Q_G \le Q_{G_{\max}} \\
& V_{\min} \le V \le V_{\max}
\end{aligned} \tag{2.10}$$

where C_s and C_d are the vectors of the supply and demand bids in \$/MWh, respectively; P_s and P_d are the supply and demand power bids, respectively, and can not exceed their maximum values; $F_{PF}(\cdot)$ represent the "classical"' power flow equations; Q_G stands for the generator reactive powers; V and δ define the bus phasor voltages; and P_{ij} and P_{ji} represent the power flowing through the lines in both directions, that are used to represent the system security by imposing limits on them, in addition to line current I_{ij} and I_{ji} thermal limits and bus voltage limits. In this model, referred to as a security-constrained OPF-based auction, P_{ij} and P_{ji} limits are typically obtained by means of off-line angle and/or voltage stability studies [70]. These limits do not present the actual stability conditions of the resulting solutions, since these limits are not the actual operating conditions that correspond to the solution of the OPF-based auction. Thus, this model can lead to insecure solutions and/or inappropriate price signals [28].

In Figures 2.13 and 2.14, the social benefit is the shaded area. Although the reactive power does not appear directly in the objective function, its effect is indirectly represented by the optimization problem constraints [67], allowing its use in other applications, such as reactive power planning. Another notable feature of the OPF is its applicability over a wide time horizon. The OPF is usually used for optimal dispatch and control actions taken every few minutes, and for medium-term planning studies months ahead, as in the case of reactive power planning. For long-term studies, the OPF is used for generation and transmission expansion planning, carried out years in advance to make decisions on investments in generation and the transmission system [67].

2.6.2 Voltage-Stability-Constrained OPF

The objective function of the OPF problem may vary, based on the target of the optimization; for example, in [71], the target is to minimize the cost of the load shedding to enhance the voltage stability of the system. The OPF-based auction can also be used to minimize a multi-objective function, as in the case of [28], where different terms in the objective function are used to maximize both the social welfare and system voltage stability margins.

The minimum singular value of the power flow Jacobian can be used as an index to predict voltage instability in power systems [25, 26]. By including a minimum limit for this index in the standard OPF-based auction, a VSC-OPF can be written as follows [27]:

$$\begin{aligned} \text{Min.} \quad & S_b = -(C_d^T P_d - C_s^T P_s) \\ \text{s.t.} \quad & F_{PF}(\delta, V, Q_G, P_s, P_d) = 0 \\ & \sigma_{min}(J_{PF}) \geq \ \sigma_{c_{PF}} \\ & 0 \leq P_s \leq P_{s_{\max}} \\ & 0 \leq P_d \leq P_{d_{\max}} \\ & I_{ij}(\delta, V) \leq I_{ij_{\max}} \\ & I_{ji}(\delta, V) \leq I_{ji_{\max}} \\ & Q_{G_{\min}} \leq Q_G \leq Q_{G_{\max}} \\ & V_{\min} \leq V \leq V_{\max} \end{aligned} \tag{2.11}$$

where $J_{PF} = [\frac{\partial F_{PF}}{\partial \delta}\big|_o \quad \frac{\partial F_{PF}}{\partial V}\big|_o]$ is the power flow Jacobian of the system, and $\sigma_{c_{PF}}$ is a minimum limit for the voltage stability index, so that voltage instability can be avoided even for the worst contingency (N-1 contingency criterion). Such a

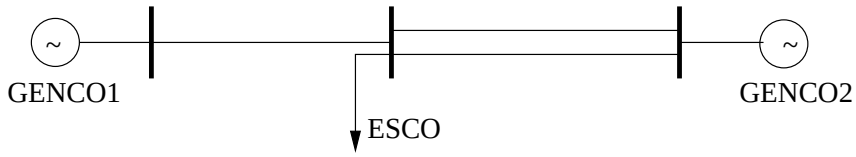

Figure 2.15: Three-bus test case.

value needs to be determined by off-line studies [27], and is used to replace the off-line-based limits on transmission power levels.

2.7 Test Systems

2.7.1 3-Bus Test System

Figure 2.15 depicts the 3-bus benchmark test system used in this thesis, which is extracted from [72]. This system was developed in [73] to study the oscillatory instabilities in a simple two machines system. Both generators are modeled by a fourth-order transient model, and the AVR model of Figure 2.3 [74]. The nominal load is assumed to be 900 MW and 300 Mvar. The dynamic data for the generators' exciters are selected from [44] and are illustrated in Appendix A, together with the market bidding data.

2.7.2 IEEE 14-Bus Test System

A single-line diagram of the IEEE 14-bus test system, in Figure 2.16, consists of five synchronous machines with IEEE type-1 exciters, two of which are synchronous compensators for reactive power support. There are 11 loads in the system, totalling 259 MW and 81.3 Mvar. The dynamic and static data for the system, generators,

and exciters are selected from [75] and are illustrated in Appendix B, together with the market bidding data.

The selection of the test system is based on the following criteria:

1. The stability of the selected system is modelled and analyzed, including FACTS, in detail in several technical documents based on the results of a variety of software packages (e.g. [9, 75]). This sample system contains enough dynamic and static elements to allow for meaningful stability and security studies.

2. The selected system represents a portion of the American Power System in the US Midwest, and hence can be considered a "realistic" example.

3. The system has enough generation and load to simulate an electricity market, and thus, produce significant results for examining the proposed techniques.

4. A larger system cannot be readily studied to illustrate the differences between the proposed SSC-OPF technique and a standard OPF auction, since a large amount of data and computations are required to reach conclusions that can be also attained with this reduced size system.

2.8 Summary

This chapter includes a brief description of power system instabilities, the basic concepts of deregulated energy markets, and the main analysis techniques and tools used in this thesis. Also, this chapter describes the models of power system components and controllers used to study the effect of system controllers on electricity

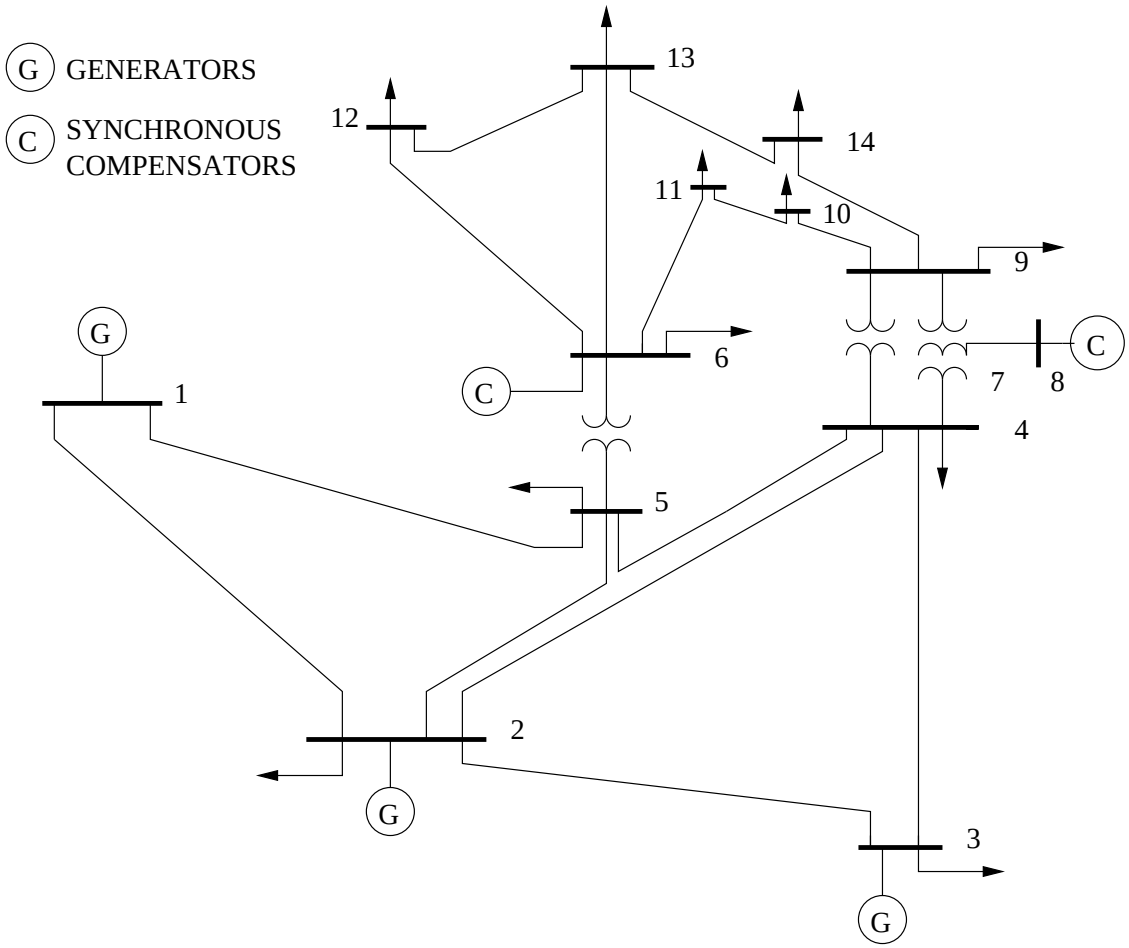

Figure 2.16: IEEE 14-bus test system.

pricing. The last part of this chapter briefly discusses and justifies the test systems used in this thesis.

Chapter 3

Small-Perturbation Stability Constrained (SSC)-OPF

3.1 Introduction

The inadequate assessment of system instability problems may lead to poor market operating conditions, which may result in unsecure system conditions and inadequate price signals [28]. Hence, in this chapter, a technique that includes the Hopf bifurcation index introduced in Chapter 2 as a stability constraint in the OPF-based auction mechanism to better represent system security, is presented. The implementation and solution techniques for the novel SSC-OPF technique are also described. Finally, the application of the SSC-OPF to several test systems is demonstrated and compared to the standard OPF and the VSC-OPF.

3.2 SSC-OPF

As discussed in Section 2.7, the minimum singular value of the modified matrix J_m (2.9) can be used as a stability index to detect voltage and oscillatory stability problems. Thus, the following new OPF-based auction, which includes this index as a constraint, is proposed as an improved alternative to properly represent these types of stability problems:

$$\begin{aligned} \text{Min.} \quad & S_b = -(C_d^T P_d - C_s^T P_s) \\ \text{s.t.} \quad & F(x, y, p) = 0 \\ & \sigma_{min}(J_m) \geq \ \sigma_c \\ & p_{min} \leq p \leq p_{\max} \\ & I_{ij}(x, y) \leq I_{ij_{\max}} \\ & I_{ji}(x, y) \leq I_{ji_{\max}} \\ & y_{\min} \leq y \leq y_{\max} \end{aligned} \tag{3.1}$$

where $F(\cdot)$ corresponds to the steady-state equations of the system dynamic model, as defined in (2.3); σ_{min} is the minimum singular value of the modified state matrix J_m, which becomes zero at a Hopf or saddle-node bifurcation point; and σ_c stands for the minimum stability index value as defined by the user. The value of σ_c depends on the system's characteristics, and must be determined from off-line stability studies, so that it reflects appropriate system security margins (e.g. the appropriate damping ratios).

It is important to highlight the differences between the proposed SSC-OPF technique (3.1) and the VSC-OPF problem (2.11). Thus:

- A full dynamic model of the system is considered in (3.1), whereas (2.11) is based on a power flow model.

- The stability index in (3.1) captures not only voltage stability problems accounted for in (2.11), but oscillatory stability problems as well.

3.2.1 OPF Solution Procedure

SSC-OPF (3.1) corresponds to a nonlinear optimization problem with an implicit constraint. Hence, "standard" optimization solution techniques must be modified to solve this problem. In this thesis, an Interior Point Method (IPM) is adopted to solve the proposed optimization problems (this technique is different than the one used in [27] to solve the VSC-OPF problem). From (3.1), the OPF auction is rewritten in the following form:

$$\begin{aligned} \text{Min.} \quad & S(\chi) \\ \text{s.t.} \quad & F(\chi) = 0, \\ & \underline{H} \leq H(\chi) \leq \overline{H}, \end{aligned} \tag{3.2}$$

where $\chi \in \Re^N$ is the vector of the optimization variables; i.e. $\chi = [x^T \quad y^T \quad p^T]^T$, $N = n+m+k$, with lower bounds $\underline{\chi}$ and upper bounds $\overline{\chi}$; $S : \Re^N \rightarrow \Re$ is the scalar optimization function; $F : \Re^N \rightarrow \Re^{n+m}$ is the vector function defined in (2.3); and $H : \Re^N \rightarrow \Re^l$ is a vector function, with the lower bounds $\underline{H}$ and upper bounds $\overline{H}$, which includes the $\underline{\chi}$ and $\overline{\chi}$ limits, used to represent all the operating limits of the system, including the stability constraint represented by the $\sigma_{min}(J_m)$ index. This optimization problem is solved by using an IPM, which transforms all the inequality constraints in (3.2) into equalities by adding non-negative slack vectors

s and q, and incorporating them into logarithmic barrier terms as follows [76, 77]:

$$\begin{aligned} \text{Min.} \quad & S(\chi) - \mu_s \sum_i (\ln s_i + \ln q_i) \\ \text{s.t.} \quad & F(\chi) = 0, \\ & -s - q + \overline{H} - \underline{H} = 0, \\ & -H(\chi) - q + \overline{H} = 0, \\ & s \geq 0, \quad q \geq 0 \end{aligned} \tag{3.3}$$

where $\mu_s \in \Re$, $\mu_s > 0$ is the barrier parameter. To solve the equality-constrained problem (3.3), the Lagrange-Newton method is used, which is based on the following Lagrangian function $L_\mu(u)$ associated with (3.3),

$$\begin{aligned} L_\mu(u) \quad = \quad & S(\chi) - \mu_s \sum_i (\ln s_i + \ln q_i) - \rho^T F(\chi) \\ & -\varsigma^T(-s - q + \overline{H} - \underline{H}) - \tau^T(-H(\chi) - q + \overline{H}) \end{aligned} \tag{3.4}$$

where $\rho \in \Re^{n+m}$, $\varsigma \in \Re^l$, and $\tau \in \Re^l$ are vectors of the Lagrange multipliers or dual variables, and $u = [\chi^T \quad s^T \quad q^T \quad \rho^T \quad \varsigma^T \quad \tau^T]^T$. The local minimum of (3.4) is expressed in terms of a stationary point of $L_\mu(u)$, which must satisfy the Karush-Kuhn-Tucker (KKT) optimality conditions $\nabla_u L_\mu(u) = 0$. Although $\nabla_u L_\mu(u) = 0$ is nonlinear, its solution is usually approximated by a single iteration of Newton's method; thus, the Hessian $\nabla^2_\chi L_\mu(u)$ is required in the algorithm. The computation of this Hessian requires an evaluation of the objective function Hessian $\nabla^2_\chi S(\chi)$ and the constraint Hessians $\nabla^2_\chi F(\chi)$ and $\nabla^2_\chi H(\chi)$, since

$$\nabla^2_\chi L_\mu(u) = \nabla^2_\chi S(\chi) - \rho^T \nabla^2_\chi F(\chi) + \tau^T \nabla^2_\chi H(\chi) \tag{3.5}$$

To solve this problem, a good estimate of $\nabla^2_\chi \sigma_{min}(J_m)$ is needed. This requires certain approximations, since $\sigma_{min}(J_m)$ is an implicit function of the optimization

variables χ. This approximation is accomplished here by first obtaining an estimate of $\nabla_\chi \sigma_{min}(J_m)$, based on [25]. Thus, if χ_* is perturbed such that $\chi_* + \Delta\chi = [z_*^T + \Delta z^T \; p_*^T + \Delta p^T]^T$, where $z = [x^T \; y^T]^T$ by using a Taylor series expansion, then

$$J|_{z_*+\Delta z} \approx J|_{z_*} + G\Delta z \tag{3.6}$$

where $G = \frac{\partial^2 F}{\partial z^2}\Big|_{z_*}$. From (2.8)

$$\begin{aligned} J_m|_{z_*+\Delta z} &\approx \begin{bmatrix} J|_{z_*+\Delta z} & \beta|_{z_*+\Delta z} B \\ -\beta|_{z_*+\Delta z} B & J|_{z_*+\Delta z} \end{bmatrix} \\ &\approx \begin{bmatrix} J|_{z_*} + G\Delta z & \beta B \\ -\beta B & J|_{z_*} + G\Delta z \end{bmatrix} \end{aligned} \tag{3.7}$$

if it is assumed that $\beta|_{z_*+\Delta z} \approx \beta|_{z_*} \approx \beta$, i.e. the frequency of the critical eigenvalues (the eigenvalues that eventually reach the imaginary axis for a Hopf bifurcation) does not change significantly, which is typically the case [29]. Then,

$$J_m|_{z_*+\Delta z} \approx J_m|_{z_*} + \begin{bmatrix} G\Delta z & 0 \\ 0 & G\Delta z \end{bmatrix} \tag{3.8}$$

Following [25], by singular value decomposition, the matrix $J_m|_{z_*}$ may be written as

$$J_m|_{z_*} = U\Sigma V^T \tag{3.9}$$

Similarly,

$$J_m|_{z_*+\Delta z} = (U + \Delta U)(\Sigma + \Delta\Sigma)(V + \Delta V)^T \tag{3.10}$$

is the singular value decomposition of $J_m|_{z_*+\Delta z}$, where ΔU, ΔV, and $\Delta\Sigma$ are small perturbations on U, V, and Σ, respectively. By substituting (3.9) and (3.10) into (3.8), expanding the matrix multiplications, and disregarding the second and third order perturbations, the following approximation is obtained:

$$U\Delta\Sigma V^T + \Delta U\Sigma V^T + U\Sigma\Delta V^T \approx \begin{bmatrix} G\Delta z & 0 \\ 0 & G\Delta z \end{bmatrix} \tag{3.11}$$

Additional constraints are given by the orthogonality of $U + \Delta U$ and $V + \Delta V$,

$$(U + \Delta U)(U + \Delta U)^T = 1 \tag{3.12}$$

and

$$(V + \Delta V)(V + \Delta V)^T = 1 \tag{3.13}$$

If (3.12) is expanded disregarding the second order terms, and substituting the unity matrix for UU^T, the result is

$$U^T\Delta U = -[U^T\Delta U]^T \tag{3.14}$$

Assume $M = U^T\Delta U$; thus, $M = -M^T$. Similarly, for $N = V^T\Delta V$. If (3.11) is premultiplied and postmultiplied by U^T and V, respectively, and including M and N,

$$\Delta\Sigma + M\Sigma + \Sigma N^T = U^T \begin{bmatrix} G\Delta z & 0 \\ 0 & G\Delta z \end{bmatrix} V \tag{3.15}$$

Since M and N have zero diagonals and Σ is a diagonal matrix, the diagonal entries of $M\Sigma$ and ΣN^T are zero. Hence, evaluating the minimum singular value of (3.15) yields

$$\Delta\sigma_{min}(J_m) = U_1^T \begin{bmatrix} G\Delta z & 0 \\ 0 & G\Delta z \end{bmatrix} V_1 \tag{3.16}$$

where U_1 and V_1 are, respectively, the left and right singular vectors corresponding to the minimum singular value of J_m. Furthermore, since at a solution point χ_*,

$$\begin{aligned} F(\chi_*) = F(z_*, p_*) &= 0 \\ \tfrac{\partial F}{\partial z}\big|_{z_*}\, dz + \tfrac{\partial F}{\partial p}\Big|_{p_*} dp &= 0 \\ \Rightarrow \Delta z = -\left[\tfrac{\partial F}{\partial z}\big|_{z_*}\right]^{-1} \tfrac{\partial F}{\partial p}\Big|_{p_*} \Delta p \\ = -J^{-1} J_p \Delta p \end{aligned} \tag{3.17}$$

one can evaluate the change of $\sigma_{min}(J_m)$ with respect to the parameters p as follows:

$$\Delta\sigma_{min}(J_m) \approx U_1^T \begin{bmatrix} -GJ^{-1}J_p\Delta p & 0 \\ 0 & -GJ^{-1}J_p\Delta p \end{bmatrix} V_1 \tag{3.18}$$

Finally, to evaluate $\nabla^2_\chi \sigma_{min}(J_m)$, the following numerical approximation is used [78]:

$$\frac{\partial^2 \sigma_{min}(J_m)}{\partial\chi_i\chi_j}\Big|_{\chi_*+\Delta\chi} \approx \frac{\frac{\partial\sigma_{min}(J_m)}{\partial\chi_i}\Big|_{\chi_*} - \frac{\partial\sigma_{min}(J_m)}{\partial\chi_i}\Big|_{\chi_*+\Delta\chi}}{\Delta\chi_j} \tag{3.19}$$

where $\frac{\partial\sigma_{min}}{\partial\chi_i}$ are obtained by using the approximations (3.16) or (3.18) as needed.

3.2.2 Implementation of SSC-OPF

Figure 3.1 depicts the computational procedure for solving the proposed SSC-OPF by an IPM, based on a Mehrotra's predictor-corrector technique programmed in MATLAB [77]. It is important to mention that the equilibrium equations of the dynamic DAE model, as well as the corresponding Jacobian and eigenvalues closer

to the imaginary axis, are computed for each iteration i. This procedure can be summarized as follows:

1. The proposed SSC-OPF is initialized by using the results obtained from applying the standard OPF (2.10) to the system.

2. The equilibrium equations of (2.3), i.e. $F(\cdot) = 0$, are solved.

3. The first and the second derivatives of the equality and inequality constraints are calculated, including the first and second derivatives of the stability constraint with respect to the optimization variables, using (3.16), (3.18), and (3.19).

4. The KKT optimality conditions are then formulated and solved by using Mehrotra's predictor-corrector technique, and the barrier parameter μ_s is updated by the techniques described in [76, 77].

5. If the barrier parameter, the objective function, and the optimization variables converge within the given tolerance limits (10^{-4}), the process ceases, otherwise, it is repeated from Step 2.

To evaluate the computational burden of the proposed SSC-OPF technique, the execution times for the VSC-OPF (2.11) and the SSC-OPF (3.1) were compared. Thus, the VSC-OPF requires about one-tenth of the CPU time needed by the SSC-OPF to obtain a solution, whereas both need approximately 40 to 50 iterations to converge to an optimal solution. This difference can be significantly reduced by optimizing the code (e.g. by using sparse matrix techniques). However, additional computational costs are expected, since the number of constraints and, especially the size of the Jacobians and Hessians, can be significantly larger than those in the proposed SSC-OPF method.

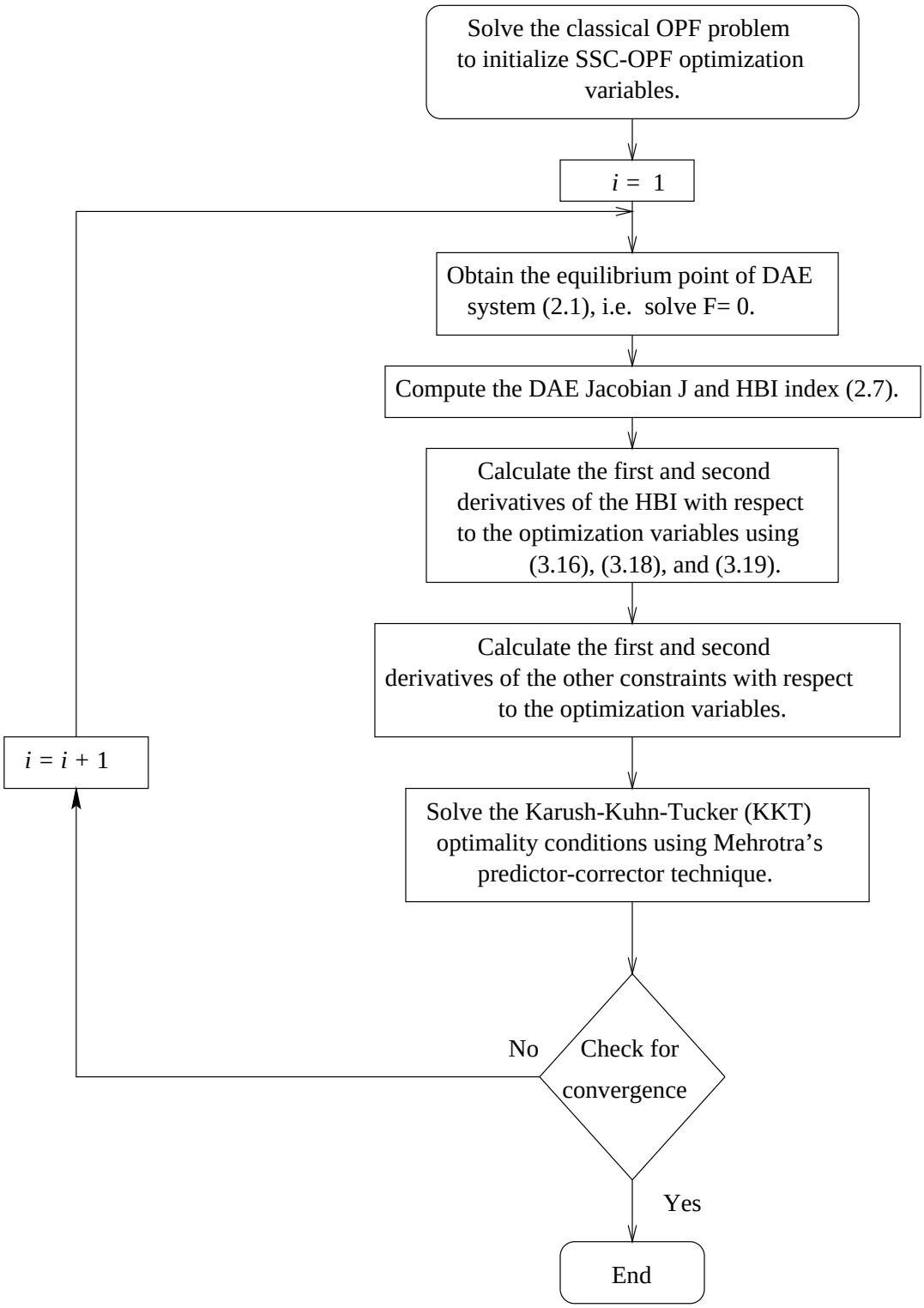

Figure 3.1: Solution procedures of the SSC-OPF.

3.2.3 Locational Marginal Prices (LMPs)

OPF-based market models produce the optimal operating point and a variety of sensitivities through the Lagrangian multipliers, which are associated with the Locational Marginal Prices (LMPs) at each node [28], providing reliable pricing indicators [69]. The Lagrangian multipliers of the power flow equations, a subset of ρ in (3.4), define the LMPs for the participants in the auction as follows:

$$\begin{aligned} \frac{\partial L_\mu(z)}{\partial P_{s_i}} &= C_{s_i} - \rho_{P_{s_i}} + \varsigma_{P_{s_{max_i}}} - \varsigma_{P_{s_{min_i}}} + \tau_{\sigma_{min}} \left(\frac{\partial \sigma_{min}(J_m)}{\partial P_{s_i}} \right) = 0 \quad (3.20) \\ \frac{\partial L_\mu(z)}{\partial P_{d_i}} &= -C_{d_i} + \rho_{P_{d_i}} + \varsigma_{P_{d_{max_i}}} - \varsigma_{P_{d_{min_i}}} + \tau_{\sigma_{min}} \left(\frac{\partial \sigma_{min}(J_m)}{\partial P_{d_i}} \right) = 0 \end{aligned}$$

Consequently, the LMPs can be calculated as follows:

$$\begin{aligned} LMP_{s_i} = \quad \rho_{P_{s_i}} &= C_{s_i} + \varsigma_{P_{s_{max_i}}} - \varsigma_{P_{s_{min_i}}} + \tau_{\sigma_{min}} \left(\frac{\partial \sigma_{min}(J_m)}{\partial P_{s_i}} \right) \quad (3.21) \\ LMP_{d_i} = \quad \rho_{P_{d_i}} &= C_{d_i} - \varsigma_{P_{d_{max_i}}} + \varsigma_{P_{d_{min_i}}} - \tau_{\sigma_{min}} \left(\frac{\partial \sigma_{min}(J_m)}{\partial P_{d_i}} \right) \end{aligned}$$

From these definitions, the LMPs are affected by the costs C_s and C_d, as well as the system constraints, particularly the stability constraint associated with $\sigma_{min}(J_m)$, and are a byproduct of the solution process. These LMPs are used to analyze the effect of the system constraints, such as security limits, in the market's prices, and are thus used here to price the dynamic controllers' services.

3.3 Comparing OPF Techniques

In the standard OPF, VSC-OPF and SSC-OPF studies, the loads are typically represented in steady-state as constant PQ loads with a constant power factor.

Hence, the loads are modelled here as follows:

$$\begin{aligned} P_L &= P_{L_o} + P_d \\ P_d &\leq P_{d_{max}} = P_{L_o}\lambda \\ Q_L &= P_L \tan\phi \end{aligned} \tag{3.22}$$

where P_{L_o} is the "base" real and power that represents the inelastic loads, ϕ stands for the constant power factor angle, and λ is a p.u. loading factor. The change in the generation bid is represented as:

$$P_G = P_{G_o} + P_s \tag{3.23}$$

where P_{G_o} is the must run generation that is not included in the market bidding.

3.3.1 Standard OPF vs. SSC-OPF

IEEE 14-Bus base case

Figure 3.2 demonstrates the HBI stability index (2.9) and the voltage stability index $\sigma_{min}(J_{PF})$ in (2.11) since the ESCOs' demand power is increased from its nominal value according to (3.23) with $P_d = P_{L_o}\lambda$. Both indices are calculated with the assumption that the total demand is shared by GENCO1, GENCO2, and GENCO3 proportionally to their inertias, i.e. the OPF technique is not applied to determine the optimal schedules. Figure 3.2 shows that there is a Hopf bifurcation point when the ESCOs' loading factor reaches 0.45 p.u., which is associated with an oscillatory instability linked to GENCO1. The voltage stability index indicates that the maximum loading factor can reach a 0.705 p.u. value, if oscillatory stability is not considered in the analysis. Figure 3.3 illustrates the HBI stability index with

different contingencies applied to the system. In this case, a line 1-5 outage is determined to be the most severe contingency from an oscillatory stability point of view, the main concern in this thesis.

A 2% damping ratio is used as the minimum value of the system damping required to maintain system security [79]. Without contingencies, this limit is reached at the ESCOs' loading factor of 0.37 p.u., which corresponds in Figure 3.2 to an HBI value of 0.00018; thus, the value of σ_c in (3.1) is chosen to be 0.0002. With an N-1 contingency criterion, the value of σ_c in (3.1), obtained from Figure 3.3, is 0.00025.

For the base case, the SSC-OPF (3.1) results with $\sigma_c = 0.0002$ are compared with those of a standard OPF (2.10). The power limits on the lines in (2.10) are obtained by considering a damping ratio of 2%, as typically done in most systems (e.g. Ontario). For the standard OPF and the SSC-OPF problems, the bus voltage limits are 0.9 p.u. and 1.1 p.u.

The supplied power by the GENCOs and their LMPs, obtained by solving (2.10) and (3.1) with respect to the ESCOs' loading factor λ, are illustrated in Figure 3.4. Notice that the power supplied by GENCO1 decreases as the demand increases when the SSC-OPF is used, which is to be expected since this generator is the reason for the low damping at $\lambda = 0.45$; this behaviour is not observed when using the standard OPF. Furthermore, the GENCOs' LMPs are higher for the standard OPF than those obtained with the SSC-OPF, since the system is more congested in (2.10) than in (3.1). All of this is due to the different security constraints used in the OPFs to represent system security, which in both cases do not allow loading levels greater than $\lambda = 0.45$. Similar results are obtained for the ESCOs' LMPs, as shown in Figure 3.5.

These results clearly show the more restrictive nature of the "classical" security constraints used in the standard OPF, as opposed to the $\sigma_{min}(J_m)$ constraint used in the proposed SSC-OPF. As a result, the bus prices for the standard OPF are higher than those for the SSC-OPF, in spite of both solutions being very similar from the stability point of view, as demonstrated by the $\sigma_{min}(J_m)$ plots depicted in Figure 3.6.

Table 3.1 summarizes the solution details for the standard OPF and SSC-OPF at the loading factor $\lambda = 0.45$, which corresponds to the maximum loading level for which there is a solution to both problems. Bus voltages and active and reactive powers for all the GENCOs and ESCOs are shown, as well as the value of the indices $\sigma_{min}(J_{pf})$ and $\sigma_{min}(J_m)$. It is evident that the standard OPF is more "restrictive" than the proposed SSC-OPF, since the supply and demand side powers are lower for the standard OPF, which is to be expected, as the SSC-OPF better represents the system stability.

IEEE 14-Bus with N-1 Security Criterion

With the N-1 security criterion, the SSC-OPF (3.1) results with $\sigma_c = 0.00025$ are compared with the standard OPF (2.10) results. The power limits on the lines in (2.10) are obtained by considering a damping ratio of 2% for the worst single contingency (line 1-5 outage). For both the standard OPF and the SSC-OPF problems, the bus voltage limits are 0.9 p.u. and 1.1 p.u.

The supplied power by GENCOs and their LMPs, obtained by solving (2.10) and (3.1) with respect to the ESCOs' loading factor λ, are illustrated in Figure 3.7. Observe that that both GENCO2 and GENCO3 supply all the demand needs, whereas GENCO1 is not dispatched. Furthermore, the GENCOs' LMPs are higher

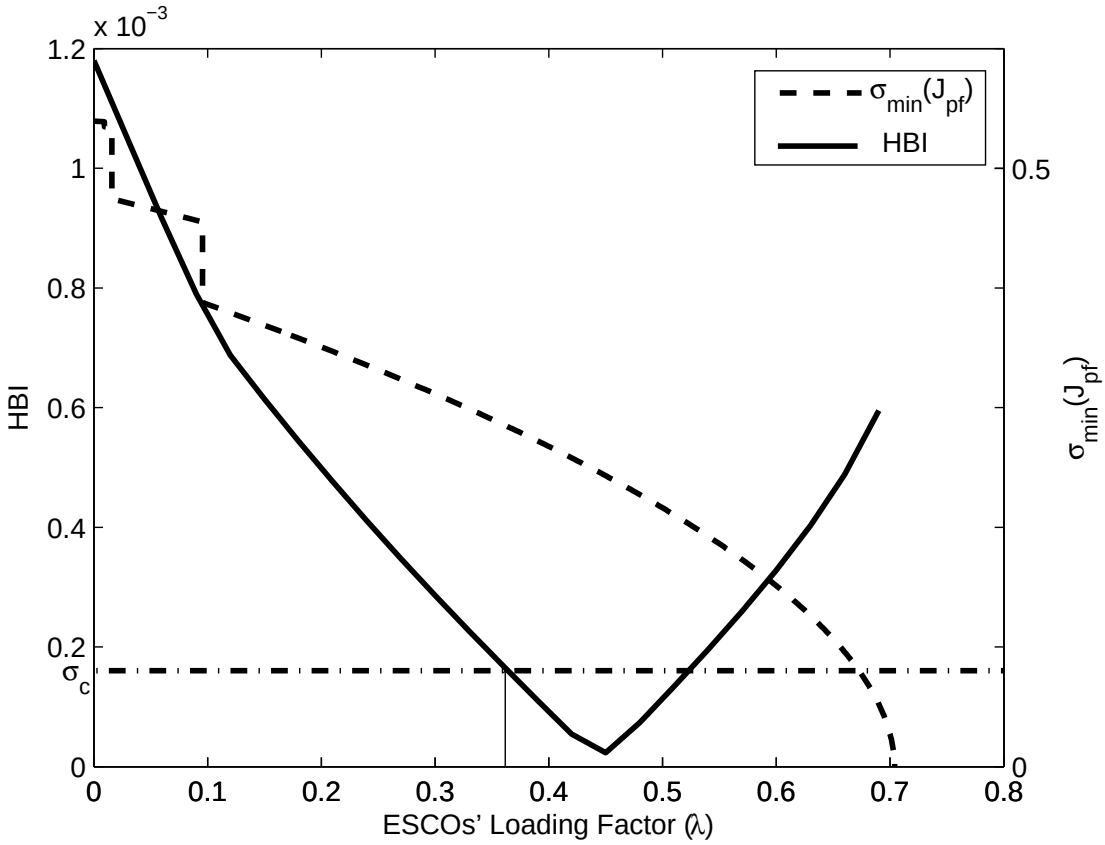

Figure 3.2: HBI and minimum singular value of power flow Jacobian versus loading factor for the IEEE 14-bus test system.

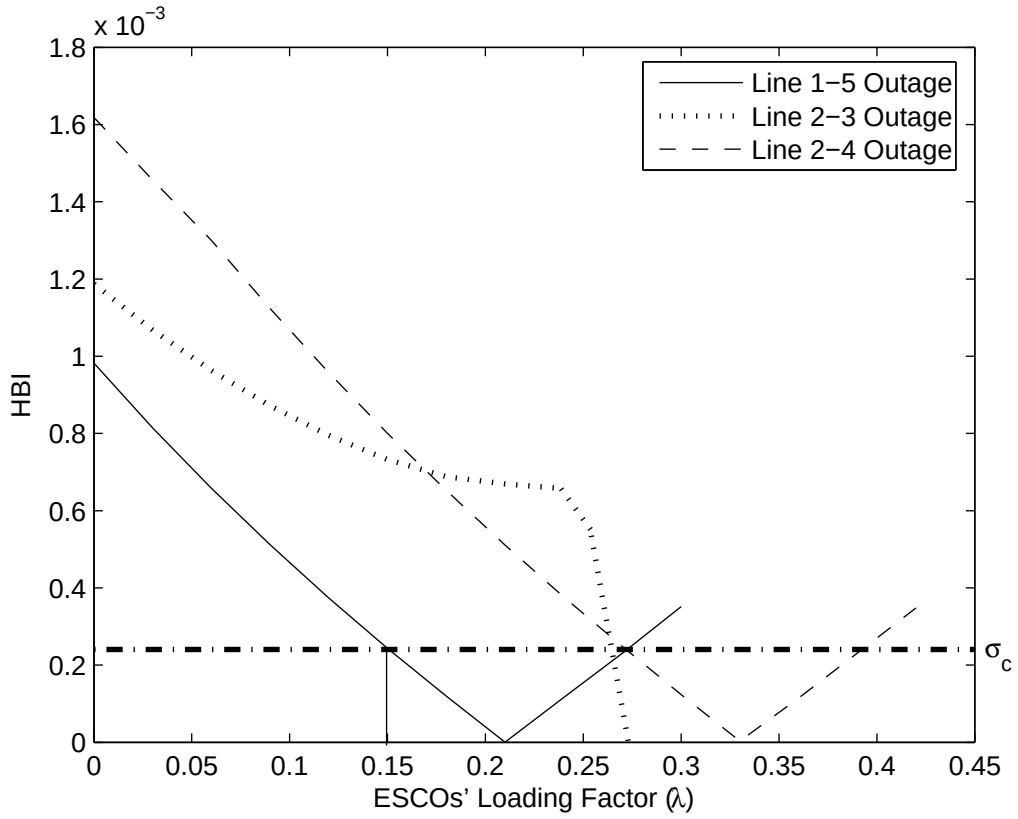

Figure 3.3: HBI stability index for different contingencies applied to the IEEE 14-bus test system.

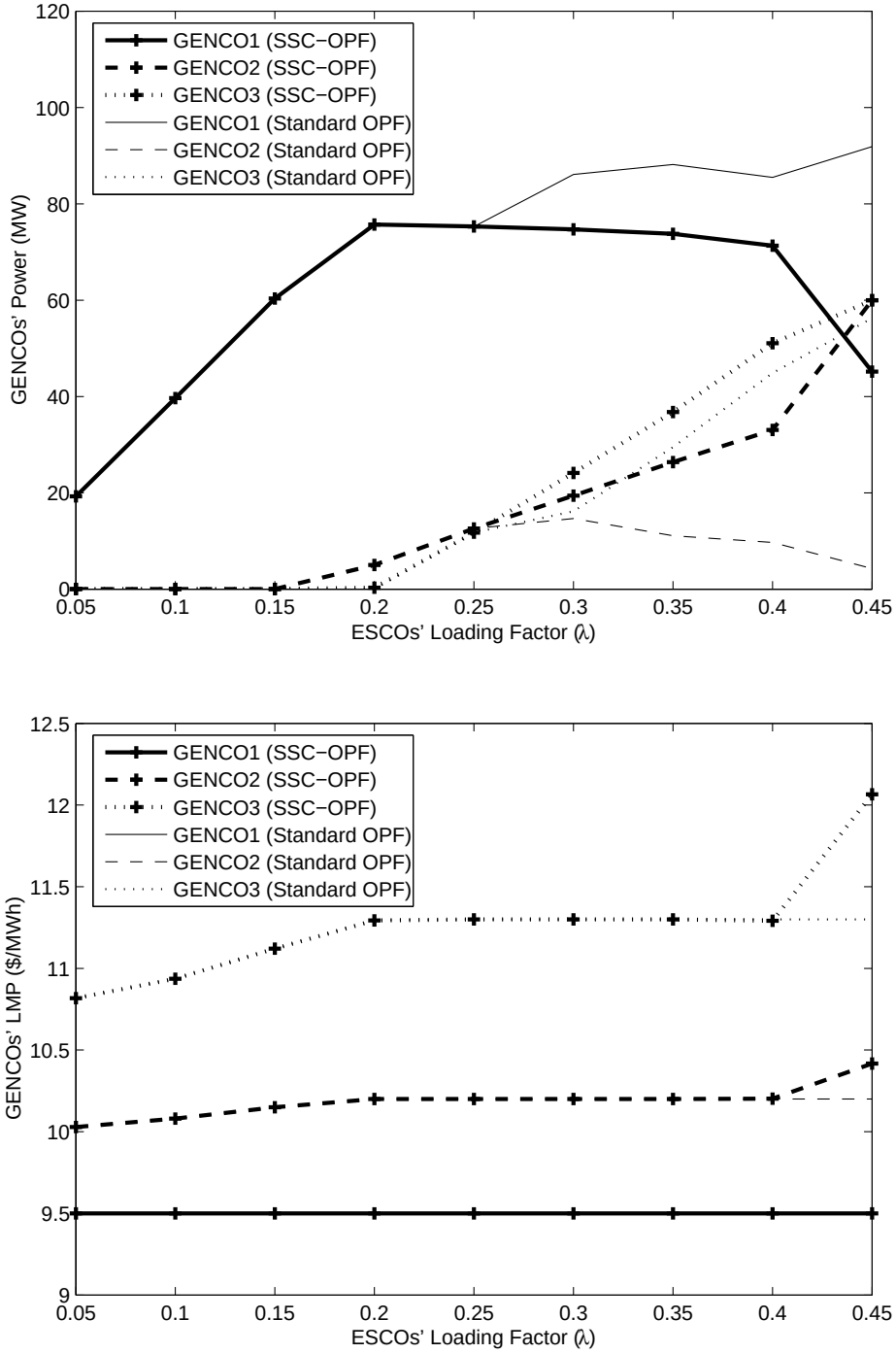

Figure 3.4: GENCOs' supplied power and LMPs with respect to the loading factor for the IEEE 14-bus test system.

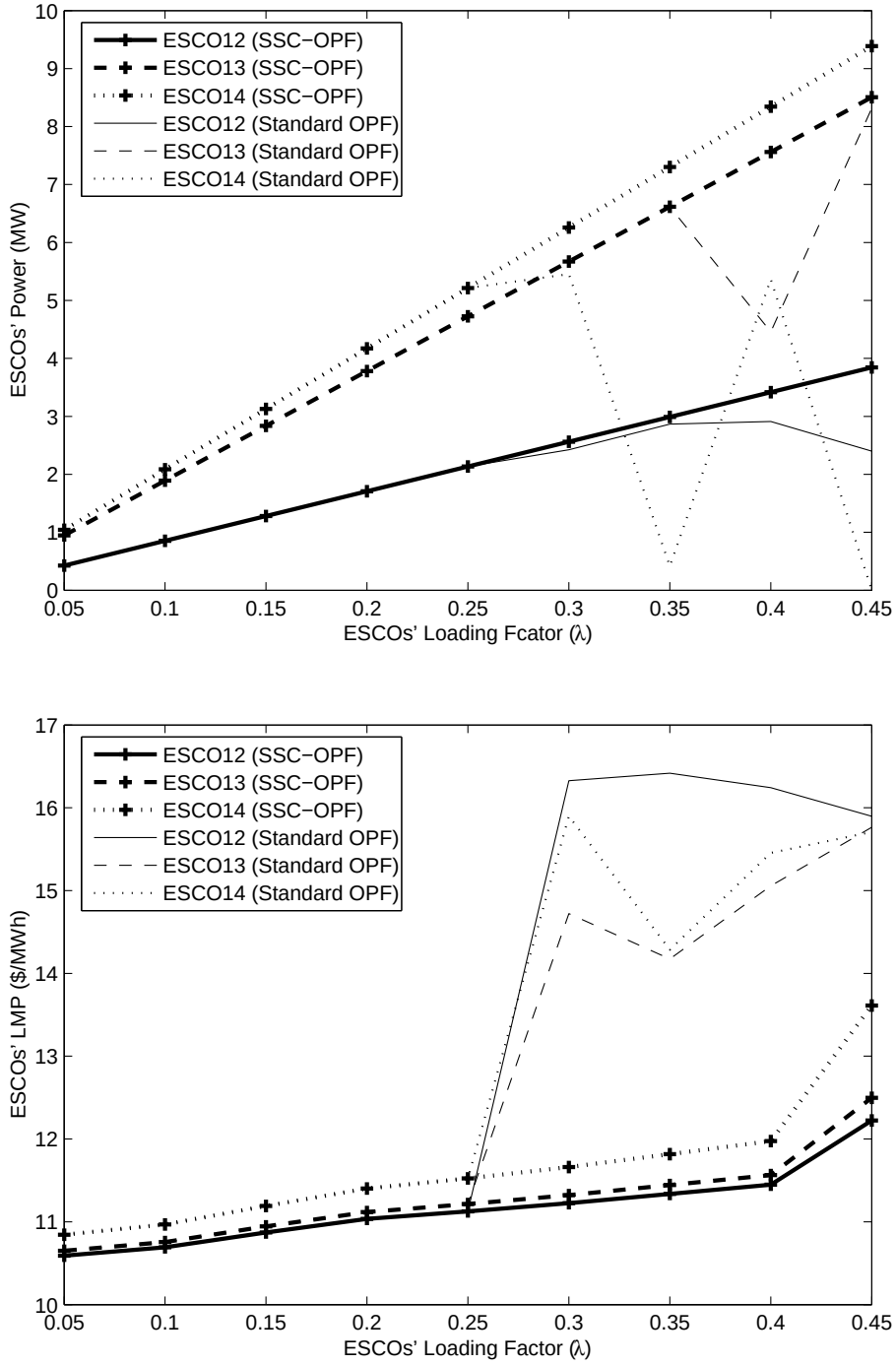

Figure 3.5: ESCOs' power and LMPs with respect to the loading factor for the IEEE 14-bus test system.

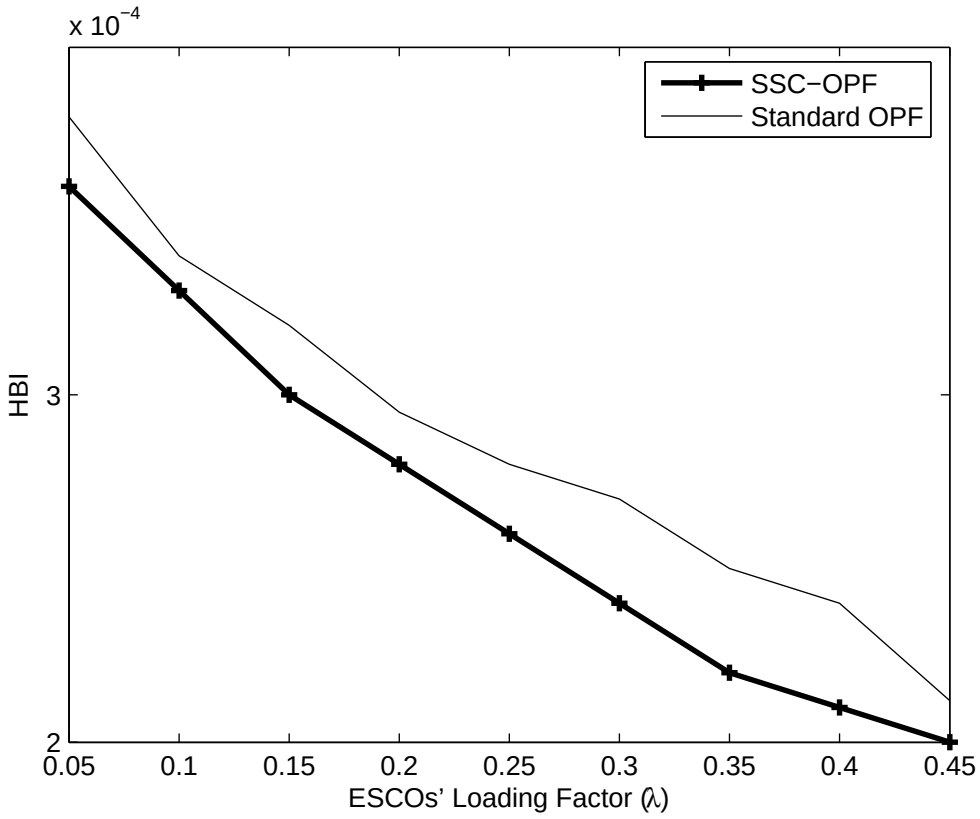

Figure 3.6: HBI results obtained by the standard OPF and the SSC-OPF for the IEEE 14-bus test system.

Table 3.1: Solution details for the standard OPF and SSC-OPF at $\lambda = 0.45$ p.u. for the IEEE 14-bus test system.

Bus	Standard OPF			SSC-OPF		
	V (p.u.)	P (MW)	Q_G (MVAr)	V (p.u.)	P (MW)	Q_G (MVAr)
GENCO1	1.1	91.87	48.6	1.1	45.148	55
GENCO2	1.0546	4.263	50	1.058	60	50
GENCO3	1.006	56.27	40	1.006	60	40
ESCO2	1.0546	13.671		1.058	13.671	
ESCO3	1.006	59.355		1.006	59.355	
ESCO4	0.9972	30.114		0.99	30.114	
ESCO5	1.0053	4.788		0.998	4.788	
ESCO6	1.0338	5.119	24	1.02	1.877	24
ESCO9	0.9916	16.48		0.97	18.585	
ESCO10	1.006	0.00		0.967	3.8836	
ESCO11	1.01	2.203		0.987	2.205	
ESCO12	1.0014	2.401		0.992	3.843	
ESCO13	0.978	8.316		0.981	8.505	
ESCO14	0.9768	0.000		0.943	9.387	
Bus 7	1.016			0.999		
Bus 8	1.056		24	1.04		24
$\sigma_{min}(J_m)$	0.000212 (stable)			0.0002 (stable)		

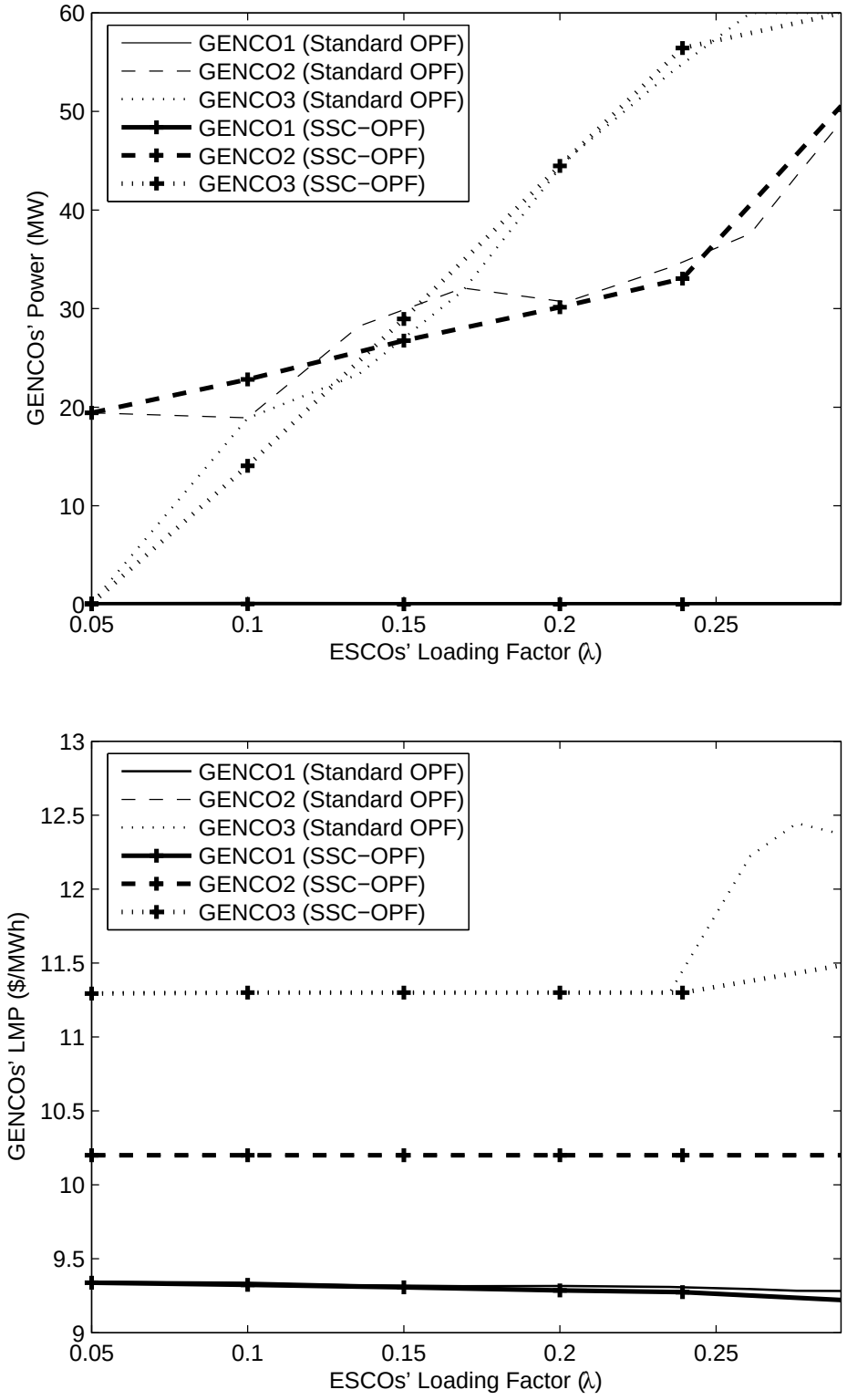

Figure 3.7: GENCOs' supplied power and LMPs with respect to loading levels for the IEEE 14-bus system with contingencies.

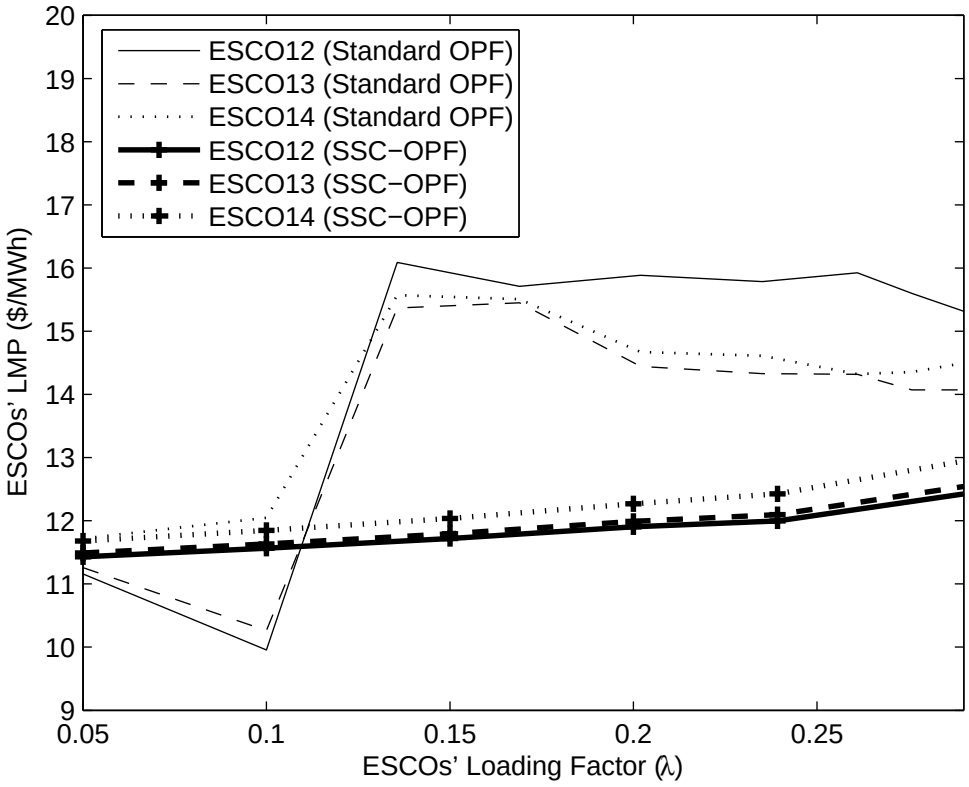

Figure 3.8: ESCOs' LMPs with respect to loading levels for the IEEE 14-bus system with contingencies.

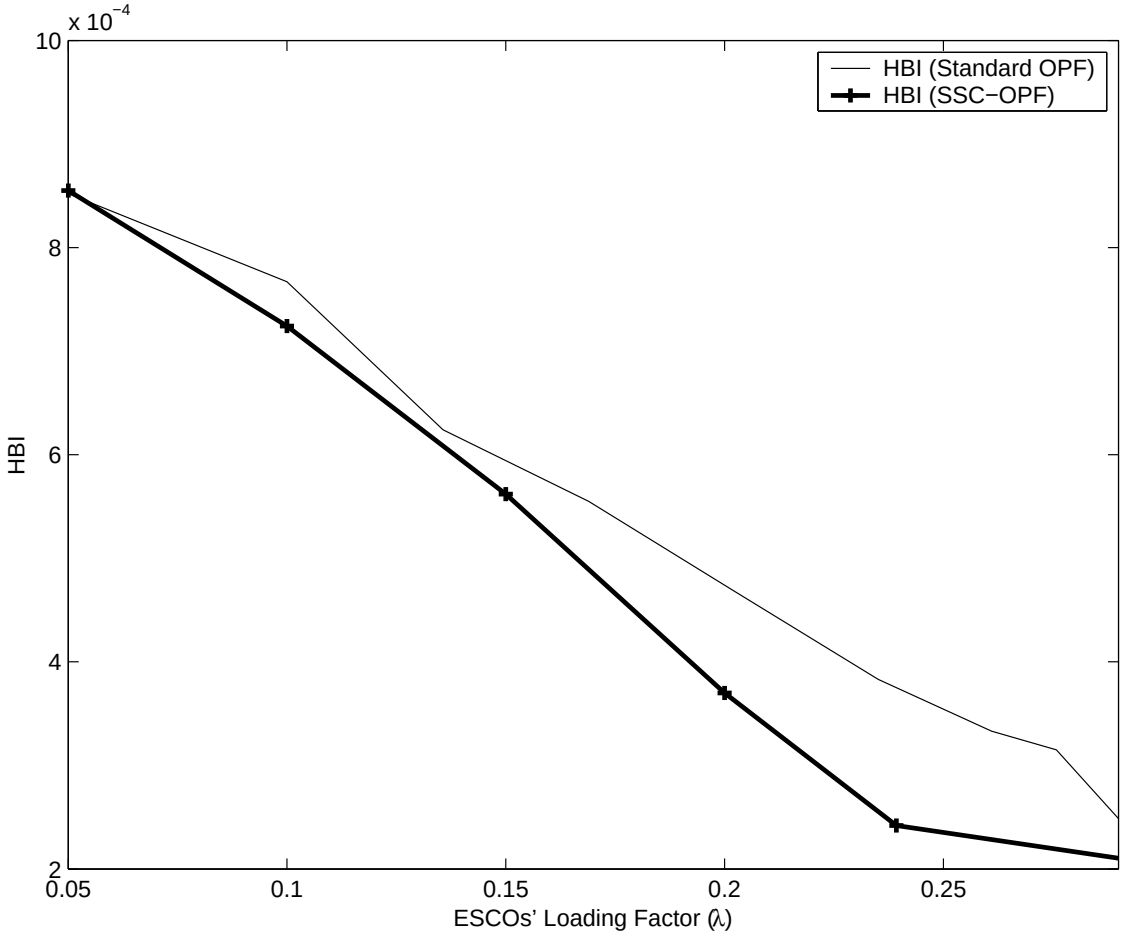

Figure 3.9: HBI results obtained with the standard OPF and the SSC-OPF for the IEEE 14-bus system with contingencies.

for the standard OPF than those obtained with the SSC-OPF, since the system is more congested in (2.10) than in (3.1) due to the different constraints used in these OPFs to represent system security. Similar results are obtained for the ESCOs' LMPs, as shown in Figure 3.8. As mentioned in the base case comparison, these results clearly demonstrate the more restrictive nature of the transmitted line power constraints used in the standard OPF, as opposed to the $\sigma_{min}(J_m)$ constraint used in the proposed SSC-OPF. Notice that both solutions are very similar from the stability perspective as demonstrated by the $\sigma_{min}(J_m)$ plots depicted in Figure 3.9.

3.3.2 VSC-OPF vs. SSC-OPF

3-Bus Test System

Figure 3.10 plots the HBI stability index (2.9) and the voltage stability index $\sigma_{min}(J_{pf})$ in (2.11) as the ESCO's demand power increases from its nominal value. Both indices are calculated by assuming that the demand of the ESCO is shared by GENCO1 and GENCO2 in proportion to their inertias.

Figure 3.10 shows that there is a Hopf bifurcation point when the ESCO demand reaches 1350 MW (there is a second Hopf at about 1880 MW, but this is of no interest from the system security point of view). The voltage stability index shows that the maximum demand power of the ESCO can reach 2150 MW, if the angle stability is not considered in the analysis. With the increase of the ESCO's demand, the system presents an oscillatory instability, associated with GENCO1, which the voltage stability index cannot detect.

Figure 3.11 presents the damping ratio of the system prior to the Hopf bifurcation point of interest. A 2% damping ratio is used here as the minimum value

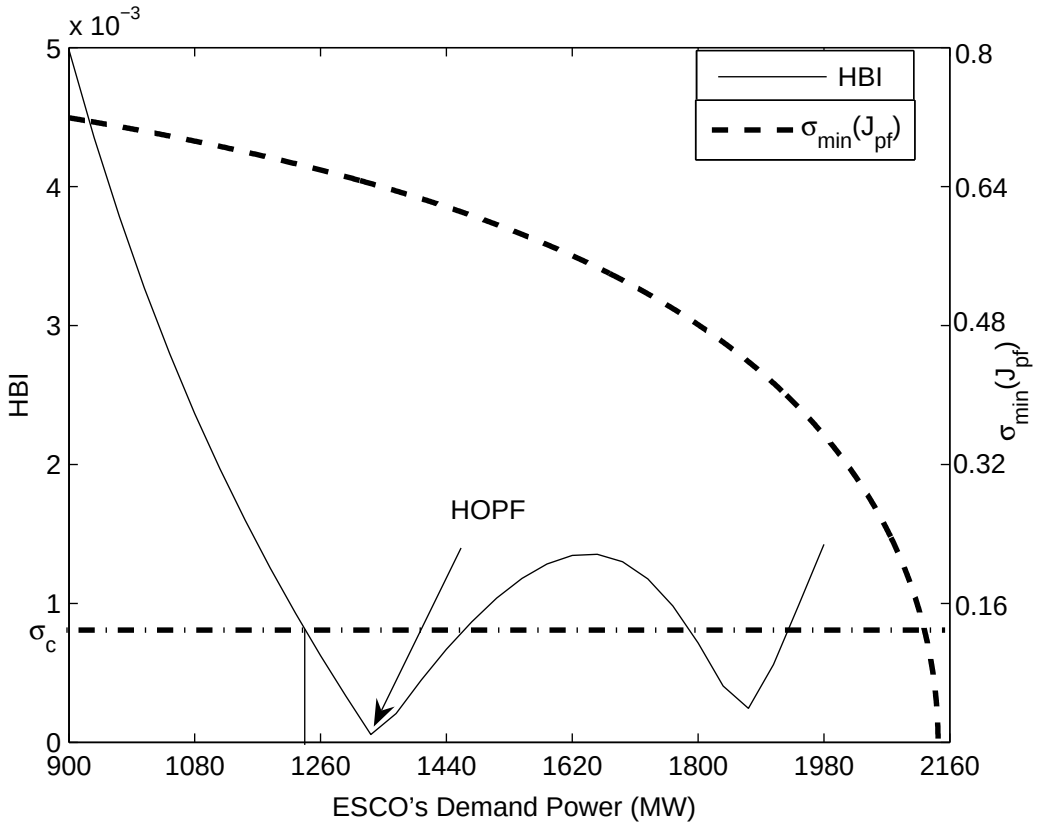

Figure 3.10: HBI and minimum singular value of power flow Jacobian versus ESCO's demand power for 3-bus test system.

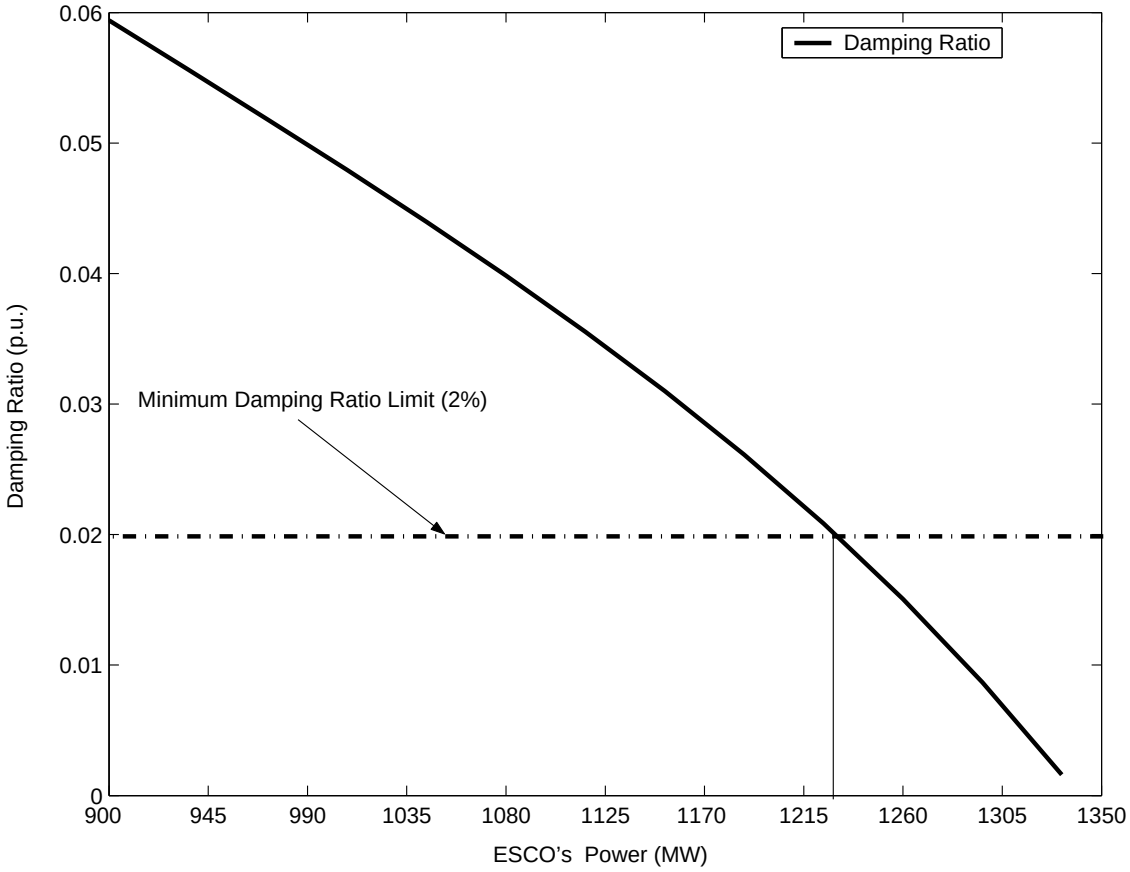

Figure 3.11: Damping ratio of the 3-bus system versus ESCO's demand power.

of the system damping required to maintain the system secure [79]. This limit is reached at an ESCO demand of 1230 MW, which corresponds, in Figure 3.10, to an HBI value of 0.0008; thus, the value of σ_c in (3.1) used here is 0.001.

The proposed SSC-OPF and the VSC-OPF are applied to the test system as the demand of the ESCO increases from 1000 to 1700 MW, which is the margin for which a solution to SSC-OPF exists for the chosen value of σ_c. Figure 3.12 displays the power supplied by GENCO1 and GENCO2 for both OPF problems. It is evident that, for the VSC-OPF, the supplied powers by GENCO1 and GENCO2 increase smoothly as the ESCO's demand increases. When the ESCO's demand approaches 1600 MW, the solutions to the VSC-OPF correspond to unstable system conditions (the system eigenvalues are on the right-half plane). This is not the case for the solutions obtained with the SSC-OPF; the solutions in this case are guaranteed to be stable due to the HBI constraint. Notice that as the ESCO's demand increases, the GENCO2's supplied power increases more rapidly than the GENCO1's power, which is expected, since GENCO1 yields oscillatory instabilities.

The LMPs of GENCO1 and GENCO2 are presented for both OPF problems, (2.11) and (3.1), in Figure 3.12. It is clear that that the LMPs of GENCOS1 or GENCOS2 are not affected by increasing the ESCO's demand for the VSC-OPF, since the system constraints are not active (the system is not congested). The GENCO2's LMP is higher than its bid, i.e. is paid more for its power, which makes sense, since GENCO1 is the reason for the system's stability problems. The ESCO's LMP is depicted in Figure 3.13 for both OPF problems; notice that the LMP in this case is not significantly affected by the stability constraint, since the load is not the reason for the stability problem.

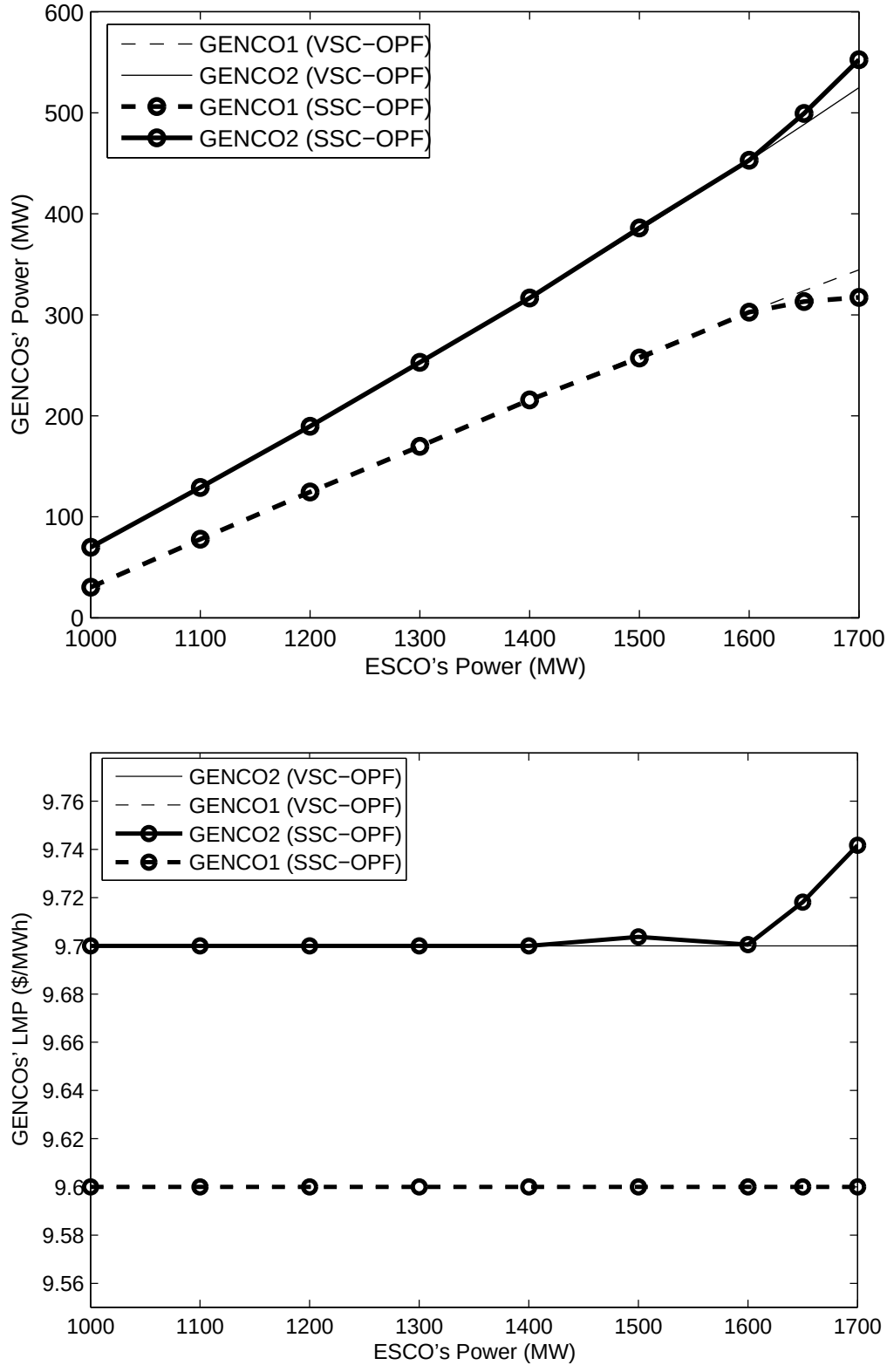

Figure 3.12: GENCOs' supplied power and LMPs with respect to ESCO's total demand power for 3-bus system.

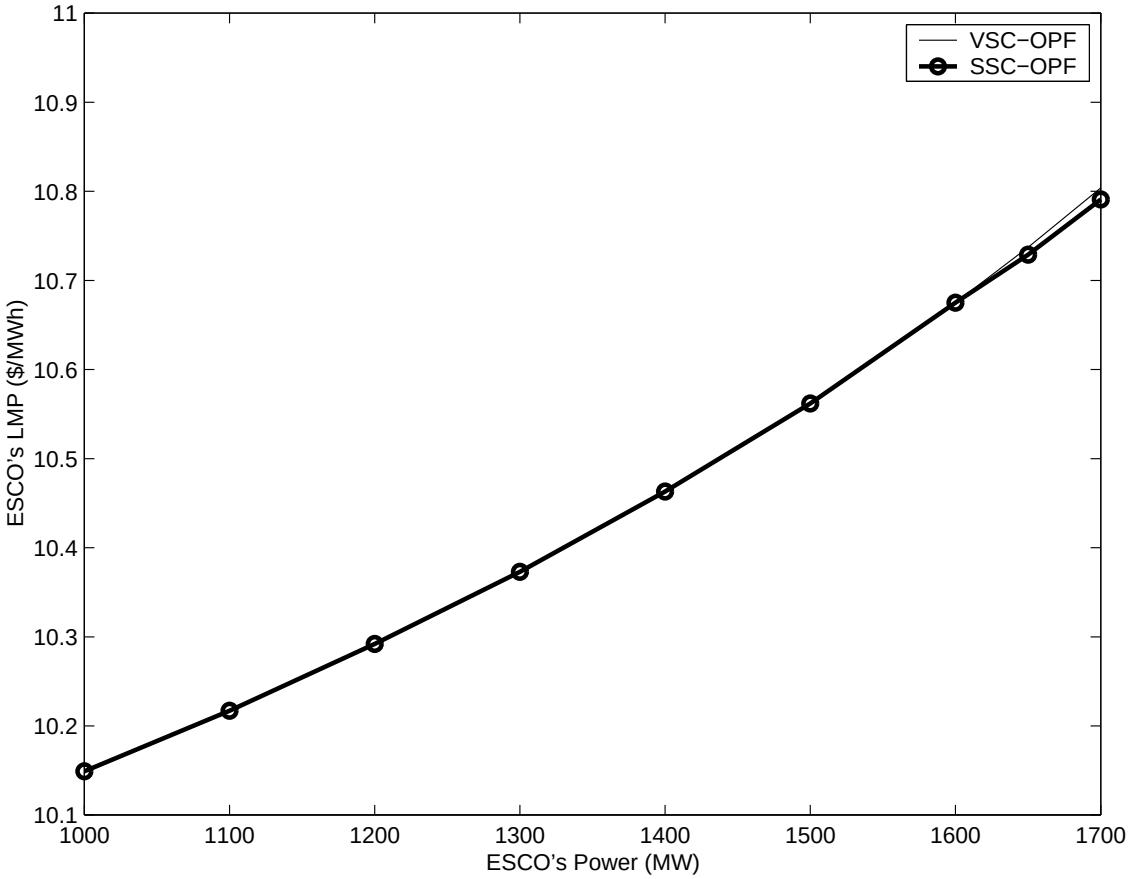

Figure 3.13: ESCO's LMP for 3-bus system.

IEEE 14-Bus System

From Figures. 3.2 and 3.3, it is evident that the range of load variations is significantly smaller in the case of contingencies; therefore, to better compare and analyze results using a wider range of load variation without loss of generality, the stability constraints in the VSC-OPF and SSC-OPF are those without contingencies. Thus, the proposed SSC-OPF is applied to the test system as the loading factor is increased from 0.05 to 0.45 p.u., which is the margin for which a solution to (3.1) exists for the chosen value of $\sigma_c = 0.0002$, to simulate various operating conditions, thus depicting the effect of different stress levels on the proposed technique. The VSC-OPF, on the other hand, is applied to the test system as the loading factor increases from 0.05 to 0.65 p.u. for a $\sigma_{c_{pf}} = 0.1$, corresponding to a load level that is 95% of the value of the maximum loading factor for the system without contingencies (this is the recommended margin by WECC). For both VSC-OPF and SSC-OPF problems, the bus voltage limits are 0.9 p.u and 1.1 p.u.

Figure 3.14 presents the power supplied by the GENCOs for both the OPF problems. For the VSC-OPF, the powers supplied by the GENCOs increase smoothly as the ESCOs' demand increases. When the loading factor exceeds 0.45 p.u., the solutions to (2.11) are unstable (a complex pair of system eigenvalues are on the right-half plane). This is not the case for the solutions obtained with the proposed SSC-OPF (3.1); the solutions in this case are guaranteed to be stable due to the HBI constraint. As the loading factor increases, the GENCO2 and GENCO3 supplied powers increase more rapidly than the power of GENCO1, which is to be expected, since GENCO1 is directly associated with the oscillatory instabilities.

The LMPs of GENCOs are also shown for both OPF problems (2.11) and (3.1) in Figure 3.14. Observe, that the LMPs of GENCOs increase smoothly as the loading

factor increases, since the system's constraints become active as the demand grows (the system becomes congested). Notice that the GENCO2 and GENCO3 LMPs are higher than their bids in the case of the proposed SSC-OPF when the system reaches its HBI limit, i.e. they are paid more for their power, which is not the case for GENCO1; this is to be expected, since GENCO1 is the principal reason for the system's oscillatory problems.

The ESCOs' powers and LMPs for "remote" loads, i.e. ESCO12, 13 and 14, are depicted in Figure 3.15 for the two OPF problems; as expected, the LMPs increase as the system become congested. Notice that for the VSC-OPF, the power of the most remote load begins to decrease as the system approaches its maximum loading conditions, since the voltage of this bus approaches its minimum limit. The "oscillations" in the power levels and the LMPs in these graphs as the loading factor increases, which are also observed in Figures 3.14 and 3.15, are due to different constraints becoming active as the load is increased.

Table 3.2 summarizes the solution for the VSC-OPF and SSC-OPF at ESCOs' loading factor $\lambda = 0.45$, which corresponds to the maximum loading level for which there is a solution to the SSC-OPF problem. The bus voltages and the active and reactive powers for all the GENCOs and ESCOs are shown as well as the values of the indices $\sigma_{min}(J_{pf})$ and $\sigma_{min}(J_m)$. It is obvious that the SSC-OPF is more "restrictive" than the VSC-OPF, i.e. the total supply and demand powers are smaller, as expected, since the SSC-OPF stability constraint properly reflects the system stability, which is not the case for the VSC-OPF. Observe that the system solution for the latter corresponds to an unstable condition.

Table 3.2: Solution details for VSC-OPF and SSC-OPF at $\lambda = 0.45$ p.u. for the IEEE 14-bus system.

Bus	VSC-OPF			SSC-OPF		
	V (p.u.)	P (MW)	Q_G (MVAr)	V (p.u.)	P (MW)	Q_G (MVAr)
GENCO1	1.1	59.11	70.41	1.1	45.148	55
GENCO2	1.051	54.94	50	1.058	60	50
GENCO3	0.995	60	40	1.006	60	40
ESCO2	1.051	13.671		1.058	13.671	
ESCO3	0.995	59.355		1.006	59.355	
ESCO4	0.977	30.114		0.99	30.114	
ESCO5	0.987	4.788		0.998	4.788	
ESCO6	0.996	7.056	24	1.02	1.877	24
ESCO9	0.951	18.585		0.97	18.585	
ESCO10	0.945	5.67		0.967	3.8836	
ESCO11	0.964	2.203		0.987	2.205	
ESCO12	0.968	3.843		0.992	3.843	
ESCO13	0.978	8.505		0.981	8.505	
ESCO14	0.92	9.387		0.943	9.387	
Bus 7	0.982			0.999		
Bus 8	1.023		24	1.04		24
$\sigma_{min}(J_m)$	0.000275 (unstable)			0.0002 (stable)		
$\sigma_{min}(J_{PF})$	0.1971			0.2632		

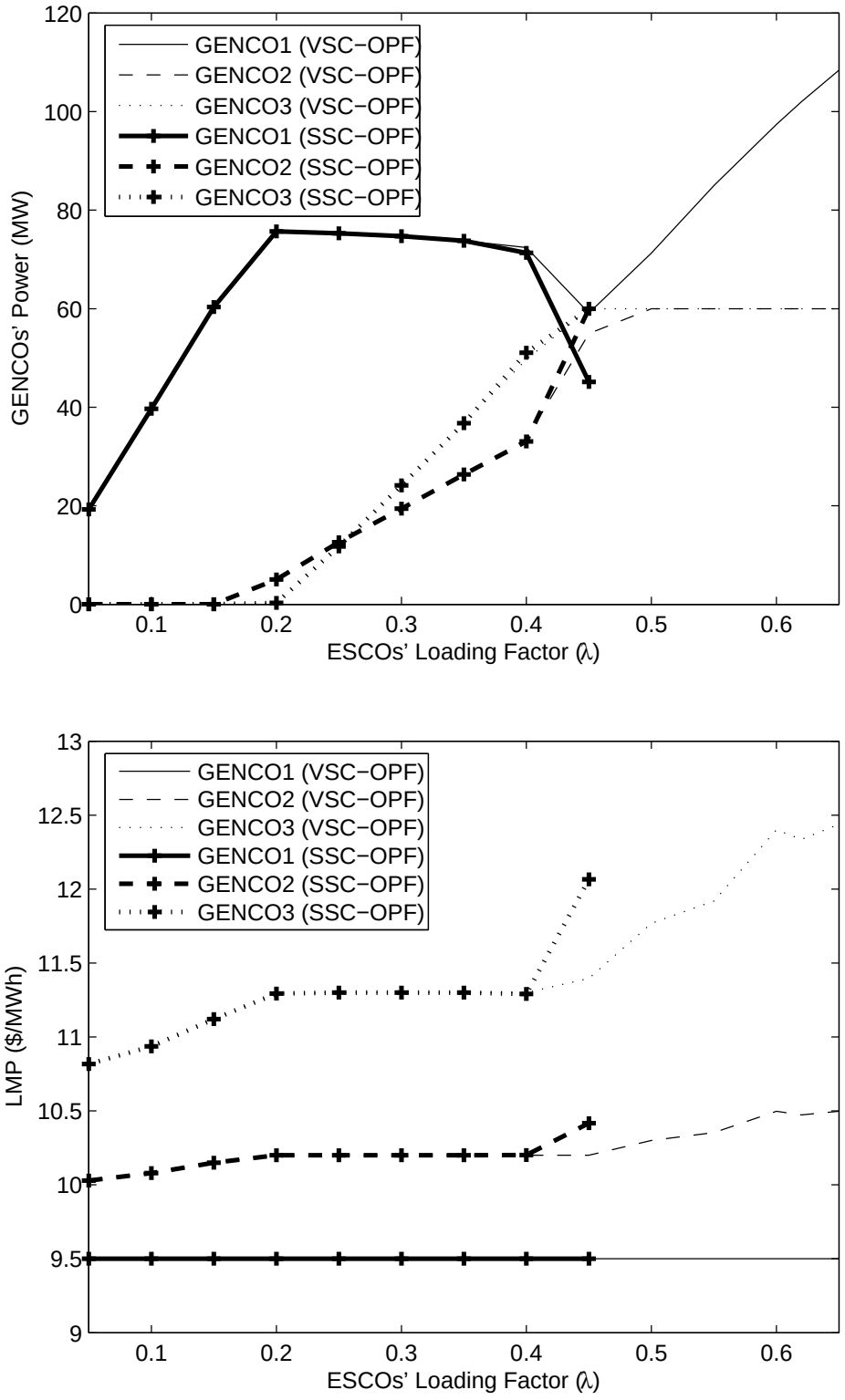

Figure 3.14: GENCOs' supplied power and LMPs with respect to the loading factor for the IEEE 14-bus system.

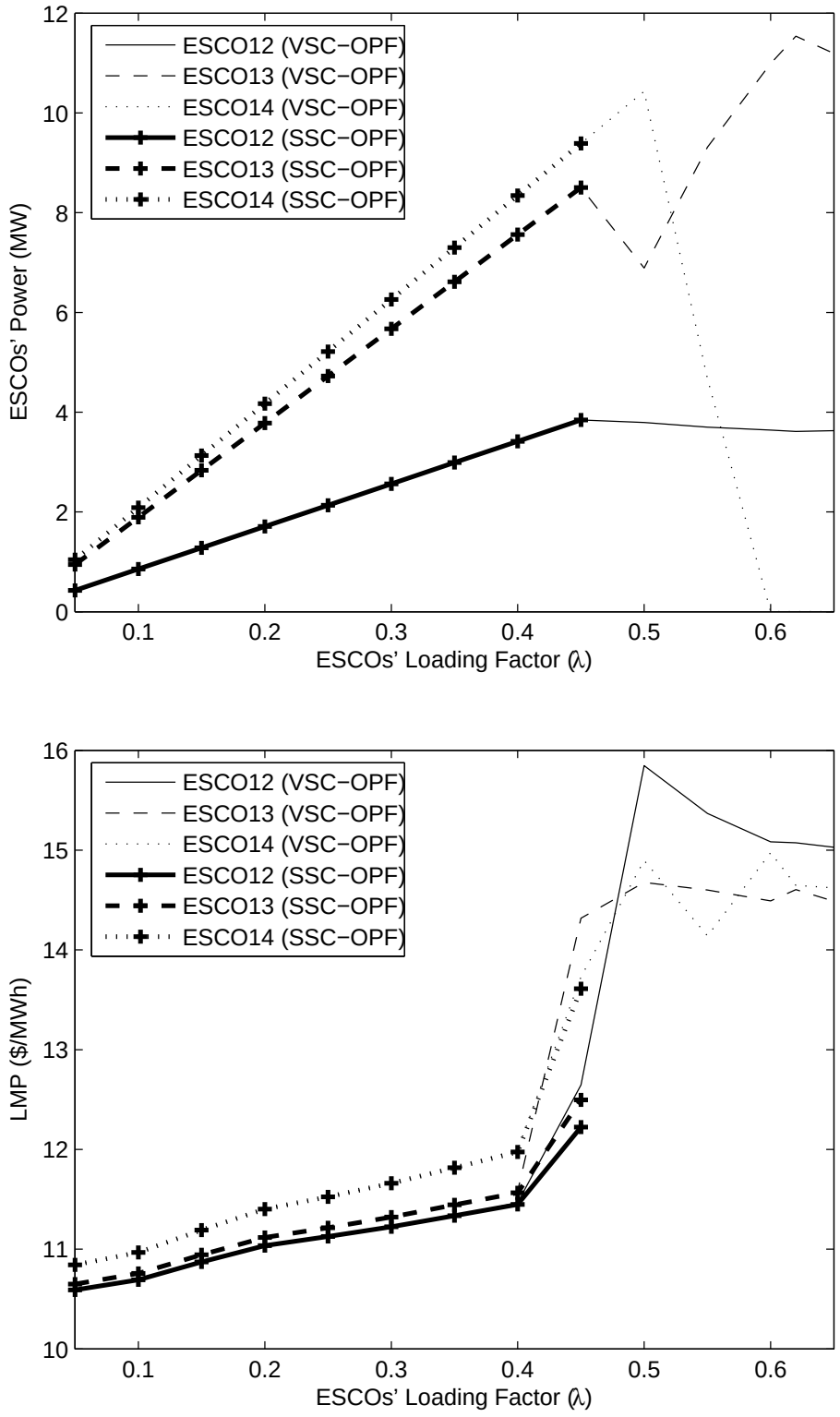

Figure 3.15: ESCOs' power and LMPs with respect to the loading factor for the IEEE 14-bus system.

3.4 Summary

Following the review and discussion of the theoretical background, an innovative approach is introduced in the form of a new SSC-OPF that predicts or detects both voltage and oscillatory instabilities. The ad-hoc approximations used to solve the SSC-OPF are also illustrated.

The proposed SSC-OPF is applied on two test systems of increasing size and complexity with and without contingencies. This illustrates the effect of the novel stability constrained OPF technique on the market signals and prices, compared to that of the standard OPF and a VSC-OPF. As clearly demonstrated, the novel SSC-OPF properly detects voltage and oscillatory instabilities, and guarantees a stable operation for the system with adequate LMPs and power signals.

Chapter 4

Pricing of Dynamic Services

4.1 Introduction

Chapter 3 introduces the new SSC-OPF and its solution procedure and application to different test systems, and it also provides comparisons among the novel SSC-OPF and a standard OPF and VSC-OPF. This comparison between the SSC-OPF and VSC-OPF is used in this chapter when power system controllers, i.e. PSS, SVC, and TCSC, are included in the power system to propose a new methodology to price the dynamic services provided by these controllers. Steady-state and dynamic models of these controllers are used in the VSC-OPF and SSC-OPF, respectively; this allows to compare the effect of these models on electricity market signals, demonstrating the importance of using dynamic models for these controllers.

4.2 Pricing Technique

PSS and FACTS controllers are well identified solutions for oscillatory instabilities in a power system. FACTS controllers such as SVC and TCSC are more expensive solutions for these types of problems, as illustrated in the approximate cost comparison of these controllers in Table 4.1 [9, 80, 81]. Since the costs associated with FACTS controllers are high, pricing methodologies for the dynamic stability services provided by these controllers should be developed.

Table 4.1: Cost comparison of the PSS and FACTS controllers.

Controller	Cost (US)
PSS	\$30,000
SVC	\$40/kvar
TCSC	\$40/kvar

The pricing techniques proposed in this thesis depends on a comparison of the market signals with and without the system controllers, based on the proposed SSC-OPF. The proposed pricing methods are based on a comparison of congestion costs and social welfare.

The congestion costs are defined as:

$$CC = \sum LMP_i P_{d_i} - \sum LMP_j P_{s_j} \tag{4.1}$$

where CC is the congestion cost in \$/h, LMP is the locational marginal price for demand bus i or supply bus j in \$/MWh, and P_{d_i} and P_{s_j} are the demand and supply power in MW. Thus, any gain in CC, due to the extension of the DLM

associated with the addition of the controllers, is considered to be a profit which cannot exist without these controllers. Consequently, the difference between the CC with and without the system controllers is used to price the dynamic services of the system controllers as follows:

$$CP = CC|_{wc} - CC|_{woc} \tag{4.2}$$

where CP is the controller pricing in \$/h, and $CC|_{wc}$ and $CC|_{woc}$ are the congestion costs with and without the controller in service, respectively. The value of the CP is not considerable if the system is not heavily loaded, i.e. for a large DLM, but as the system loading approaches its DLM, these costs increase significantly.

The social welfare S_b in (2.10) could also be used as a tool for pricing the dynamic services provided by the controllers. Although S_b can be viewed as a "theoretical" measure for the controllers' benefits, this value in principal can be used to determine the "worth" of the controller. The social welfare pricing SP can hence be defined as:

$$SP = SP|_{wc} - SP|_{woc} \tag{4.3}$$

where SP is the social welfare controller pricing in \$/h, and $SP|_{wc}$ and $SP|_{woc}$ are the social welfare with and without the controller in service, respectively. Similar to the CP, the value of the SP is not considerable if the system is not heavily loaded.

This pricing techniques are applied in the following sections to the PSS for the 3-bus system and the IEEE 14-bus system, and to FACTS controllers, SVC and TCSC, for the IEEE 14-bus system.

4.3 Pricing PSS Services

In this section, the pricing methodology is applied to PSS controller to predict the benefits of the controller for the system. Although the cost of PSS controller is relatively cheap, its benefits for system stability should be "valued" to help convince generating facilities to properly use and tune this controller, since these are no longer under the control of the system operators.

When a PSS is added to the AVR of GENCO1 in the 3-bus test system, the Hopf bifurcation point is removed. Consequently, when the SSC-OPF is applied to the system with the PSS, the results are similar to those of the VSC-OPF. This is expected, since the oscillatory instabilities are removed by the introduction of the PSS, and thus, both OPF problems are basically the same, i.e. constrained by the system voltage stability limits and other constraints.

As illustrated in Figures 4.1 and 4.2, the inclusion of the PSS benefits the system congestion costs and social welfare. In terms of percentage of the CP and SP values with respect to the GENCO1 power payment, the value is not significant, especially if it is compared to the benefits for the entire system, which are quite significant, since a proper damping ratio and much larger transaction levels are attained by the introduction of the PSS.

The IEEE 14-bus test system is also analyzed with the inclusion of PSS and FACTS controllers. A SVC, a TCSC, and a PSS are added to the system, as shown in Figure 4.3, to study their effect on system stability and LMPs. The PSS and TCSC are added to remove oscillatory instabilities, whereas the SVC is added to improve the system voltage stability. The static and dynamic data of these controllers are provided in Appendix B.

Figure 4.4 reflects the effect of the PSS on the HBI of the system, assuming the

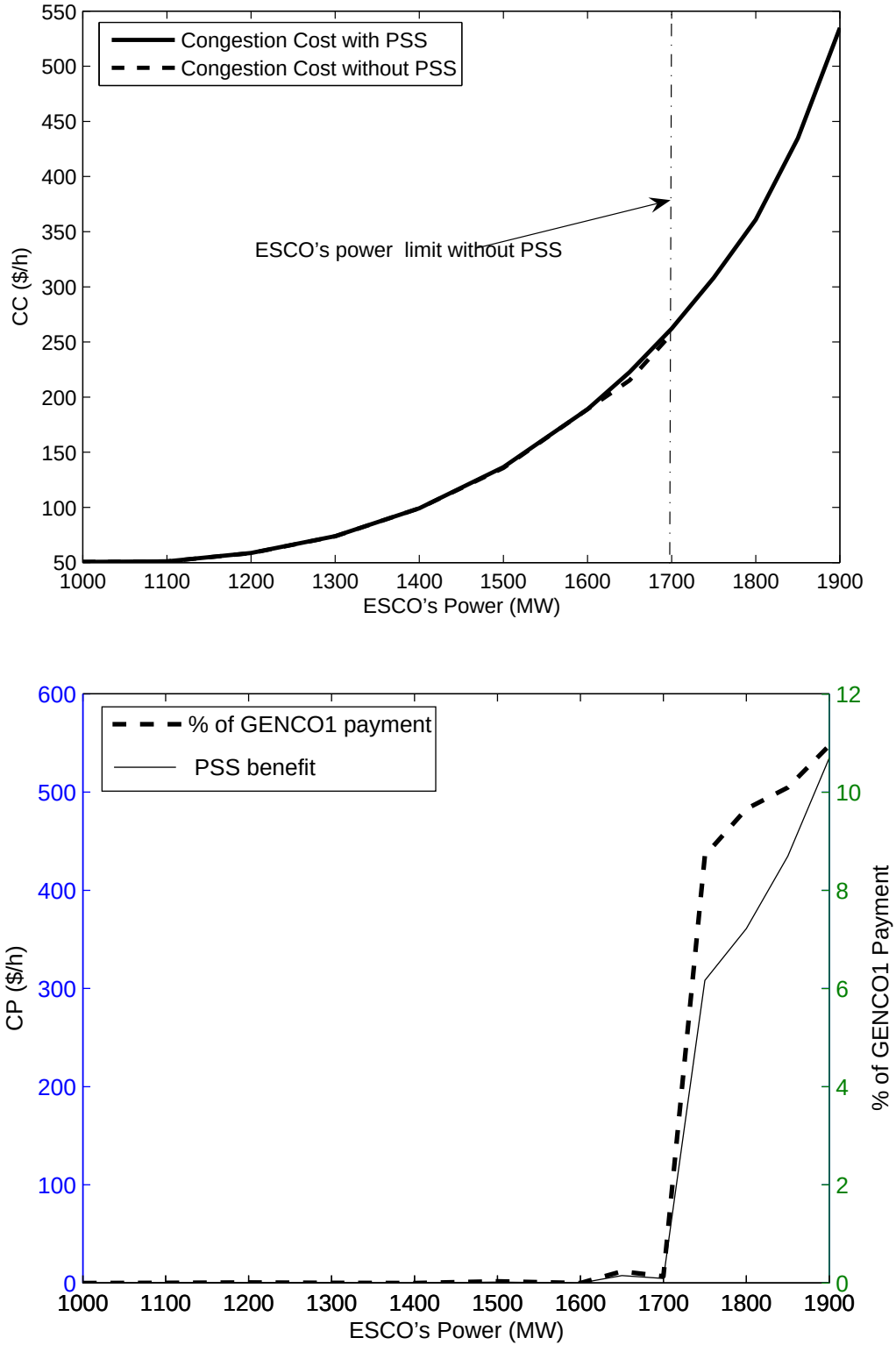

Figure 4.1: *CC* and benefits with and without the PSS in the 3-bus test system.

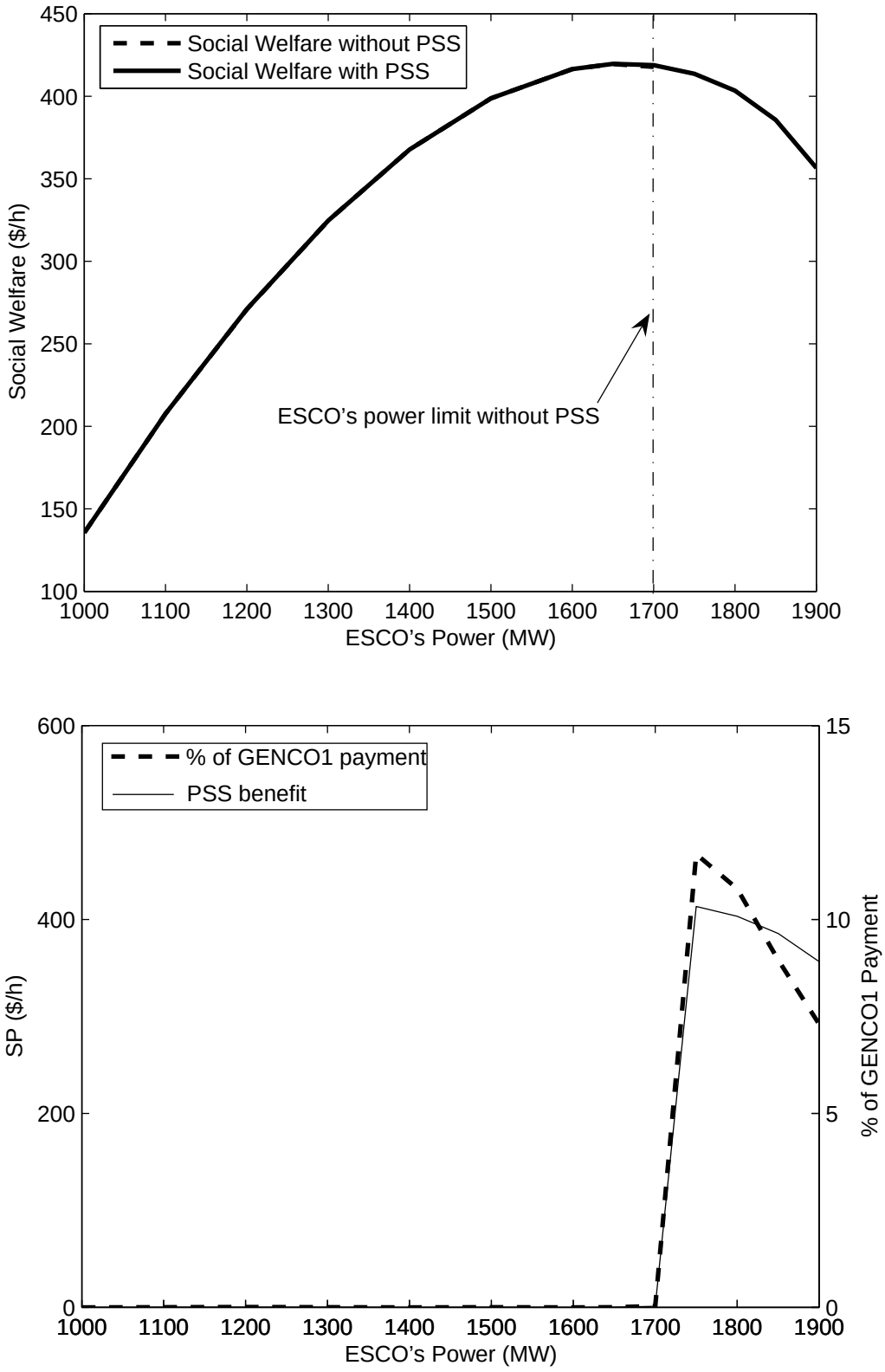

Figure 4.2: S_b and benefits using social welfare with and without the PSS in the 3-bus test system.

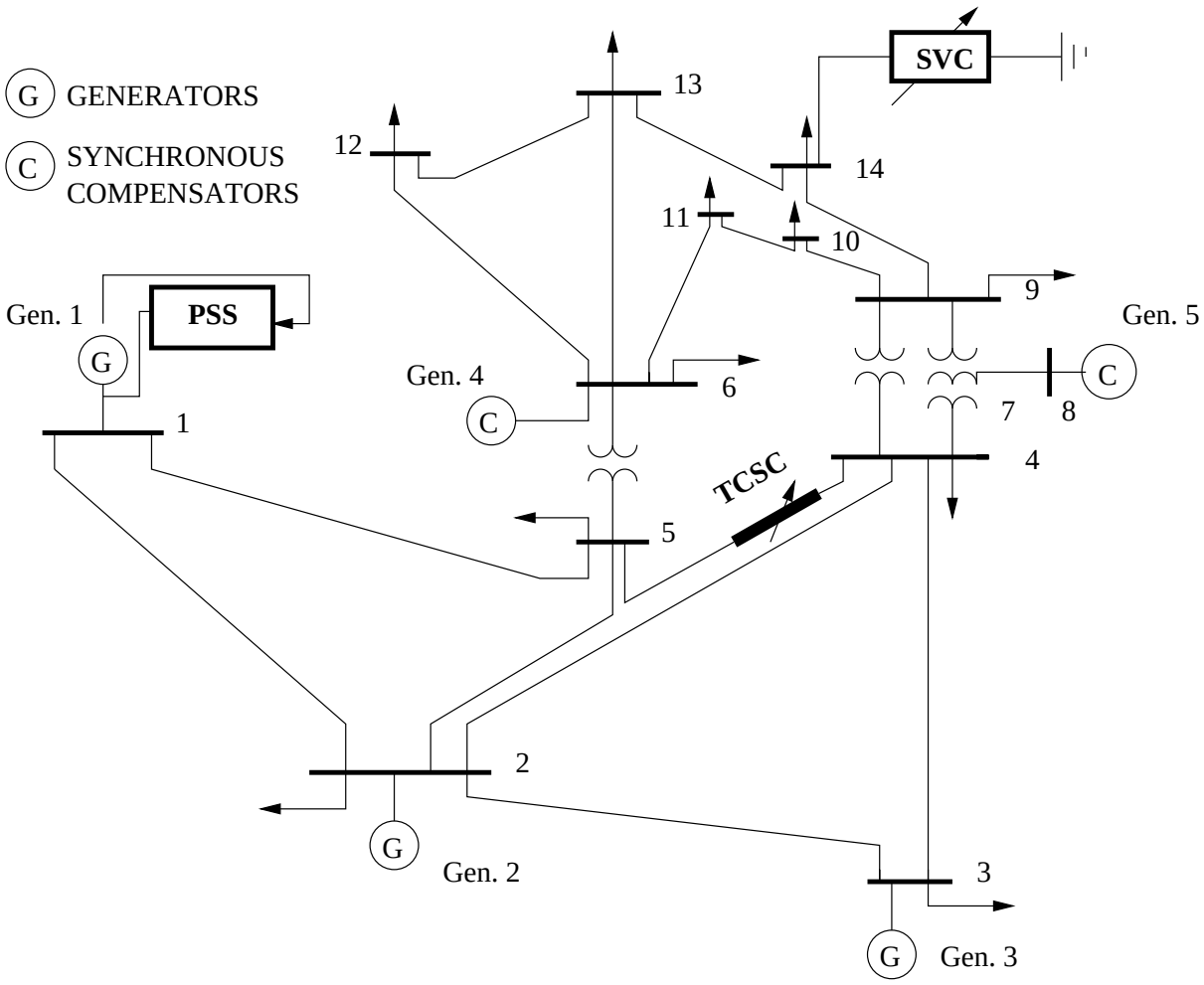

Figure 4.3: IEEE 14-bus test system with the PSS, SVC and TCSC.

load increase in (3.23) with $P_d = P_{L_o}$ (the OPF techniques are not applied in this case). The PSS is installed on GENCO1, since this is the source of oscillatory instability, completely removing the Hopf bifurcation from the system. Consequently, when the SSC-OPF is applied to the test system with the PSS, the results are similar to those obtained with the VSC-OPF. This is expected, since both OPF problems are the same, i.e. mainly constrained by the system voltage stability limits and current, and voltage constraints.

As depicted in Figures 4.5 and 4.6, the inclusion of the PSS results in a reduction in the system congestion costs and an increase in the social welfare, as expected. The difference between the CC and S_b of the system with and without the PSS may then be used for pricing the PSS control services as proposed in (4.2) and (4.3). In terms of percentage of the PSS payment with respect to the GENCO1 payment, this payment is somewhat significant. However, when compared to the benefits for the whole system, which are quite significant, since proper damping ratios and much larger transaction levels are attained by the introduction of the PSS, these costs for the system are certainly justifiable. Notice that the benefits for the system with the PSS are negative in the region, where the system without PSS is near its stability limits; this is to be expected, since the stability constraint for the system without PSS becomes active close to the point where there is an angle stability problem, which is not the case for the system with the PSS. It should be stressed that these costs should not necessarily correspond to a payment for the services provided by the PSS, and it is only an indication of the benefits accrued by the system with this controller.

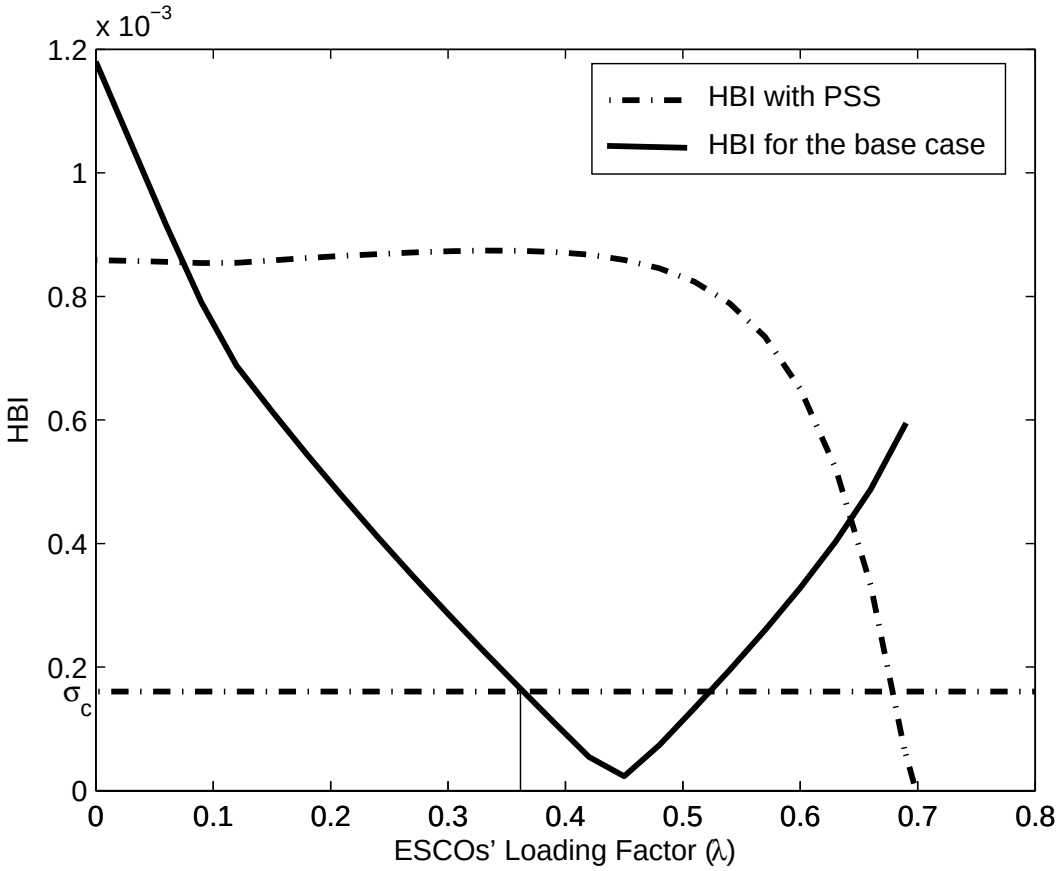

Figure 4.4: HBI with and without the PSS versus the loading factor for the IEEE 14-bus test system.

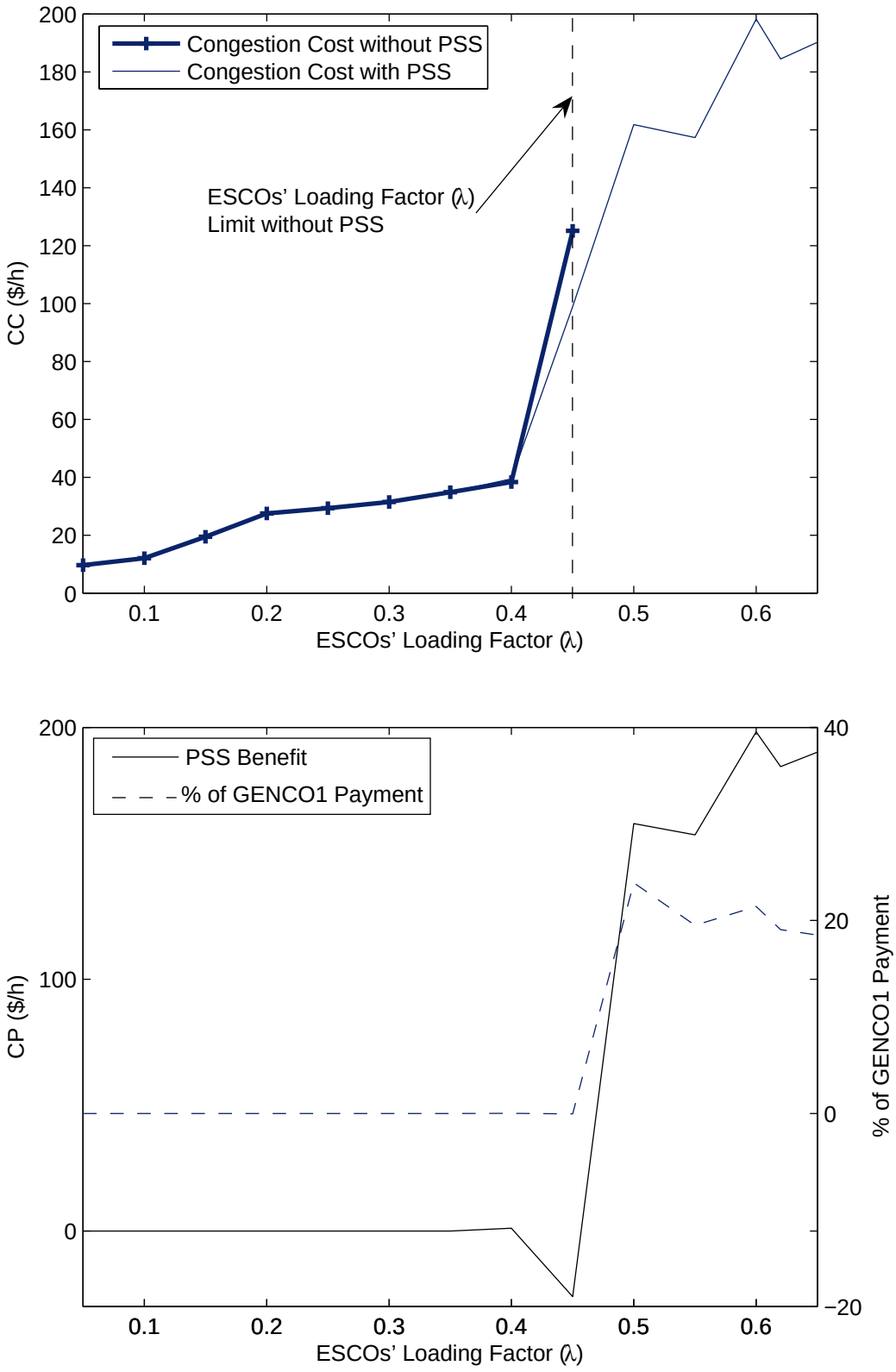

Figure 4.5: *CC* and benefits with and without the PSS for the IEEE 14-bus test system.

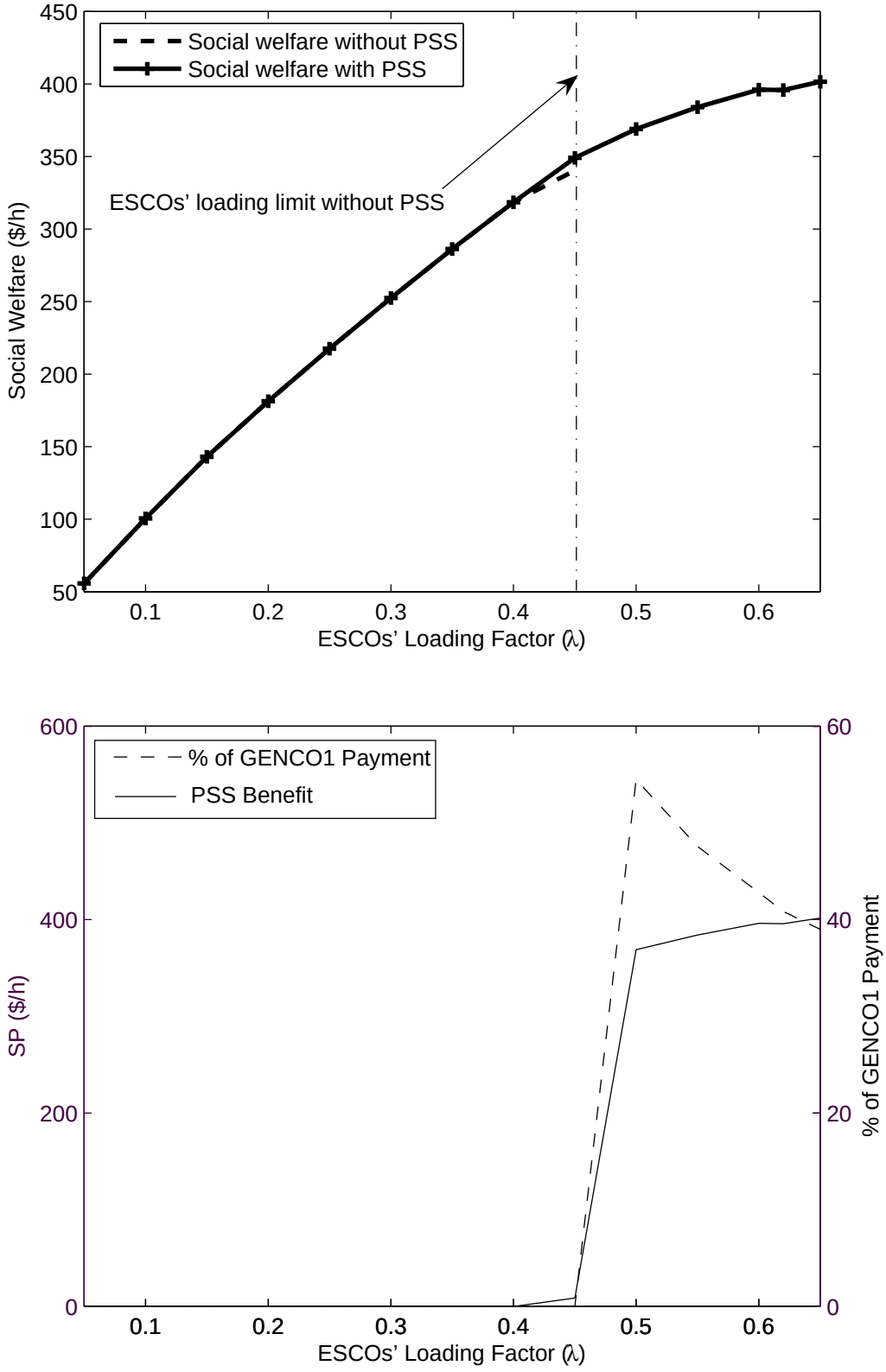

Figure 4.6: S_b and benefits with and without the PSS for the IEEE 14-bus test system.

4.4 Pricing FACTS Services

Figure 4.7 plots the effect of the SVC and TCSC controllers on the HBI for the test system, as the system load is increased according to (3.23) with $P_d = P_{L_o}$ (the OPF techniques are not applied in this case). The SVC controller moves the Hopf bifurcation point from a loading factor of 0.45 to 0.62. The TCSC controller is installed in series with the line connected between buses 4 and 5 with a 50 % compensation level, using the active power flow in this line as the input signal for the oscillation damping [34]; in this case, the Hopf bifurcation point moves from a loading factor of 0.45 to 0.6.

4.4.1 SVC Controller

The power levels and LMPs of GENCOs are shown for both OPF problems (2.11) and (3.1) with a SVC controller in Figure 4.8. In the VSC-OPF, the steady state model of the SVC controller described in [23] is used. For the SSC-OPF, the dynamic stability constraints force the LMPs of GENCO2 and GENCO3 to increase with respect to the VSC-OPF. Observe that near the Hopf bifurcation point (at $\lambda \approx 0.6$), the power levels at GENCO1 decrease, as expected, since GENCO1 is the principal contributer to the angle stability problem.

The ESCOs' LMPs are depicted in Figure 4.9 for the two OPF problems. Both the power and LMP of ESCO14 increases significantly with respect to the case without the SVC. This is due to the SVC controller, connected to this bus, which enhances the supply conditions for this load (this bus is the one that benefits the most from the installation of the controller).

Figure 4.10 represents the effect of the dynamic modelling of the SVC controller

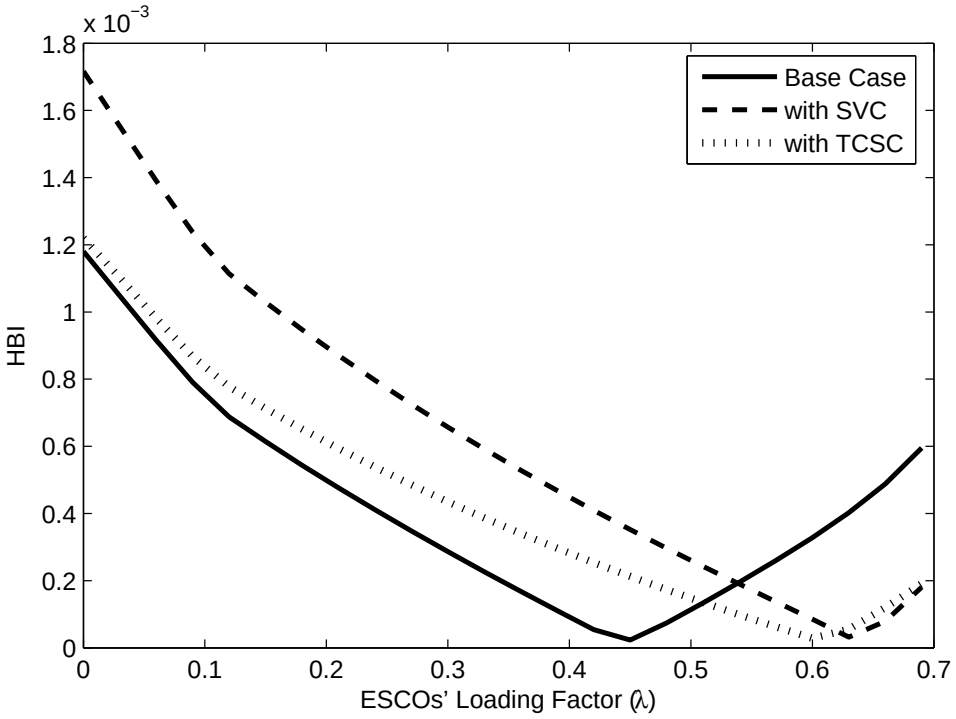

(a)

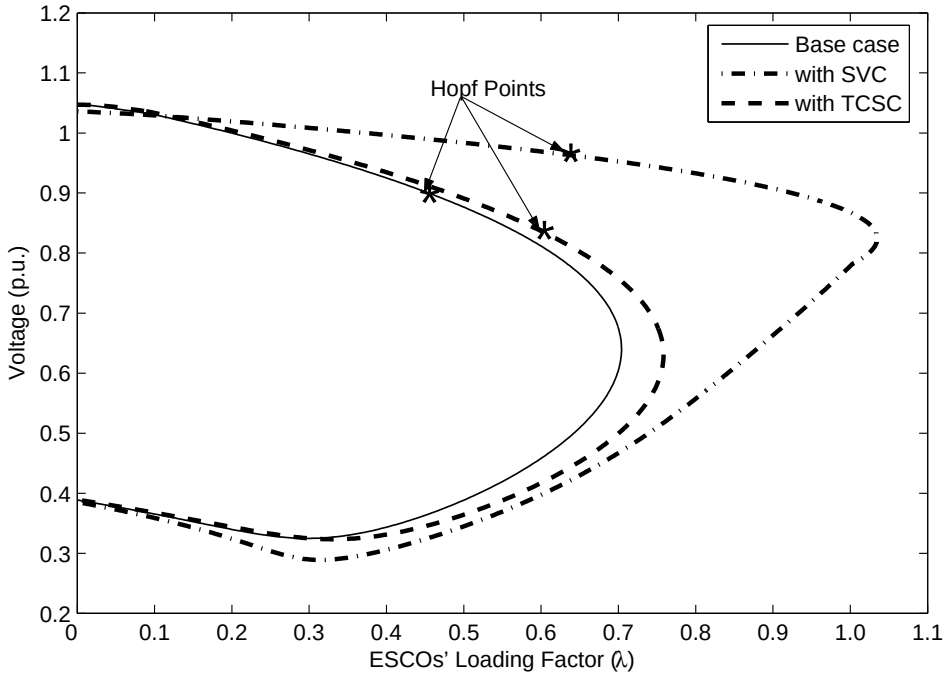

(b)

Figure 4.7: Effect of FACTS on the angle stability as the loading factor increases for the IEEE 14-bus test system: (a) HBI and (b) PV curves.

on market prices. When the results obtained with the SSC-OPF are compared with the ones obtained with the VSC-OPF, which includes the SVC steady-state model, there is a significant discrepancy between these results, especially close to the Hopf bifurcation point at $\lambda \approx 0.6$, even at "low" loading conditions. This demonstrates the importance of accounting for the FACTS controller dynamics within the market auction mechanisms.

In Figures 4.11 and 4.12, the inclusion of the SVC controller result in a positive effect on the system's CC and S_b, as expected. The difference between the CC and S_b resulting from the SSC-OPF with and without the SVC controller may then be used for pricing the SVC dynamic stability control services. Notice that at approximately the original Hopf bifurcation point ($\lambda \approx 0.4$), the introduction of the SVC does yield savings for the system, similarly to the PSS. Furthermore, with respect to the percentage of GENCOs' power payments, the SVC price is not that significant, especially if it is compared to the benefits for the whole system, since proper damping and higher transaction levels are attained by the introduction of the SVC controller.

4.4.2 TCSC Controller

The power levels and LMPs of GENCOs are depicted in Figure 4.13 for the OPF problems (2.11) and (3.1) with the addition of a TCSC controller, using the TCSC steady state model described in [23] in the VSC-OPF problem. Notice that the power levels and the LMPs of the GENCOs behave similarly, as observed in the previous examples, when the loading factor is increased, and similarly for the ESCOs' power levels and LMPs, shown in Figure 4.14.

Figure 4.15 shows the difference between the market prices obtained with and

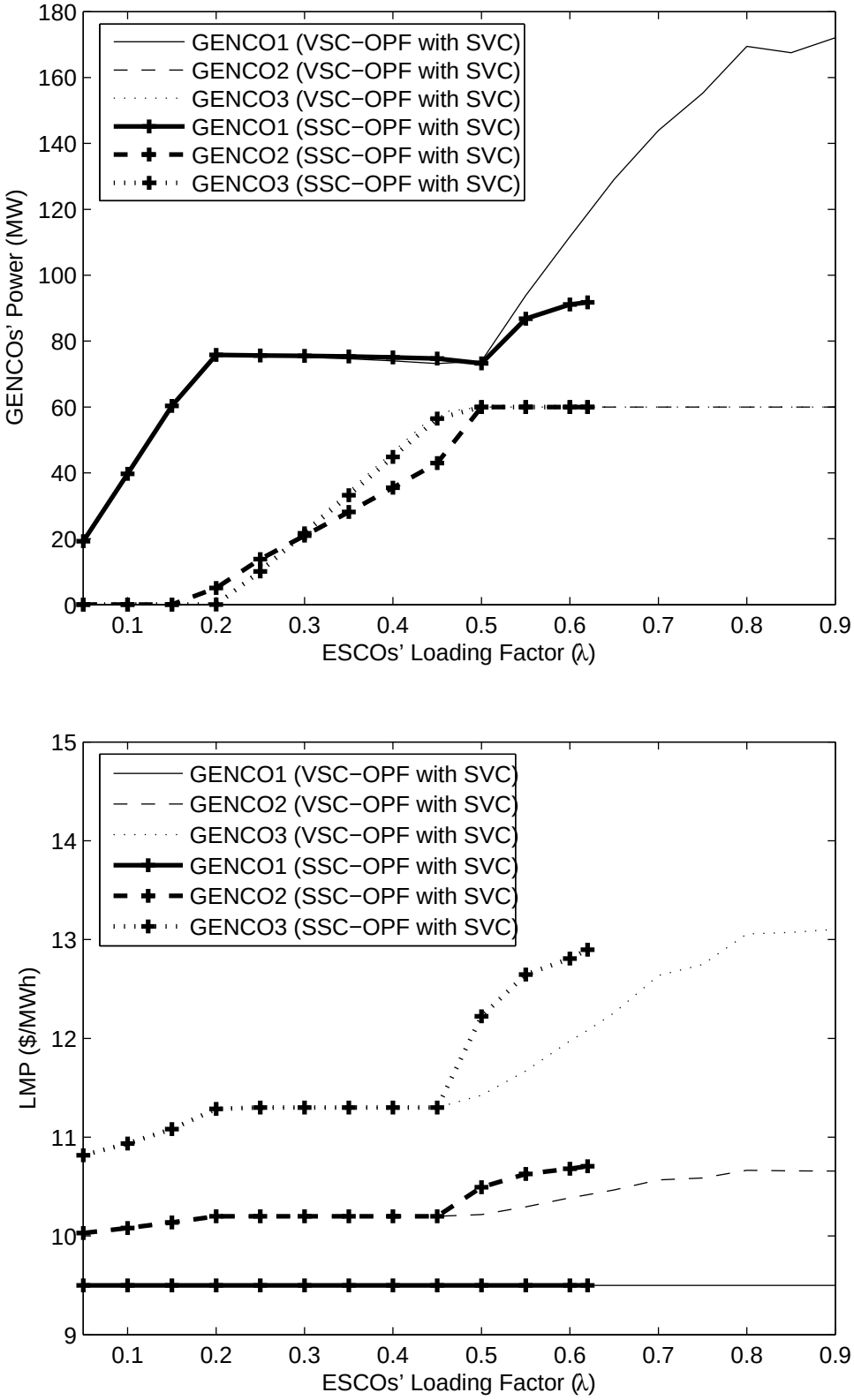

Figure 4.8: GENCOs' supplied power and LMPs with respect to the loading factor with the SVC controller in the IEEE 14-bus test system.

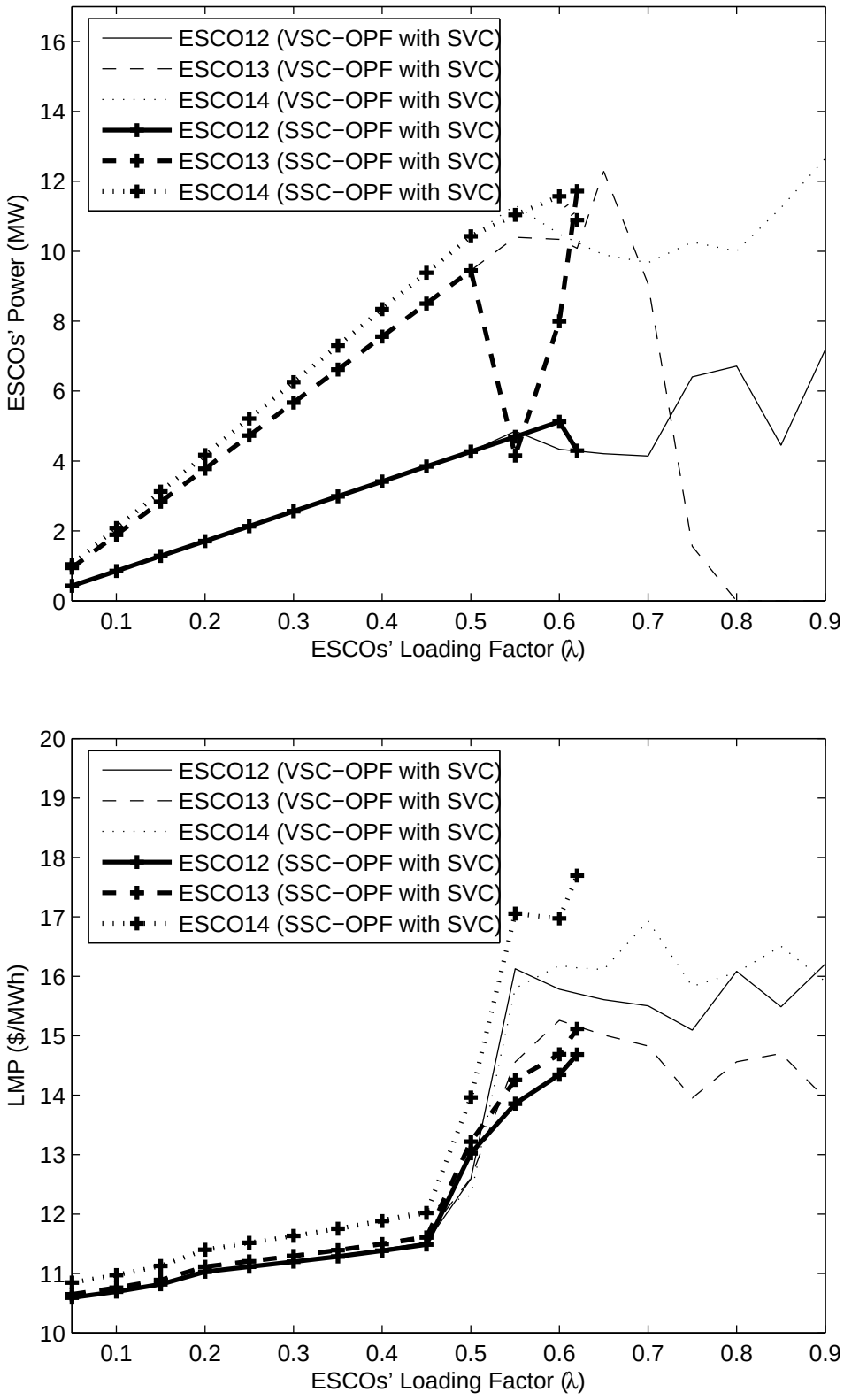

Figure 4.9: ESCOs' power and LMPs with respect to the loading factor with the SVC controller in the IEEE 14-bus test system.

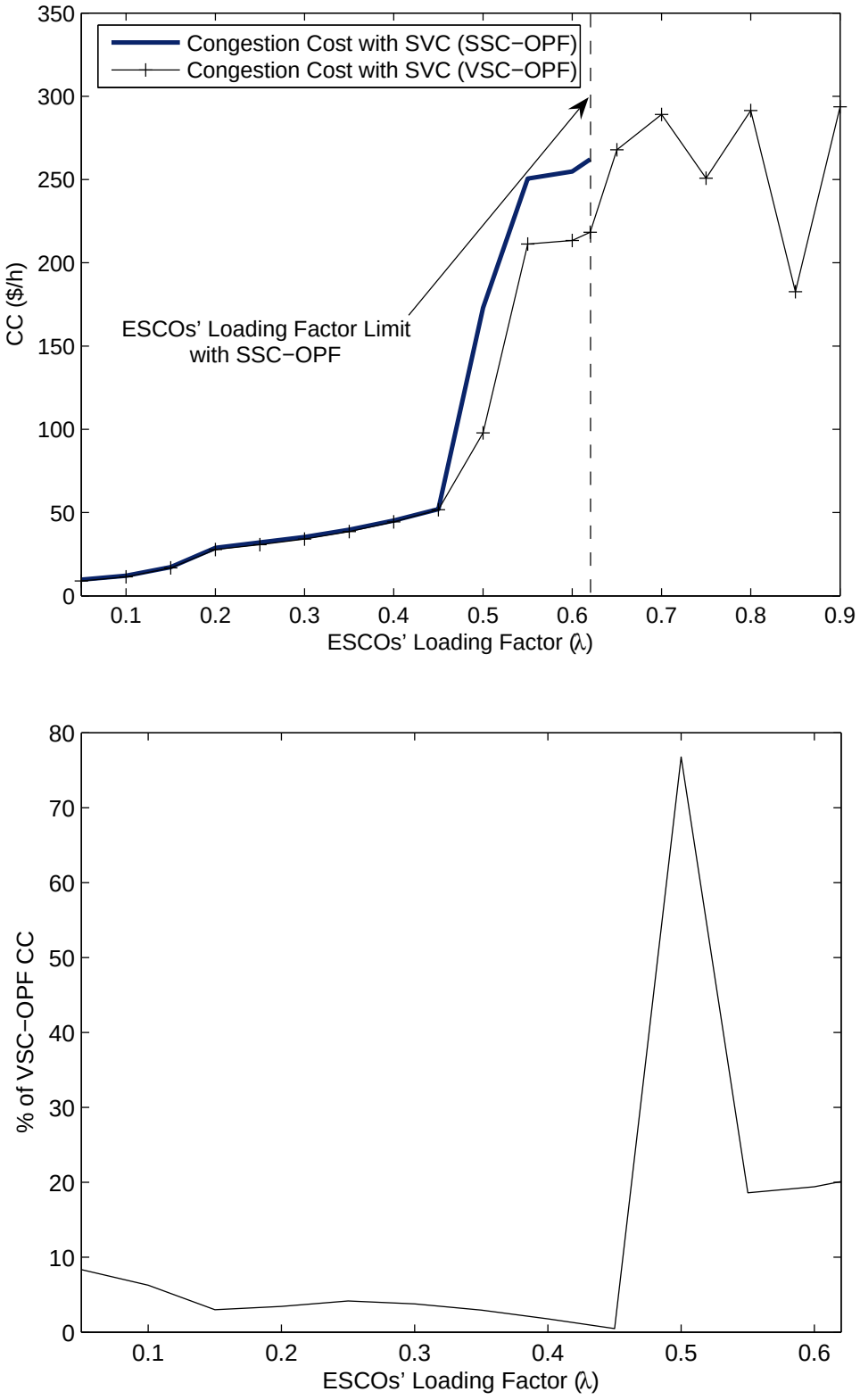

Figure 4.10: Cost analysis for the SVC dynamic model in the IEEE 14-bus test system.

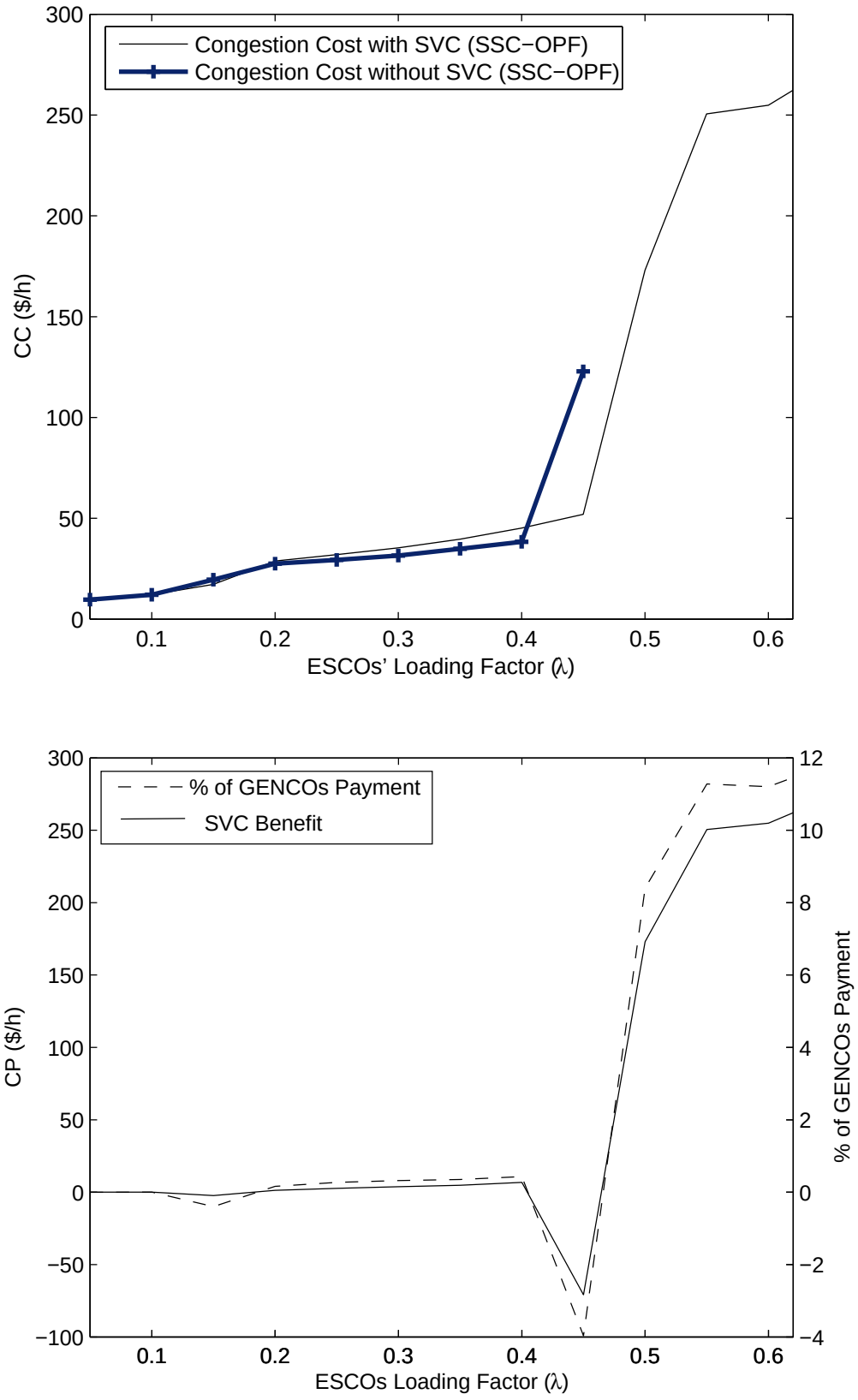

Figure 4.11: SVC benefit and pricing analysis for the IEEE 14-bus test system using congestion costs.

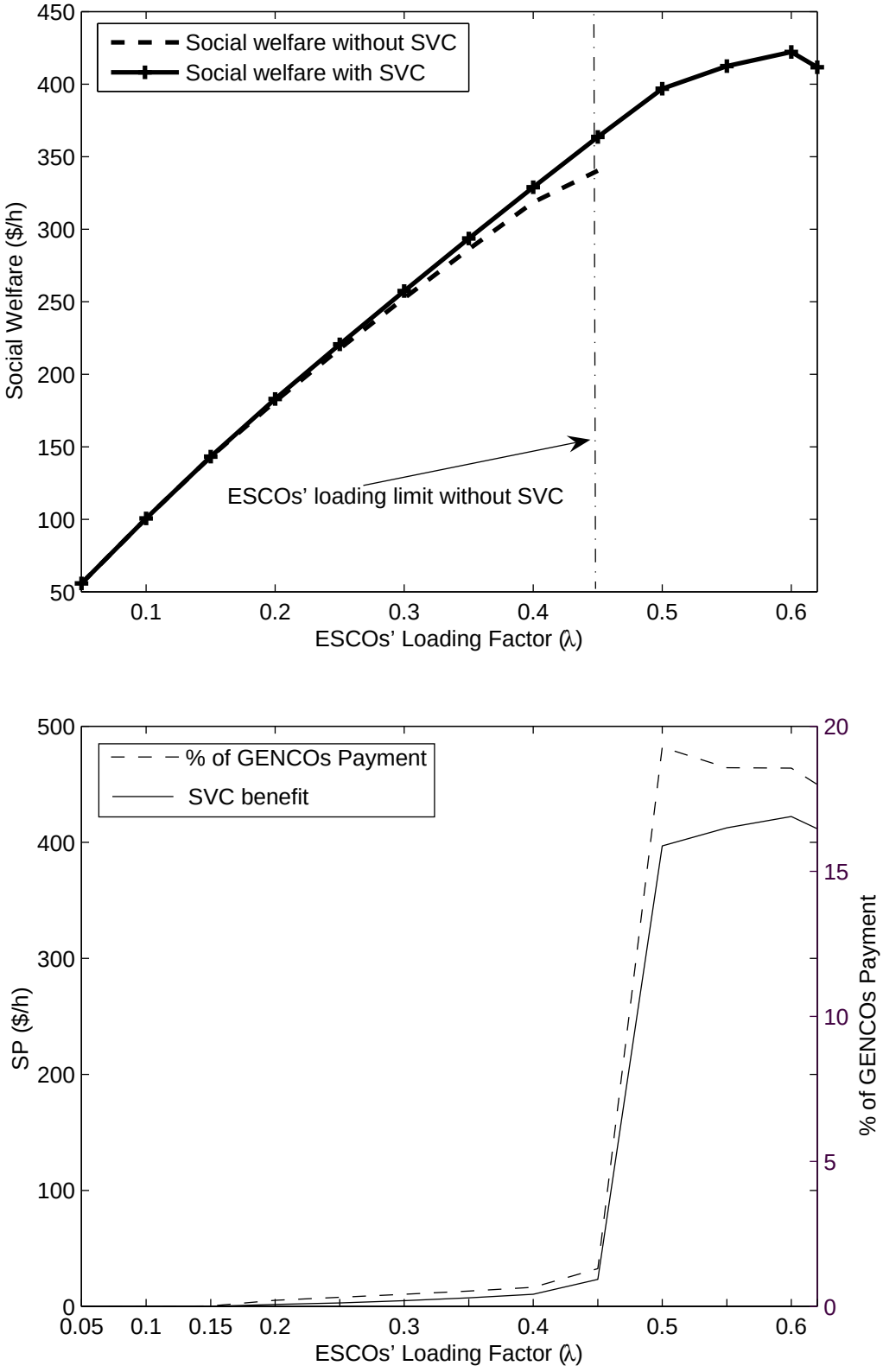

Figure 4.12: SVC benefit and pricing analysis for the IEEE 14-bus test system using social welfare.

without a dynamic model of the TCSC controller. Like the SVC controller, the difference in the social welfare is significant, especially near the Hopf bifurcation point ($\lambda \approx 0.6$). Again, these results highlight the need for considering the FACTS controller dynamics in the market auction mechanisms.

Figures 4.16 and 4.17 depict the effect of including the TCSC controller in the system's CC and S_b. By using a similar pricing methodology as that of the PSS and SVC, the difference between the CC and S_b resulting from the proposed SSC-OPF with and without the TCSC controller may be used for pricing the TCSC dynamic stability control services. In terms of percentage of the GENCOs' power payments, these prices are not that significant, especially if they are compared to the benefits for the entire system, as in the case of the other controllers.

4.5 Summary

A new technique for pricing dynamic services provided by the system controllers is presented and discussed for the PSS, SVC, and TCSC. The methodology is applied to two different test systems and the effect of the dynamic modelling of these controllers on the market signals is demonstrated. This chapter also demonstrates the importance of dynamic modelling of system controllers in the context of energy markets.

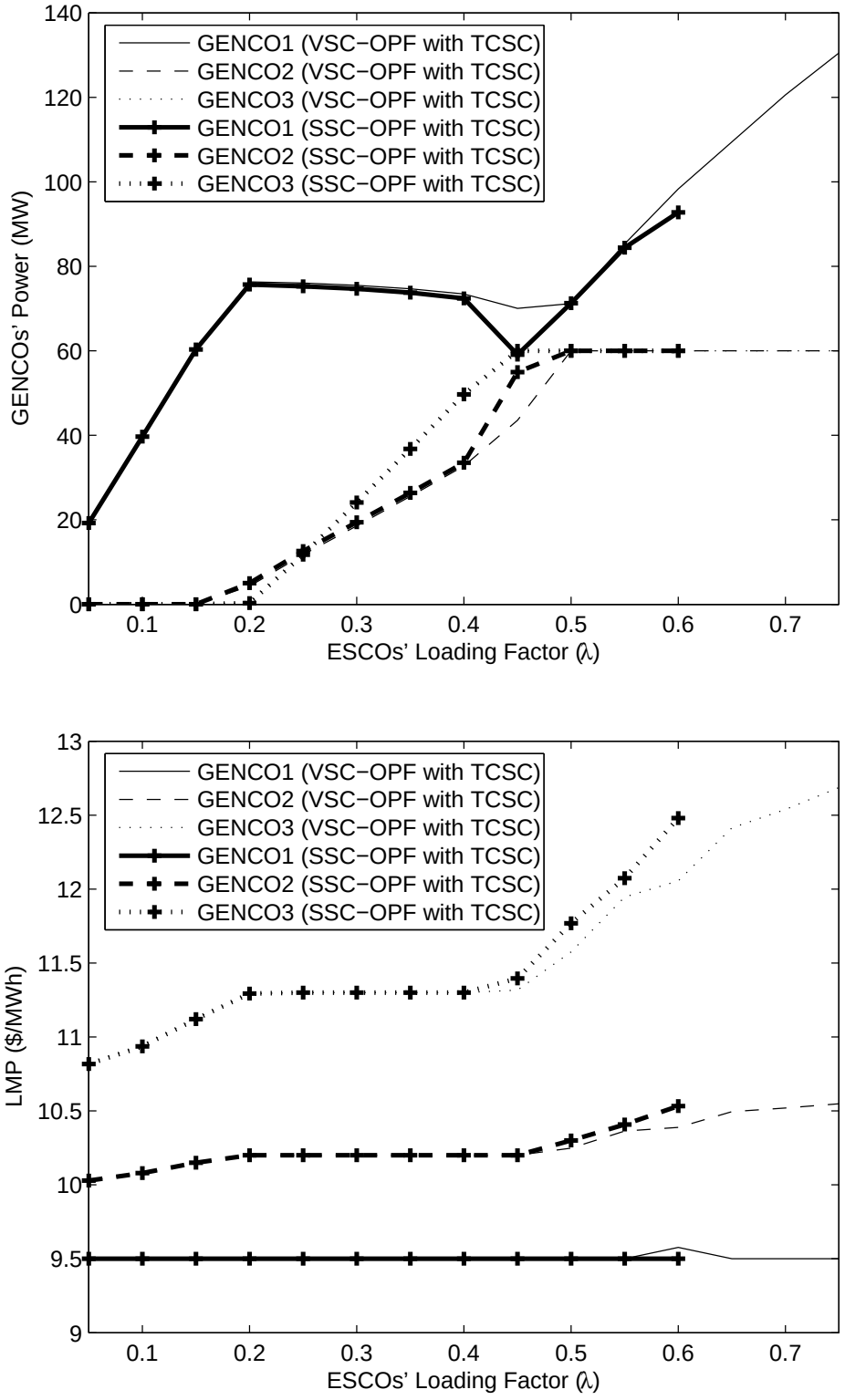

Figure 4.13: GENCOs' supplied power and LMPs with respect to the loading factor with the TCSC controller for the IEEE 14-bus test system.

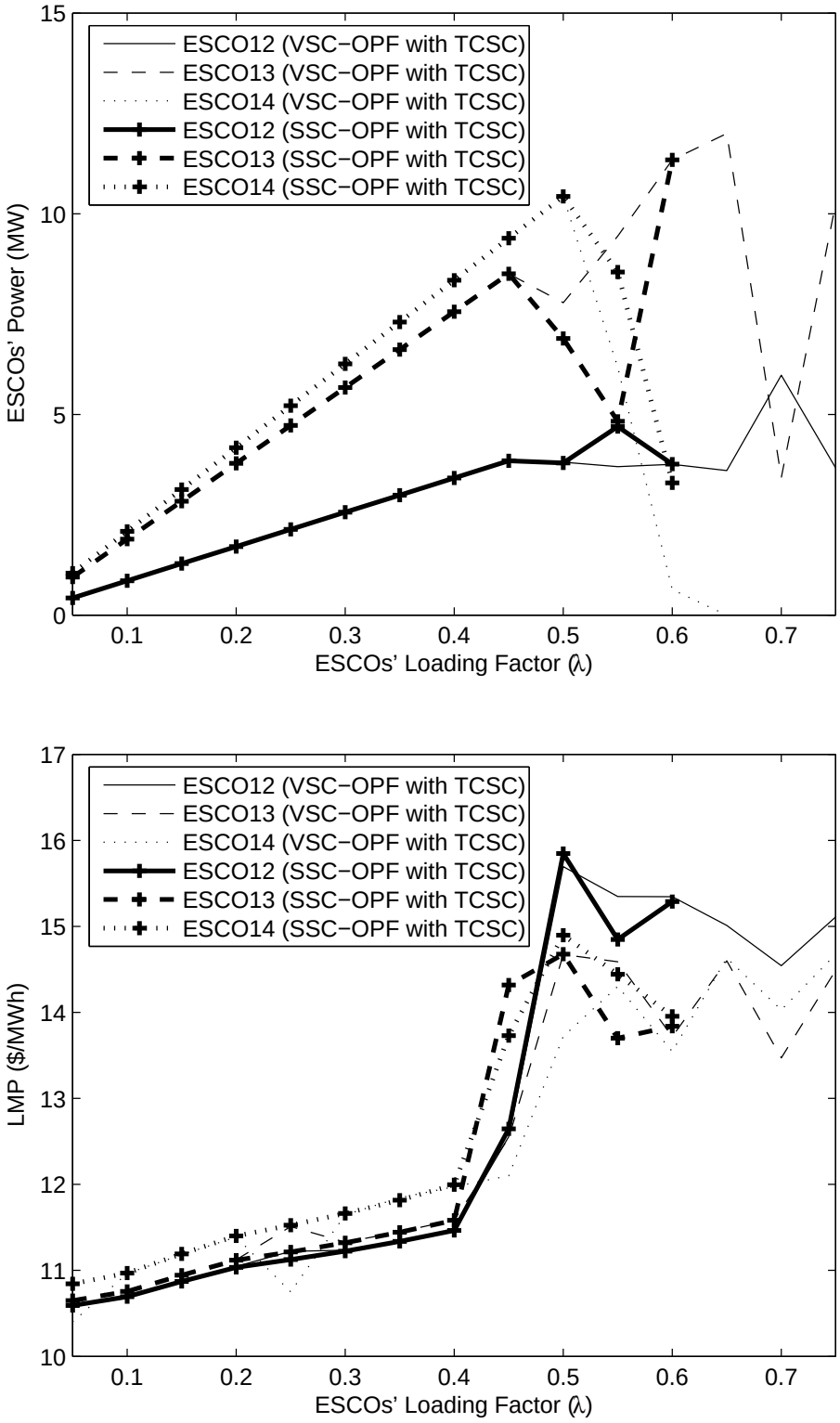

Figure 4.14: ESCOs' power and LMPs with respect to the loading factor with the TCSC controller for the IEEE 14-bus test system.

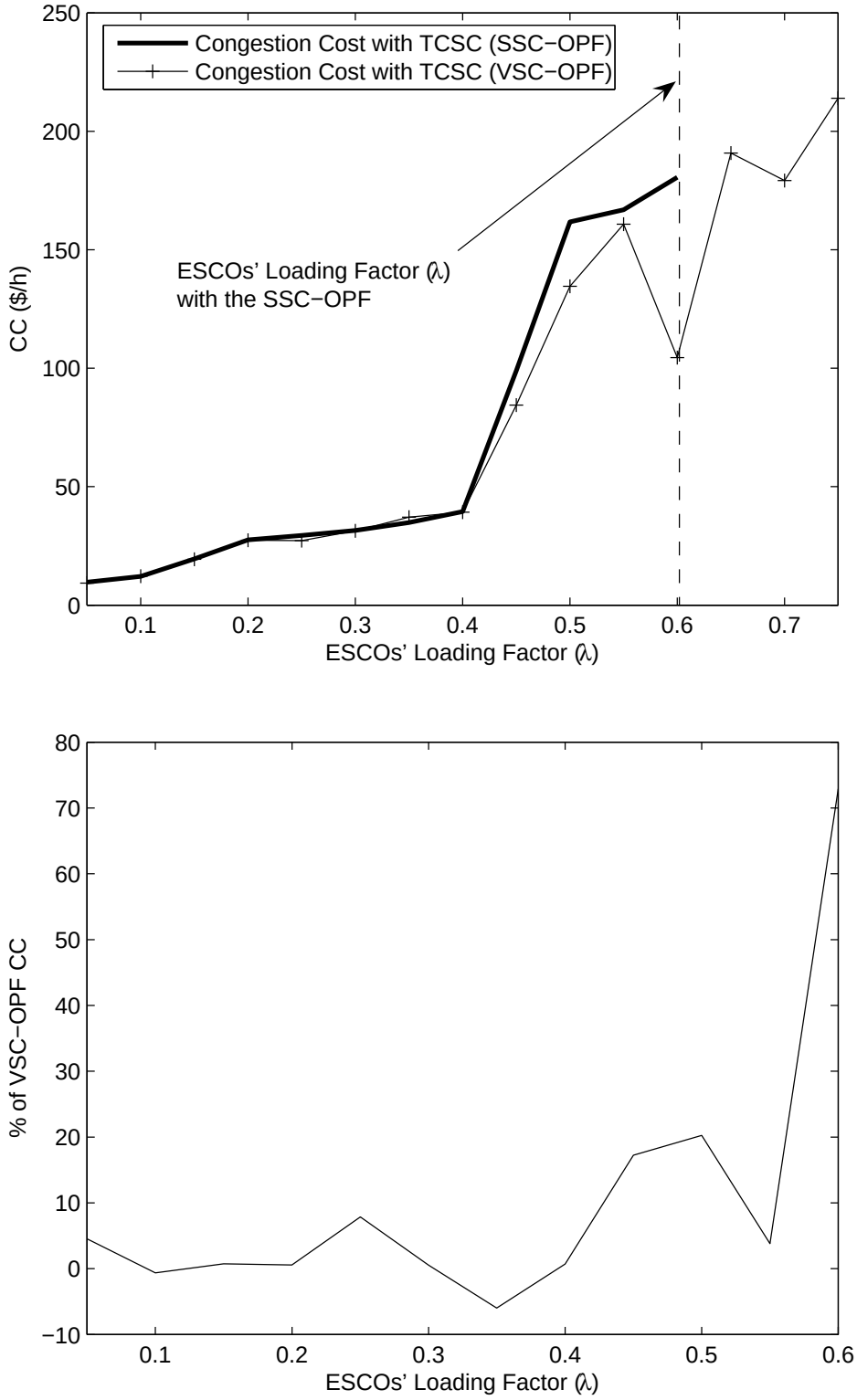

Figure 4.15: Benefit analysis for the TCSC dynamic model in the IEEE 14-bus test system.

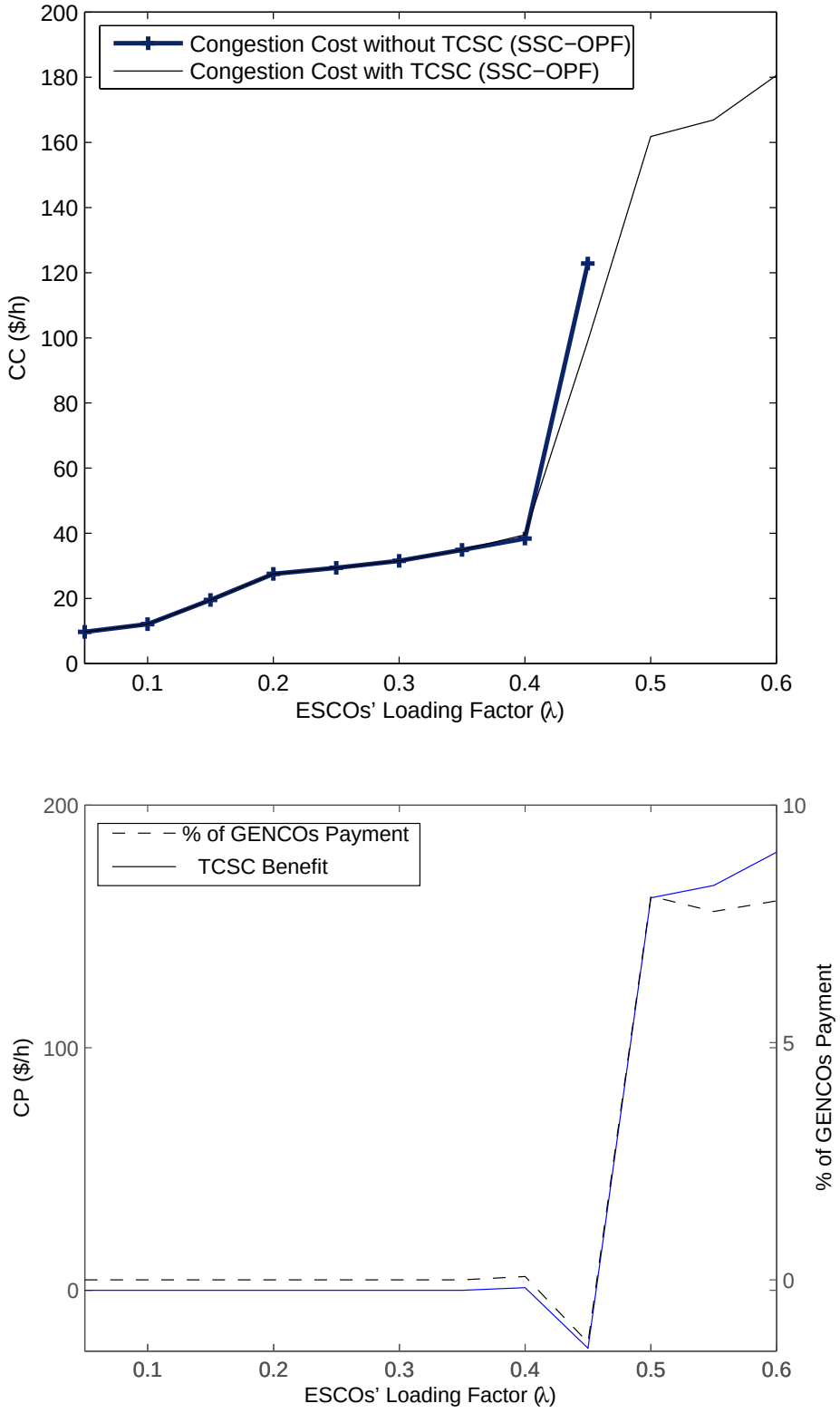

Figure 4.16: TCSC benefit and pricing analysis for the IEEE 14-bus test system using congestion costs.

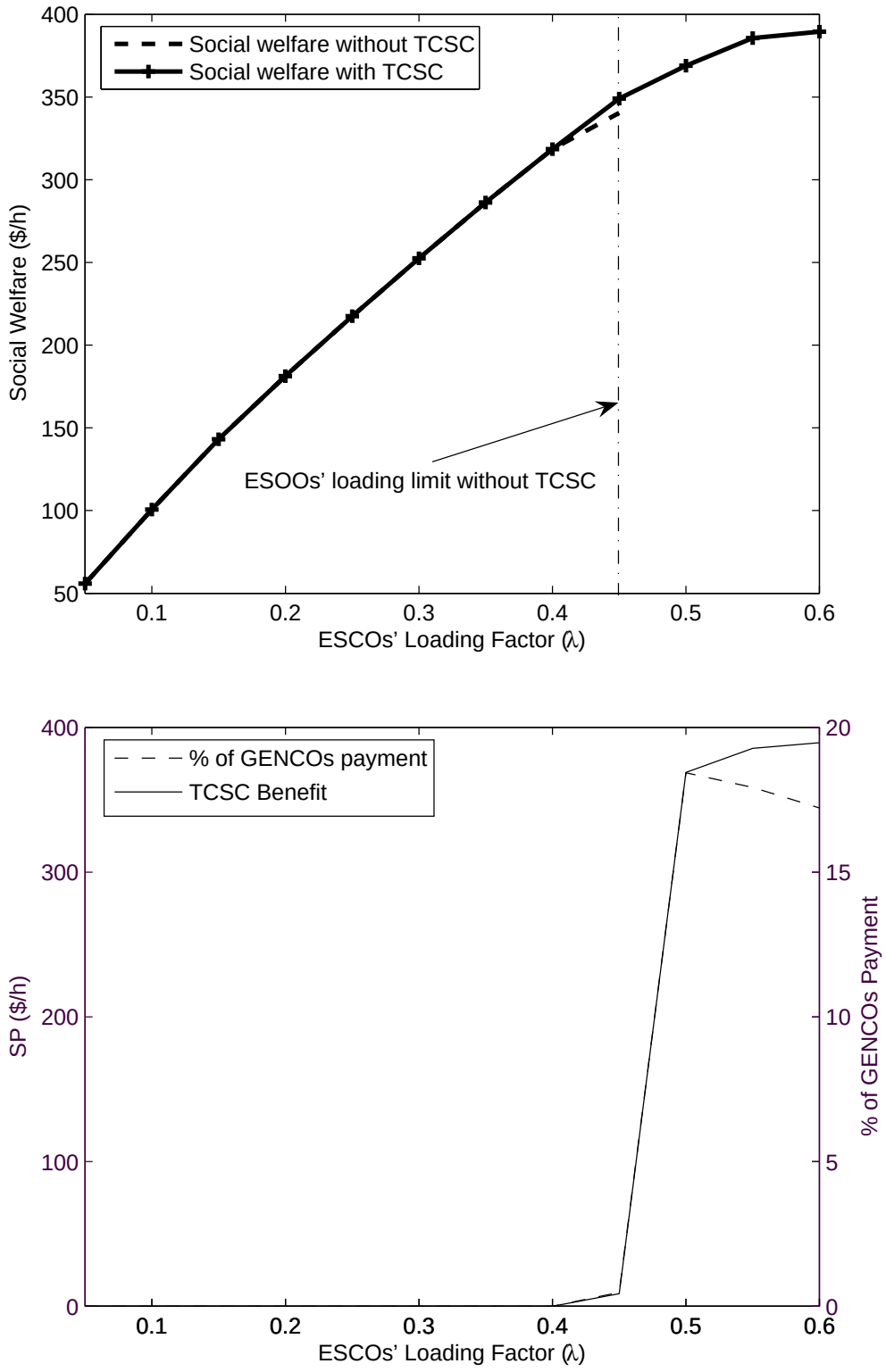

Figure 4.17: SVC benefit and pricing analysis for the IEEE 14-bus test system using social welfare.

Chapter 5

Optimal Tuning of Oscillation Damping Controllers

5.1 Introduction

Chapter 4 offers a new methodology for pricing the dynamic services provided by the PSS or other controllers such as FACTS. First though, these controllers should be "optimally" tuned to improve of market operating conditions, i.e. power dispatch and price levels, as well as guaranteeing an adequate level of system security. Thus, this chapter compares the use of the proposed SSC-OPF versus a standard OPF auction when oscillation damping controllers (e.g. PSS and TCSC) are included. Furthermore, the adoption of the SSC-OPF for optimally tuning these controllers within the context of an electricity market clearing mechanism is also discussed.

5.2 Comparing OPF Techniques

In this section, the standard OPF auction is compared with respect to the newly developed SSC-OPF when the PSS and TCSC are added to the IEEE 14-Bus test system (Figure 4.3), demonstrating the benefits of using the proposed SSC-OPF, which incorporates the dynamic models of these controllers.

The results in this section are obtained without considering system contingencies, since this significantly limits the loading range for stability studies. There is no reason to expect that contingencies would affect the conclusions of the analysis presented here.

5.2.1 PSS and the Standard OPF

Figures 5.1 and 5.2 depict the supply and demand power and LMPs, respectively, when the standard OPF (2.10) and SSC-OPF (3.1) are applied to the IEEE 14-bus system, with the PSS included. The PSS gain is chosen to be $K_{PSS} = 2.5$ for the SSC-OPF, since this yields a 2% damping ratio at the original Hopf bifurcation point at $\lambda = 0.45$ p.u. The power limits on the lines used in (2.10) are computed off-line, considering a damping ratio of 2% for the system when the PSS is included. The bus voltage limits in both OPF problems are 0.9 p.u. and 1.1 p.u. Higher LMPs are obtained by using the standard OPF, and the supply and demand powers are lower as the system becomes more congested for the standard OPF compared to the results obtained from the SSC-OPF. A comparison of the congestion cost between both OPFs is illustrated in Figure 5.3, which, as expected, shows the more restrictive nature of the standard OPF auction.

The solution details, i.e. bus voltage, reactive powers and supply and demand

powers, are illustrated in Table 5.1 for the loading factor $\lambda = 0.5$. It is evident that the SSC-OPF leads to higher supply and demand powers compared to the standard OPF's results. This is because the stability constraint in the SSC-OPF reflects better the effect of PSS on the system than the transmission line power limits used in the standard OPF.

5.2.2 TCSC and the Standard OPF

Figures 5.4 and 5.5 present the power and LMPs for supply and demand side, respectively, for the OPF problems (2.10) and (3.1) when applied to the IEEE 14-bus system including the TCSC. The TCSC gain is chosen to be $K_{TCSC} = 1.3$ for the SSC-OPF, since this gain yields a 2% damping ratio at the original Hopf bifurcation point $\lambda = 0.45$ p.u. The power limits on the lines in (2.10) are obtained off-line with a damping ratio of 2% for the case when the TCSC is included. The bus voltage limits are 0.9 p.u. and 1.1 p.u. in both problems. Observe that the LMPs obtained by using the standard OPF are higher, and the supply and demand powers are lower when compared to the SSC-OPF results, as the system becomes more congested. The CC comparsion between the OPFs depicted in Figure 5.6 shows the more restrictive nature of the standard OPF.

The solution details, i.e. bus voltage, reactive powers and supply and demand powers, are listed in Table 5.2 at a loading factor of $\lambda = 0.6$. The SSC-OPF results in higher supply and demand powers when compared to the standard OPF solution. This is due to the SSC-OPF properly modelling the TCSC and its effect on oscillation damping control on the market auction.

Table 5.1: Solution details for the standard OPF and the SSC-OPF with the PSS at $\lambda = 0.5$ p.u. and $K_{PSS} = 2.5$ for the IEEE 14-bus test system with PSS.

Bus	Standard OPF			SSC-OPF		
	V (p.u.)	P (MW)	Q_G (MVAr)	V (p.u.)	P (MW)	Q_G (MVAr)
GENCO1	1.1	103.59	55.56	1.1	67.734	80
GENCO2	1.051	0.00	50	1.058	60	50
GENCO3	0.999	60.00	40	1.006	60	40
ESCO2	1.051	15.19		1.058	15.19	
ESCO3	0.999	65.95		1.006	65.95	
ESCO4	0.992	33.46		0.99	33.46	
ESCO5	1.001	3.219		0.998	5.32	
ESCO6	1.029	4.315	24	1.02	6.489	24
ESCO9	0.986	17.32		0.97	19.406	
ESCO10	0.985	0.00		0.967	6.199	
ESCO11	1.008	2.45		0.987	2.45	
ESCO12	1.006	2.40		0.992	3.89	
ESCO13	0.997	7.9076		0.981	8.252	
ESCO14	0.972	0.00		0.943	8.445	
Bus 7	1.01			0.999		
Bus 8	1.051		24	1.04		24
$\sigma_{min}(J_m)$	0.000263			0.0002		

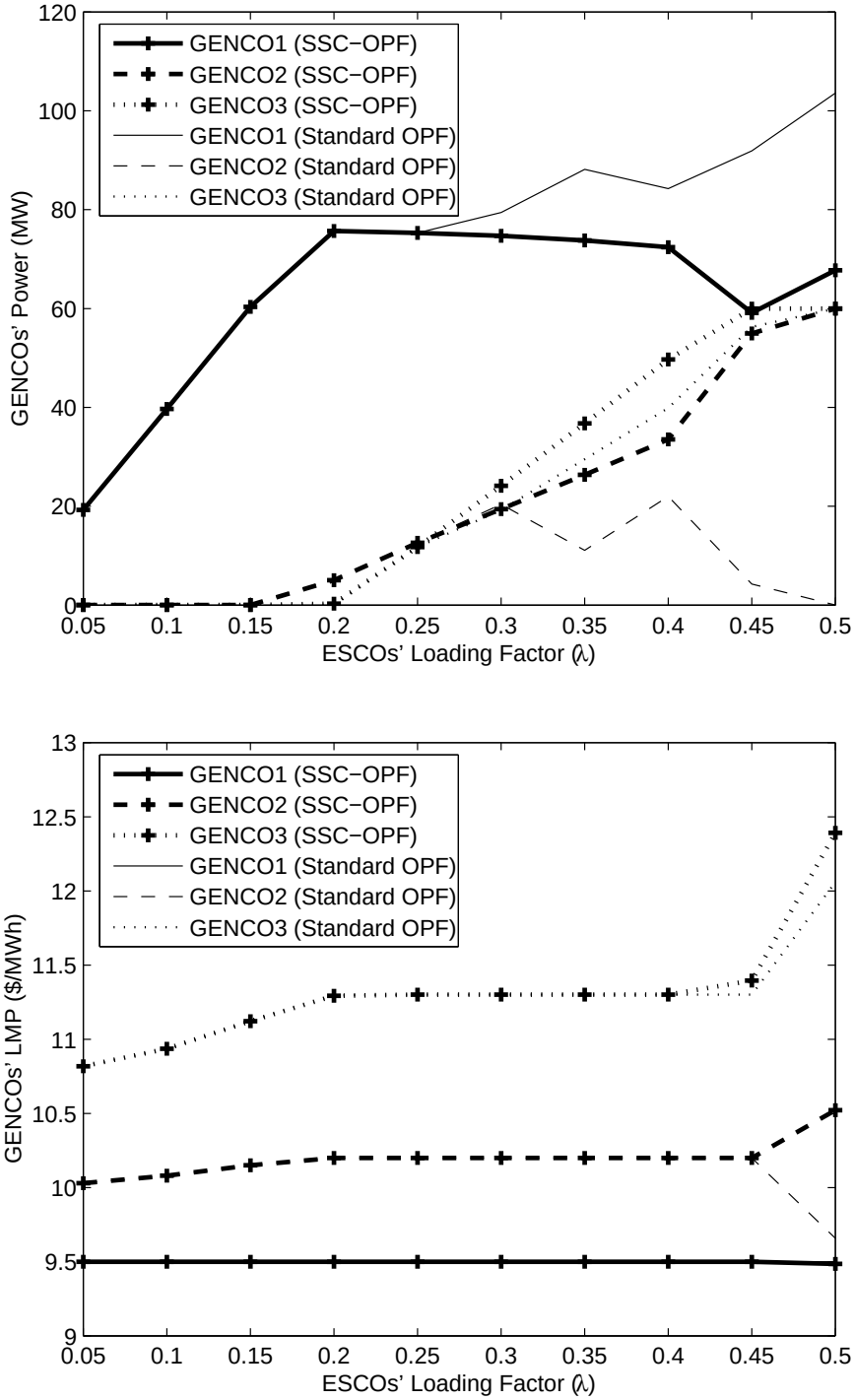

Figure 5.1: GENCOs' supplied power and the LMPs with respect to the loading factor for the IEEE 14-bus test system with PSS.

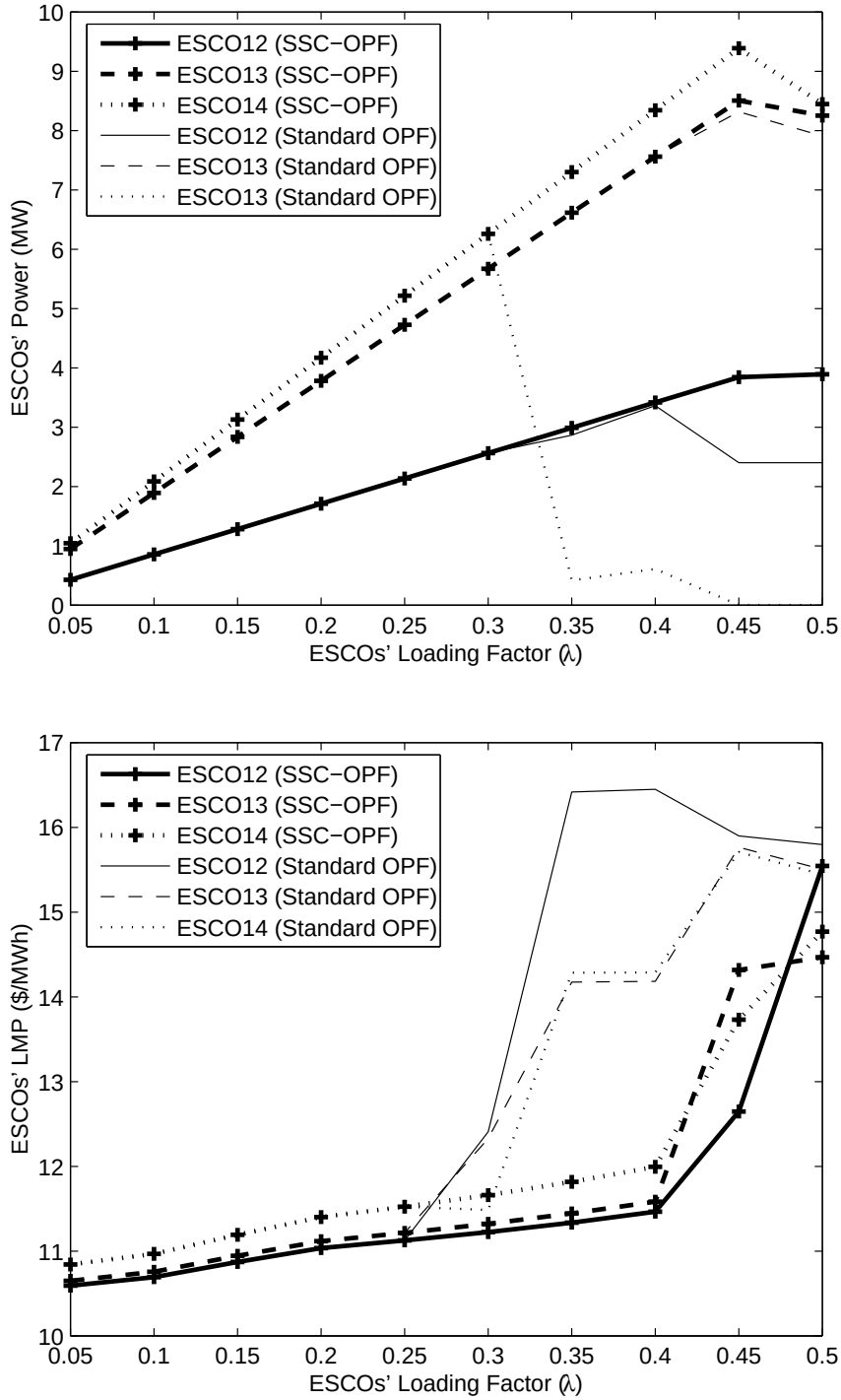

Figure 5.2: ESCOs' power and the LMPs with respect to the loading factor for the IEEE 14-bus test system with PSS.

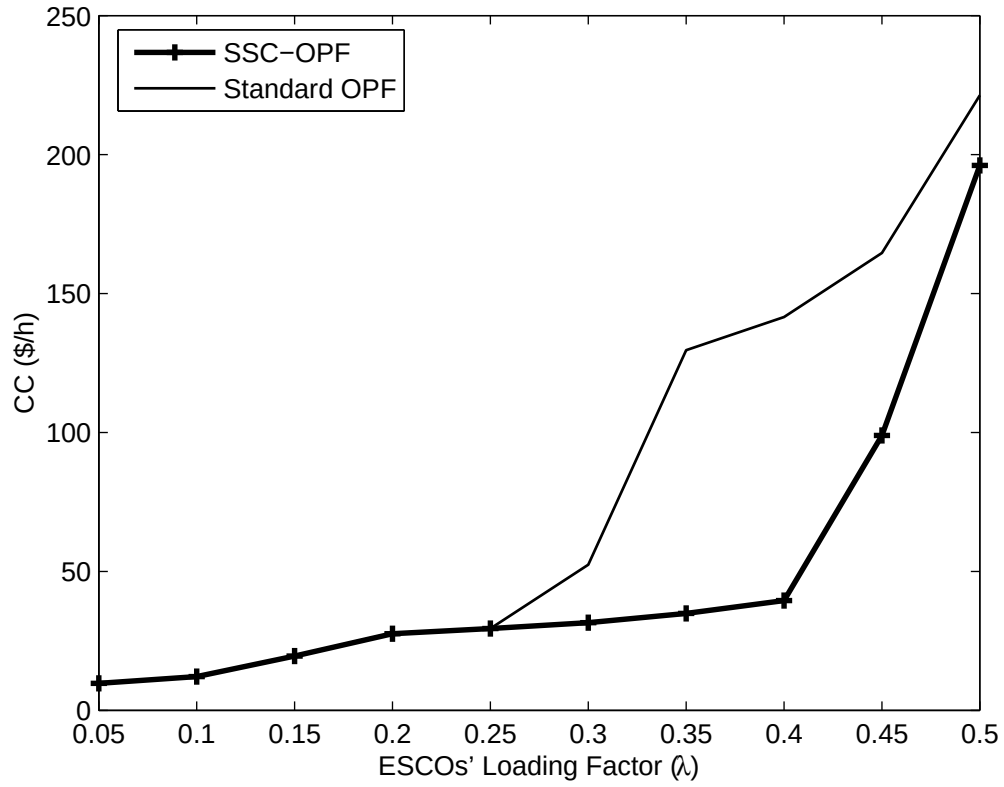

Figure 5.3: Congestion Cost comparison between the standard OPF and the SSC-OPF when the PSS is included in the IEEE 14-bus test system.

Table 5.2: Solution details for the standard OPF and the SSC-OPF at $\lambda = 0.6$ p.u. and $K_{TCSC} = 1.3$ for the IEEE 14-bus test system with TCSC.

Bus	Standard OPF			SSC-OPF		
	V (p.u.)	P (MW)	Q_G (MVAr)	V (p.u.)	P (MW)	Q_G (MVAr)
GENCO1	1.1	131.34	75.83	1.1	94.516	98.7
GENCO2	1.041	0.00	50	1.038	60	50
GENCO3	0.978	60.00	40	0.965	60	40
ESCO2	1.041	18.228		1.038	18.228	
ESCO3	0.978	79.14		0.965	79.14	
ESCO4	0.977	36.033		0.996	40.152	
ESCO5	0.988	6.384		0.969	6.384	
ESCO6	1.013	5.457	24	0.976	4.926	24
ESCO9	0.97	10.486		0.926	24.78	
ESCO10	0.967	2.731		0.921	5.413	
ESCO11	0.983	2.94		0.941	2.94	
ESCO12	0.987	3.829		0.948	3.735	
ESCO13	0.981	3.322		0.937	11.34	
ESCO14	0.946	6.727		0.909	3.293	
Bus 7	0.995			0.958		
Bus 8	1.036		24	1.00		24
$\sigma_{min}(J_m)$	0.000259			0.0002		

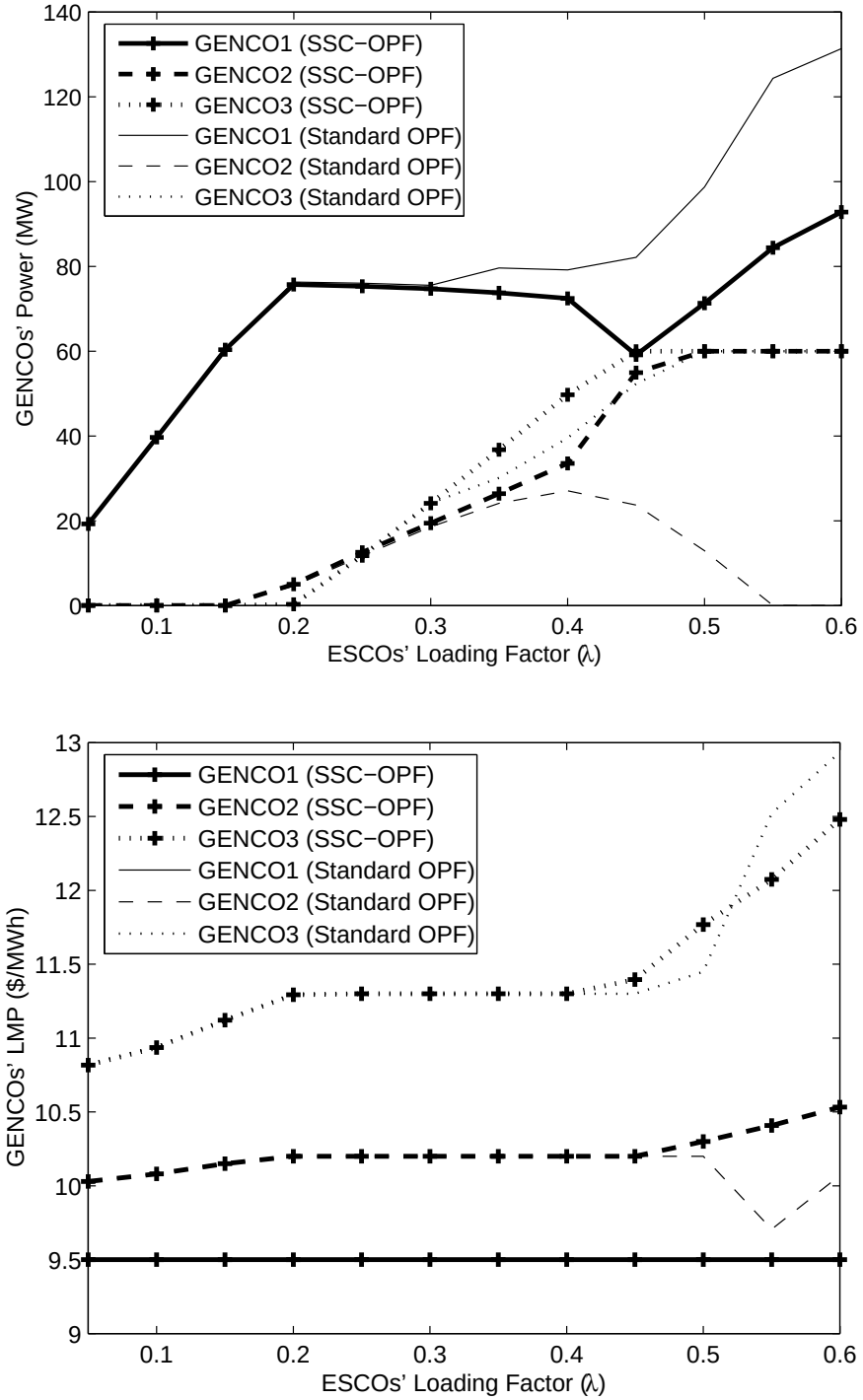

Figure 5.4: GENCOs' supplied power and the LMPs with respect to the loading factor for the IEEE 14-bus test system with TCSC.

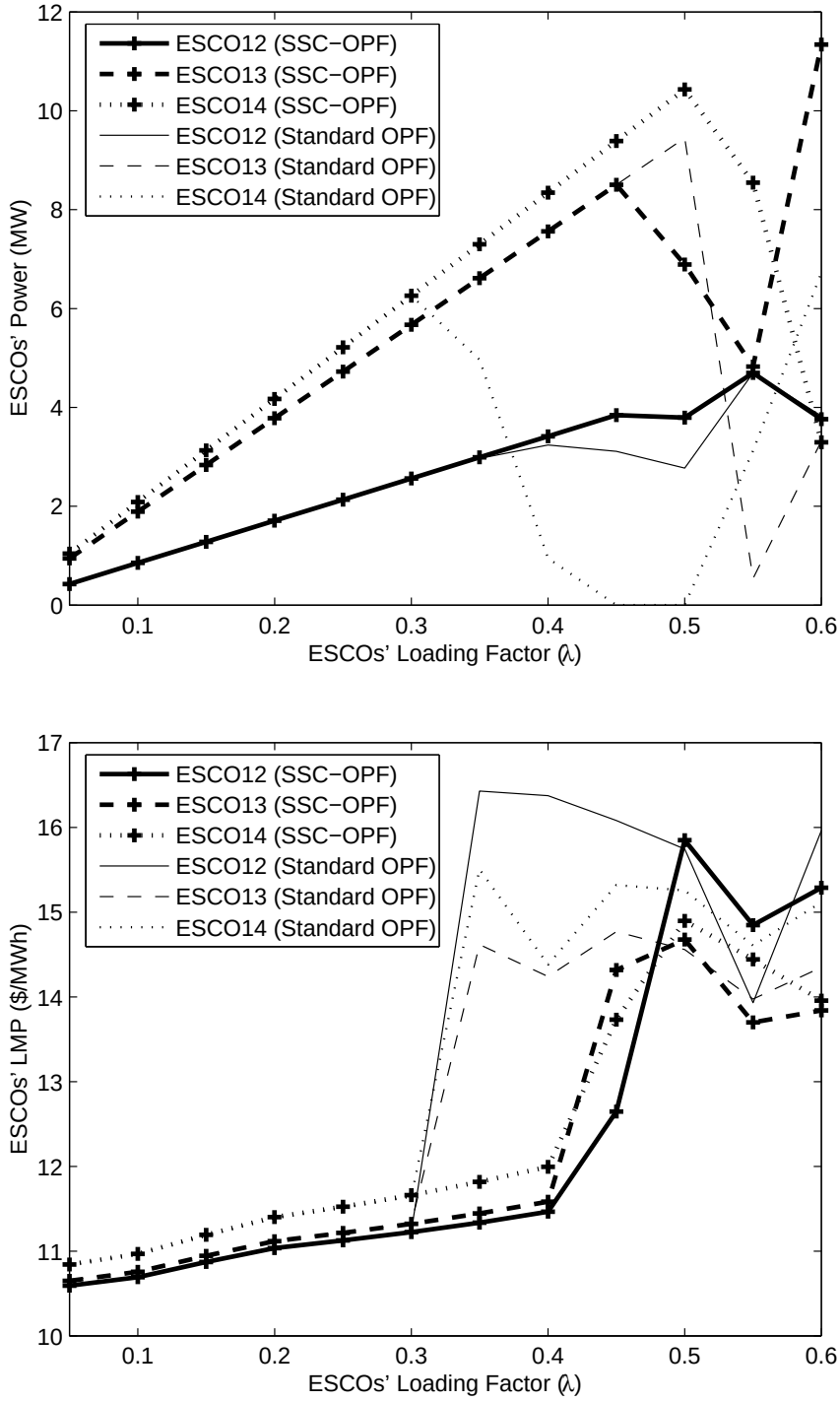

Figure 5.5: ESCOs' power and the LMPs with respect to the loading factor for the IEEE 14-bus test system with TCSC.

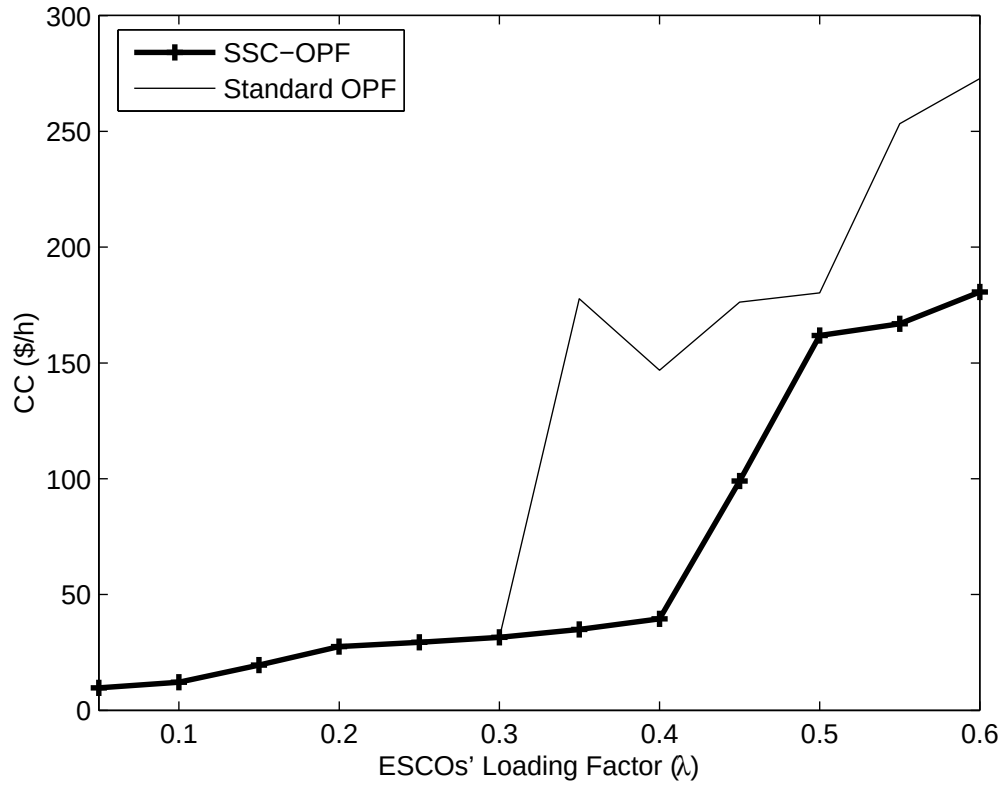

Figure 5.6: Congestion Cost comparison between the standard OPF and the SSC-OPF when the TCSC is included in the IEEE 14-bus test system.

5.3 Optimal Tuning

As shown in the previous section, the SSC-OPF appropriately models the oscillation damping controllers, resulting in more adequate market and system conditions. In this section, the PSS and TCSC gains, i.e. K_{PSS} and K_{TCSC}, are optimally tuned by using the proposed SSC-OPF. The novel optimal tuning technique is illustrated on the IEEE 14-bus system without contingencies.

5.3.1 Optimal Tuning of the PSS

Figure 5.7 presents the effect of the PSS gain (K_{PSS}) on the HBI, as the ESCOs' demand power is increased from its nominal value, according to (3.23) with $P_d = P_{L_o}$. The HBI index is calculated assuming that the total demand is shared between GENCO1, GENCO2 and GENCO3 in proportion to their inertias, i.e. OPF techniques are not applied in this case to determine the optimal schedules. Notice that as this gain is increased, the loadability margin increases, and the system becomes more stable. This significant effect of K_{PSS} on system stability illustrates the need to choose the appropriate PSS gain.

Figures 5.8 and 5.9 portray the results of solving the SSC-OPF problem in (3.1) with and without optimal tuning for supply and demand, respectively. The PSS gain is chosen to be $K_{PSS} = 2.5$, since it yields a 2% damping ratio at the original Hopf bifurcation point at $\lambda = 0.45$ p.u. For the optimal tuning of the PSS, the overall system and market conditions improve as the system changes due to demand increase; thus, the operating margin of the system expands beyond the loading factor of 0.5 p.u., which is the limit for the SSC-OPF with a fixed K_{PSS}. The K_{PSS} optimal values, with respect to load increase obtained from the SSC-

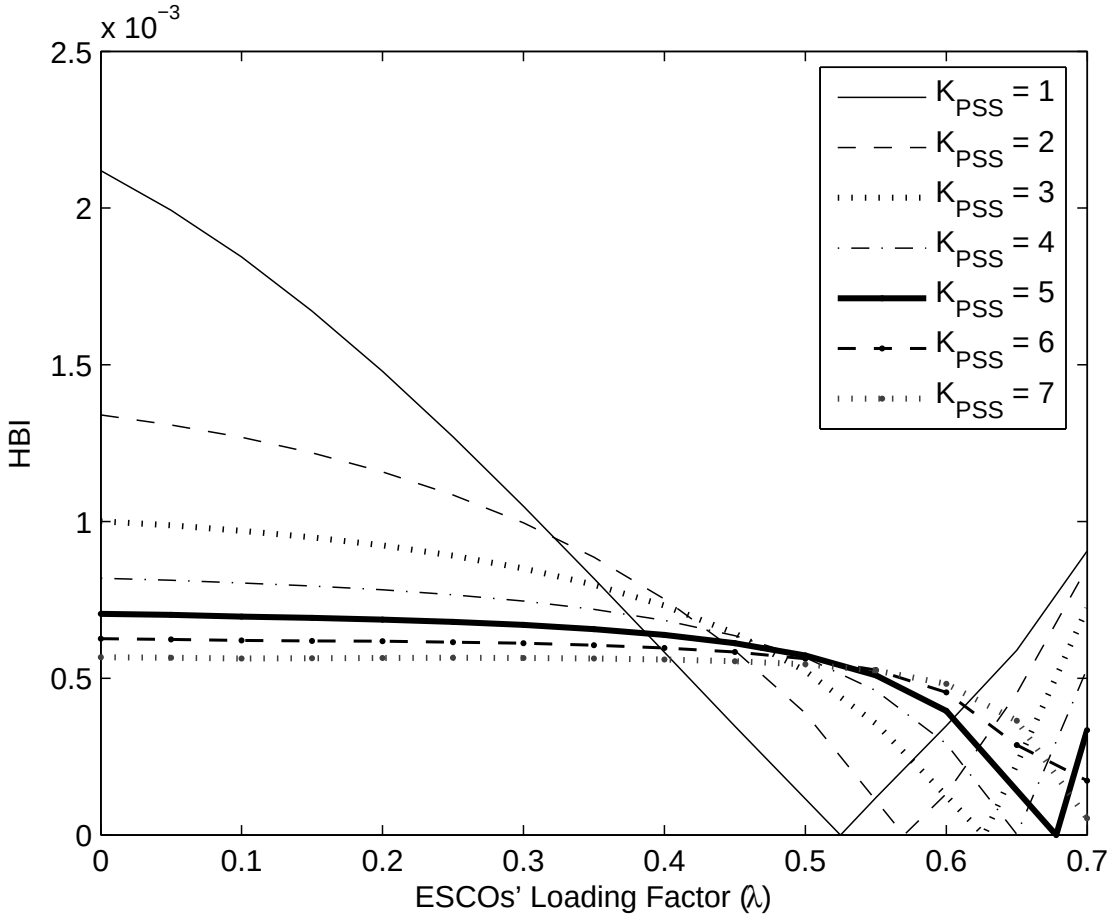

Figure 5.7: Effect of the PSS gain on the HBI for the IEEE 14-bus test system.

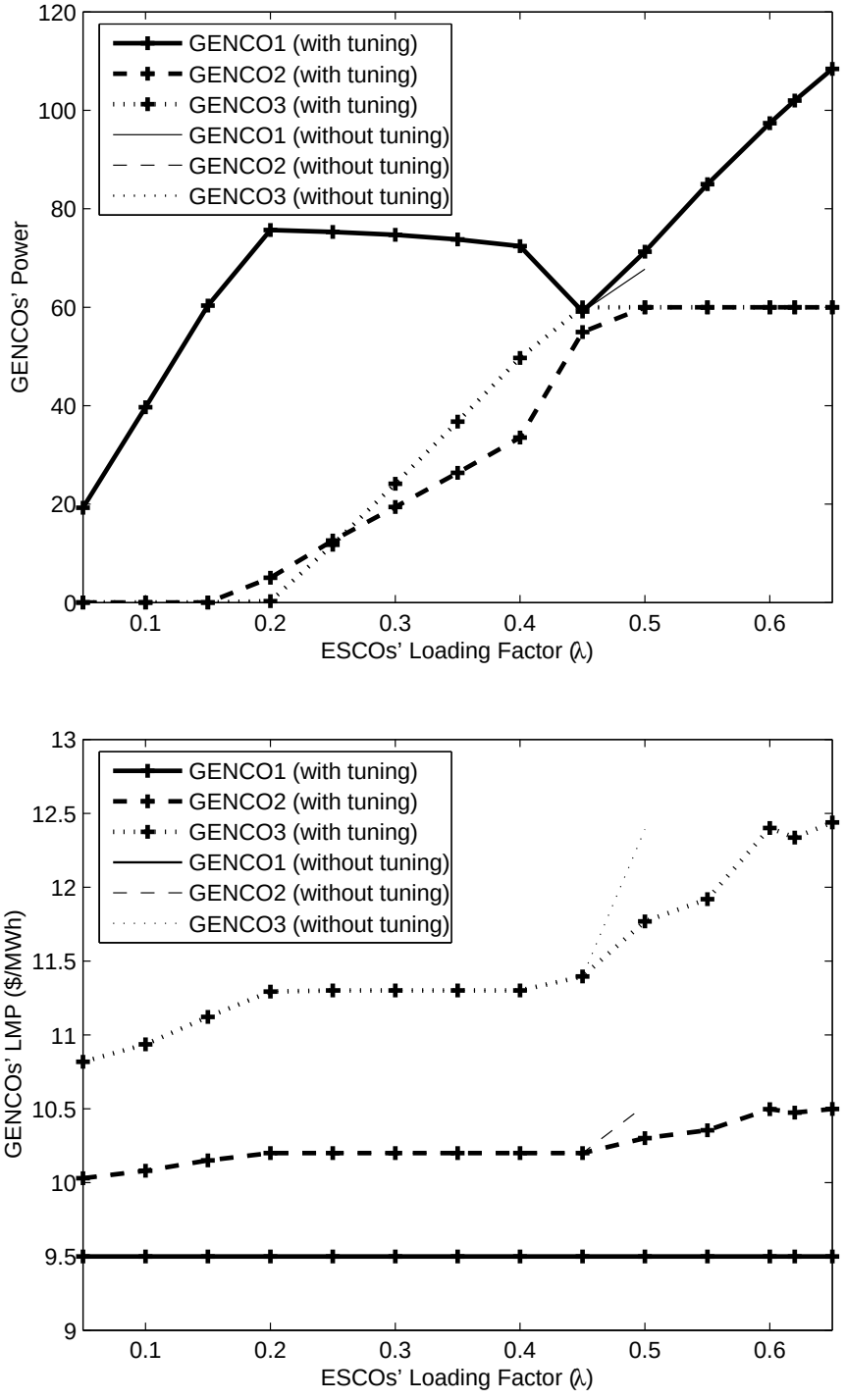

Figure 5.8: GENCOs' supplied power and the LMPs with respect to the loading factor for the IEEE 14-bus test system with PSS.

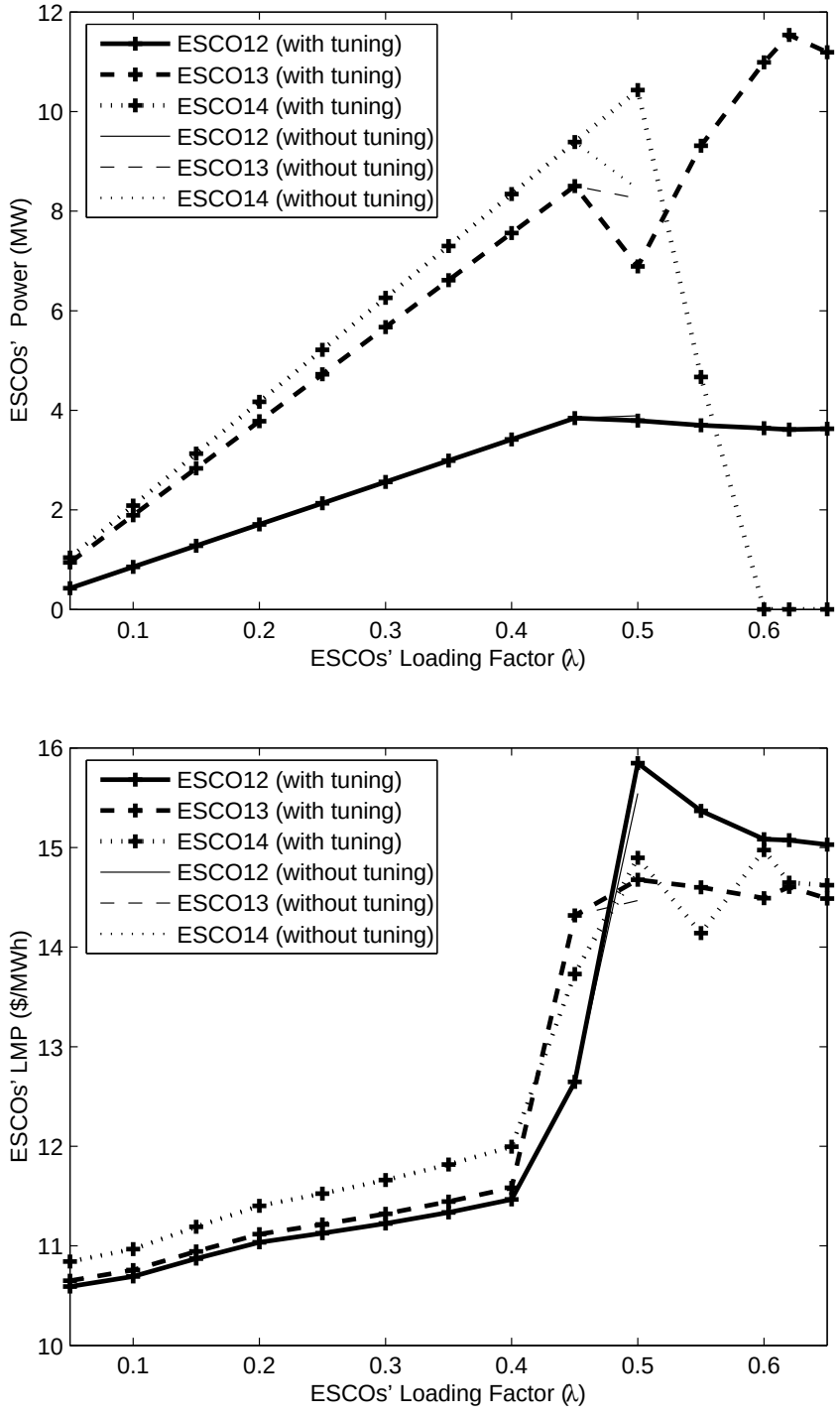

Figure 5.9: ESCOs' power and the LMPs with respect to the loading factor for the IEEE 14-bus test system with PSS.

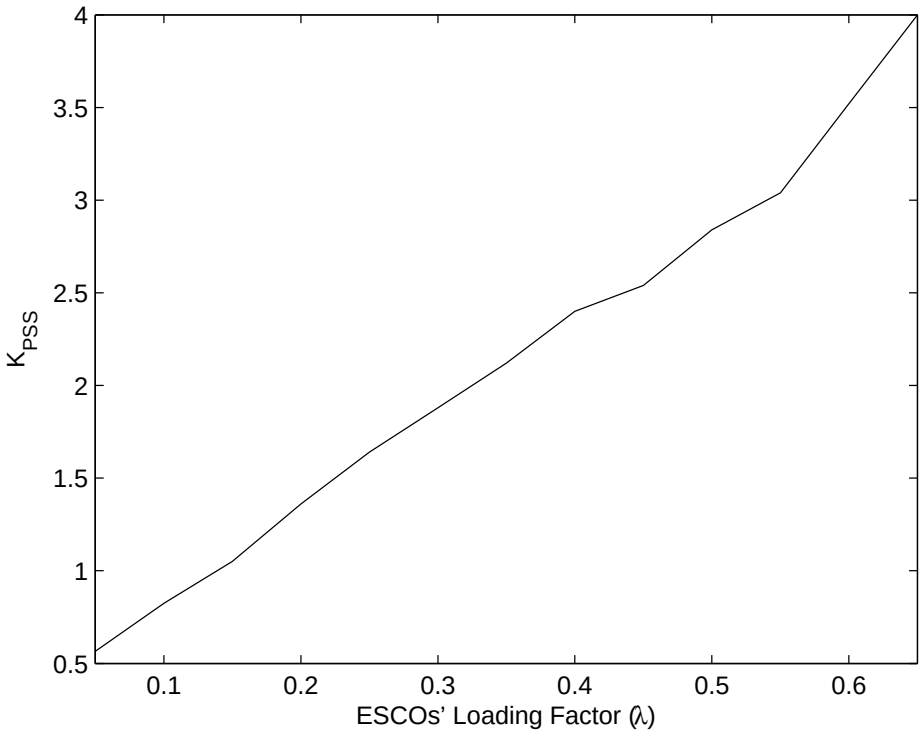

Figure 5.10: Optimal value of the PSS gain with respect to the loading factor for the IEEE 14-bus test system.

Table 5.3: Solution details for the SSC-OPF at $\lambda = 0.5$ p.u. with and without optimal tuning for the IEEE 14-bus test system with PSS.

Bus	SSC-OPF without tuning			SSC-OPF with tuning		
	V (p.u.)	P (MW)	Q_G (MVAr)	V (p.u.)	P (MW)	Q_G (MVAr)
GENCO1	1.1	67.734	80	1.1	71.286	83.9
GENCO2	1.058	60	50	1.044	60	50
GENCO3	1.006	60	40	0.981	60	40
ESCO2	1.058	15.19		1.044	15.19	
ESCO3	1.006	65.95		0.981	65.95	
ESCO4	0.99	33.46		0.964	33.46	
ESCO5	0.998	5.32		0.975	5.32	
ESCO6	1.02	6.489	24	0.979	7.84	23.3
ESCO9	0.97	19.406		0.931	20.65	
ESCO10	0.967	6.199		0.926	5.75	
ESCO11	0.987	2.45		0.946	2.45	
ESCO12	0.992	3.89		0.951	3.791	
ESCO13	0.981	8.252		0.941	6.89	
ESCO14	0.943	8.445		0.900	10.43	
Bus 7	0.999			0.964		
Bus 8	1.04		24	1.006		24
$\sigma_{min}(J_m)$	0.0002			0.00028		
K_{PSS}	2.5			2.84		

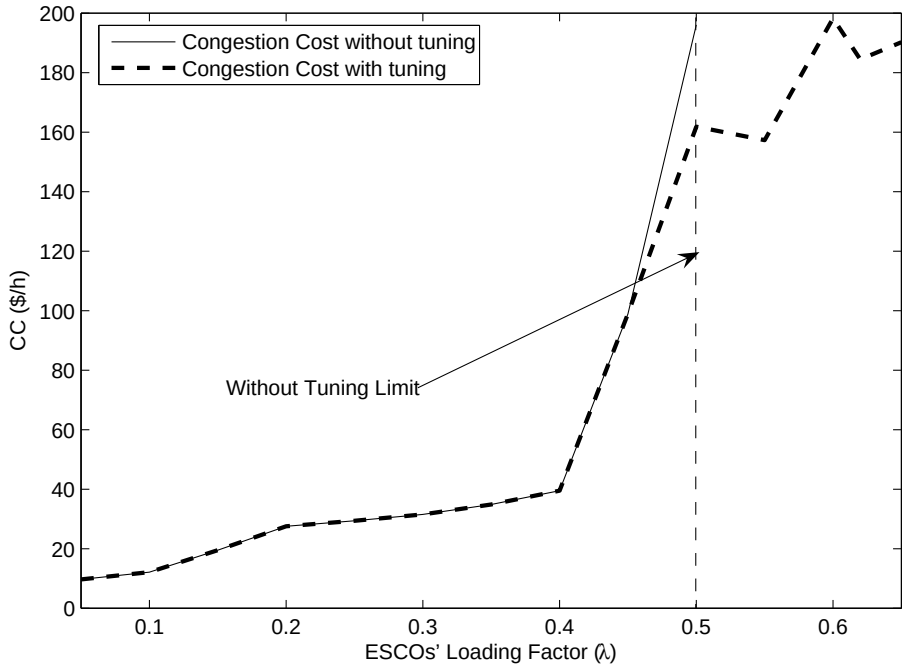

Figure 5.11: Benefit analysis of PSS tuning for the IEEE 14-bus test system.

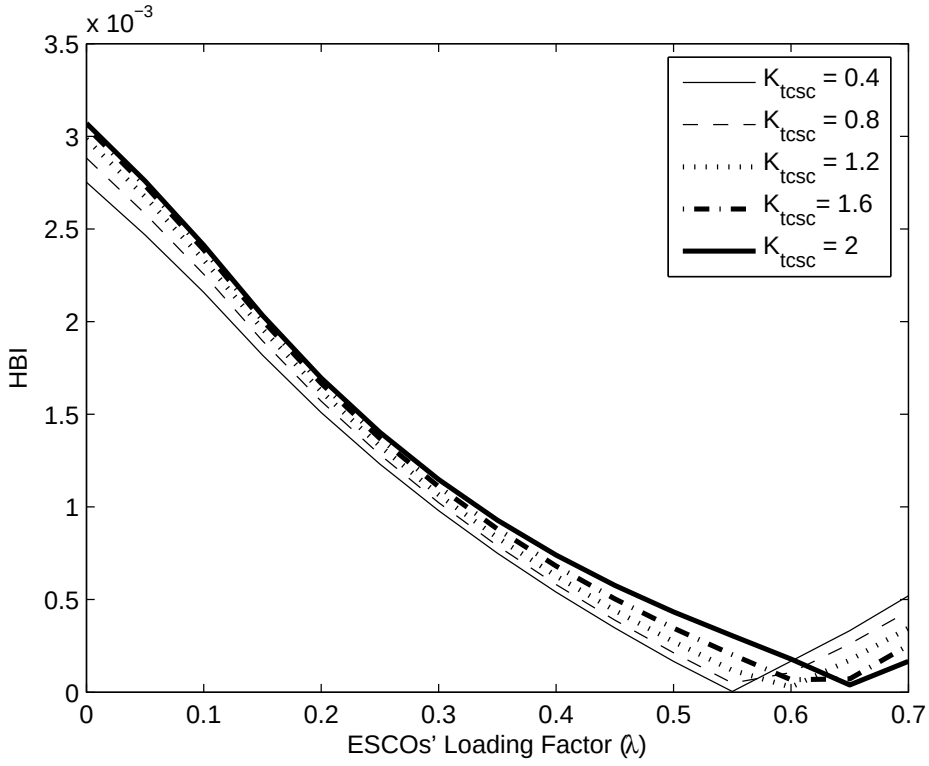

Figure 5.12: Effect of TCSC gain on the HBI for the IEEE 14-bus test system.

OPF, are illustrated in Figure 5.10. Observe that the PSS gain increases as the demand increases, as expected from the results in Figure 5.7.

Table 5.3 summarizes the bus voltages, reactive powers, and the supply and demand powers for the SSC-OPF with and without PSS tuning, at a loading power factor of $\lambda = 0.5$. It is evident that the SSC-OPF leads to higher transaction levels when the optimal tuning occurs. Notice that optimal tuning further enhances system stability, as the value of HBI increases.

To illustrate the "value" of the optimal tuning of the PSS gain for the market, the effect of the PSS tuning on CC is compared in Figure 5.11. The results reveal that, with the optimal tuning of the PSS gain, the system becomes less congested.

5.3.2 Optimal Tuning of the TCSC

Figure 5.12 denotes the effect of the TCSC gain K_{TCSC} on the HBI, as the ESCOs' demand power is increased from its nominal value according to (3.23), with $P_d = P_{L_o}$. The HBI index is calculated by assuming that the total demand is shared with GENCO1, GENCO2, and GENCO3 in proportion to their inertias, i.e. OPF techniques are not applied in this case to determine optimal schedules. The effect of the changes of K_{TCSC} on the system's stability clearly indicates that, as this gain is increased, the system becomes more stable, resulting in increased loadability margins.

The power outputs and LMPs of all the GENCOs are shown in Figure 5.13 for the SSC-OPF problem (3.1) with and without optimal tuning. The TCSC gain for the SSC-OPF problem with a fixed K_{TCSC} is set to 1.3, which corresponds to a 2% damping ratio at the original Hopf bifurcation point at $\lambda = 0.45$ p.u. Notice that the powers and LMPs of the GENCOs behave similarly to those of

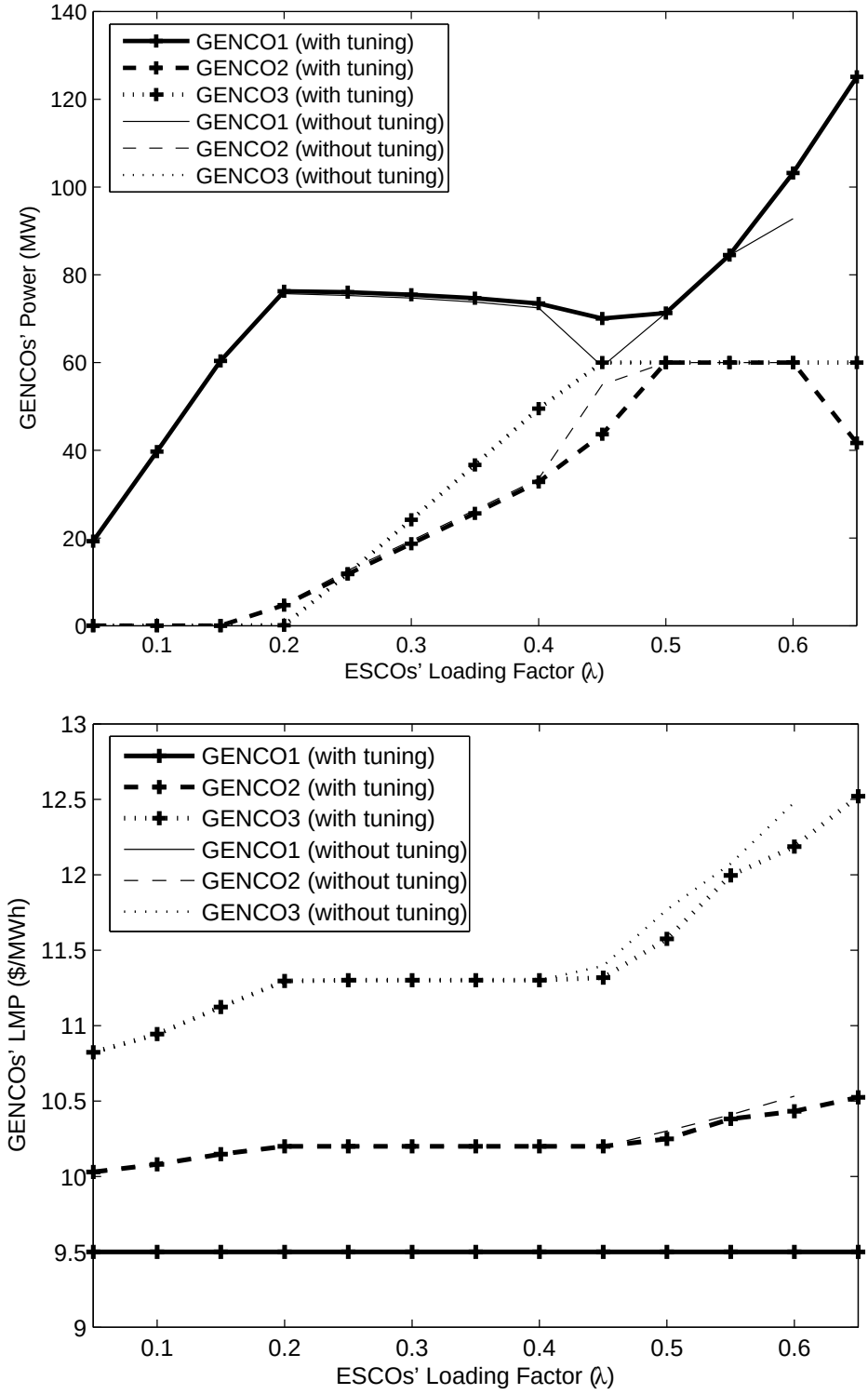

Figure 5.13: GENCOs' supplied power and the LMPs with respect to the loading factor for the IEEE 14-bus test system with TCSC.

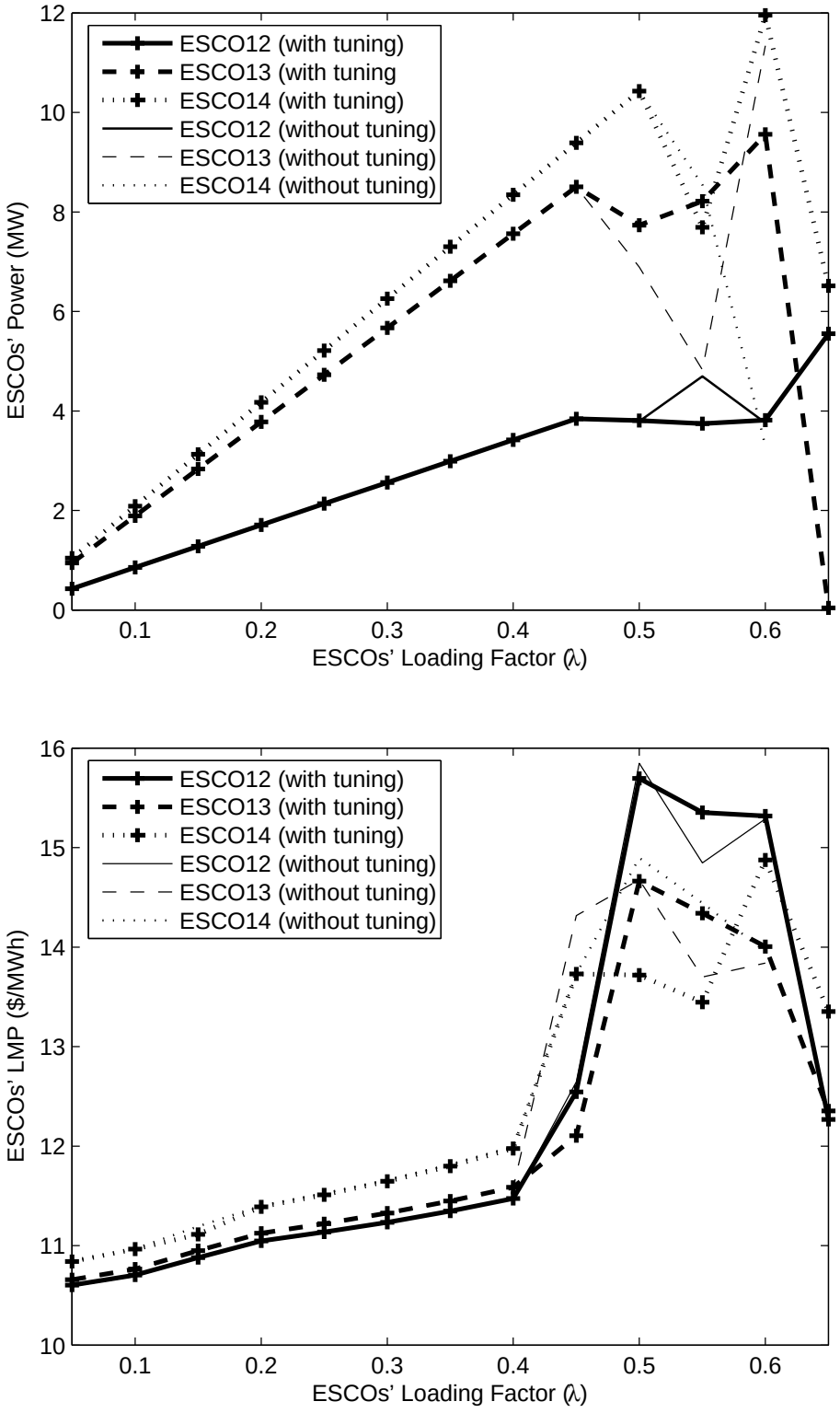

Figure 5.14: ESCOs' power and the LMPs with respect to the loading factor for the IEEE 14-bus test system with TCSC.

Table 5.4: Solution details of the SSC-OPF for the IEEE 14-bus test system with TCSC at $\lambda = 0.6$ p.u. with and without optimal tuning.

Bus	SSC-OPF without tuning			SSC-OPF with tuning		
	V (p.u.)	P (MW)	Q_G (MVAr)	V (p.u.)	P (MW)	Q_G (MVAr)
GENCO1	1.1	94.516	98.7	1.1	103.18	107.6
GENCO2	1.038	60	50	1.03	60	50
GENCO3	0.965	60	40	0.957	60	40
ESCO2	1.038	18.228		1.03	18.228	
ESCO3	0.965	79.14		0.957	79.14	
ESCO4	0.996	40.152		0.959	40.152	
ESCO5	0.969	6.384		0.942	6.384	
ESCO6	0.976	4.926	24	0.963	5.91	24
ESCO9	0.926	24.78		0.922	24.76	
ESCO10	0.921	5.413		0.918	5.641	
ESCO11	0.941	2.94		0.938	2.94	
ESCO12	0.948	3.735		0.941	3.81	
ESCO13	0.937	11.34		0.929	9.561	
ESCO14	0.909	3.293		0.900	11.96	
Bus 7	0.958			0.953		
Bus 8	1.00		24	0.992		24
$\sigma_{min}(J_m)$	0.0002			0.00021		
K_{TCSC}	1.3			2.08		

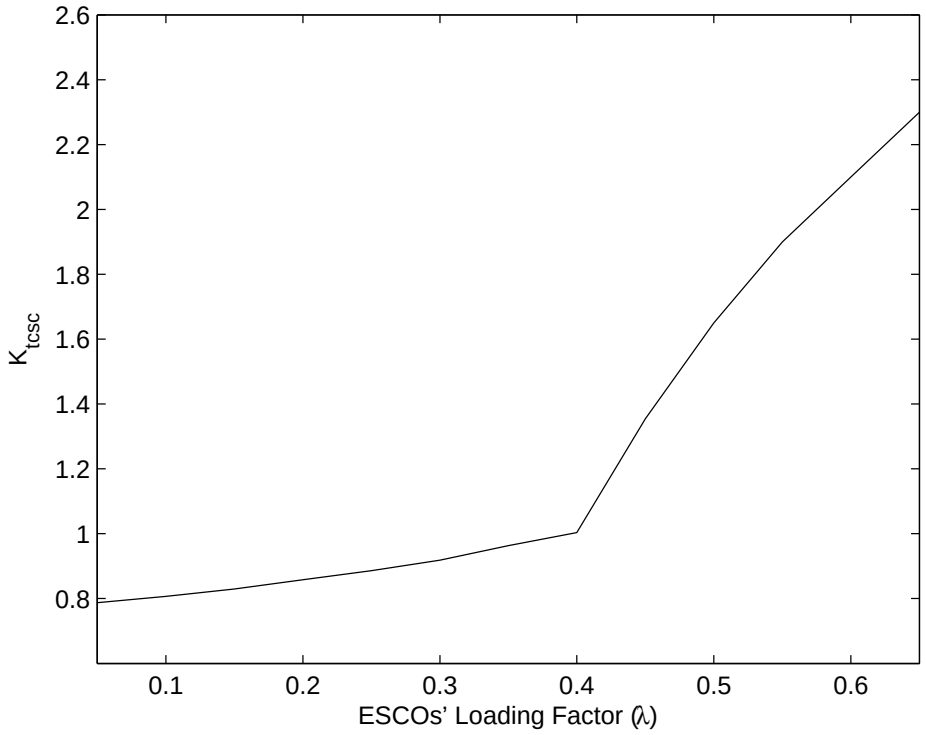

Figure 5.15: Optimal value of the TCSC gain with respect to the loading factor for the IEEE 14-bus test system.

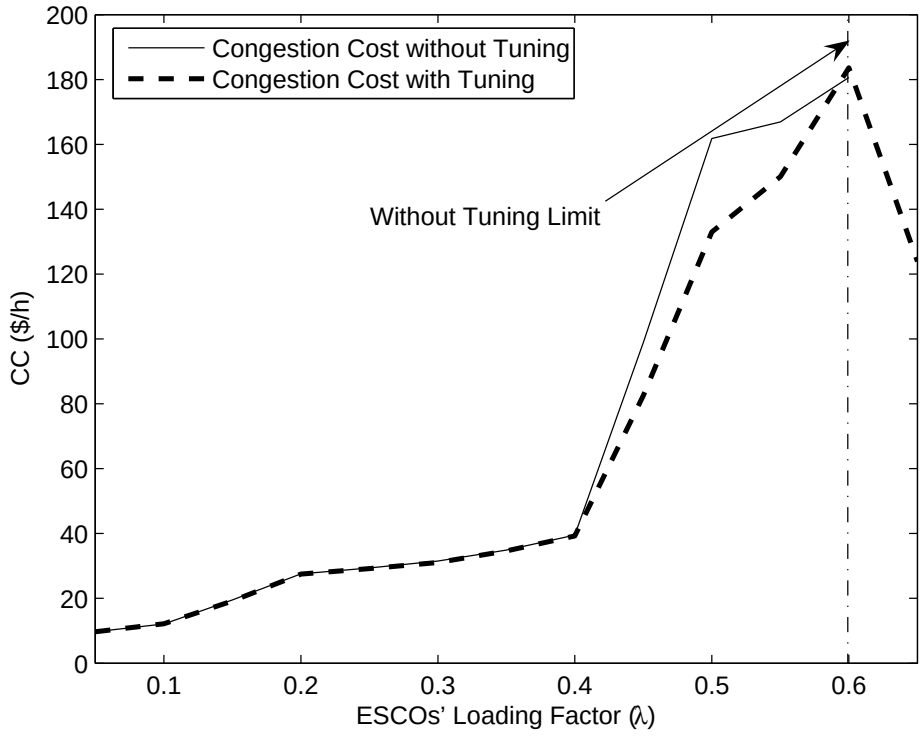

Figure 5.16: Price of the TCSC tuning.

the PSS example, as the loading factor increases. Similar results are obtained for the ESCOs' powers and LMPs, as depicted in Figure 5.14. Figure 5.15 depicts the optimal TCSC gain as the demand increases; as expected, the optimal TCSC gain increases more rapidly when the loading factor gets closer to the original Hopf bifurcation point ($\lambda \approx 0.45$ p.u.).

Table 5.4 provides a comparison between the SSC-OPF results with and without optimal tuning for a loading factor $\lambda = 0.6$ p.u. Observe that the optimal tuning technique results in better market prices and increased transacted powers, since the system is less congested; the system stability is enhanced as well.

Figure 5.16 demonstrates the difference between the CC obtained with and without optimal tuning. Notice that the difference in CC can be significant, especially near the Hopf bifurcation point for the system without optimal tuning ($\lambda \approx 0.6$). Again, these results highlight the importance of optimally tuning the controllers as the ESCOs' demand changes.

5.4 Summary

A novel technique to optimally tune these controllers is demonstrated, so that system controllers can be better utilized in a market environment. This chapter also compares the modelling of the oscillation damping controllers in the standard OPF and SSC-OPF auctions. The results obtained for the IEEE 14-bus test system with PSS and TCSC show the importance of properly modelling these controller in the market auctions.

Chapter 6

Conclusions

This thesis presents a novel stability-constrained OPF which properly represents both voltage and oscillatory instabilities in the system. The proposed SSC-OPF is used to suggest a new methodology to price the dynamic services provided by PSS and FACTS controllers. The newly developed SSC-OPF is also used to propose a novel tuning technique for oscillation damping controllers. The following summarizes the content and main conclusions of this thesis:

- A newly developed SSC-OPF for managing and pricing oscillatory instability is proposed and tested on different test systems. The proposed OPF technique is devised by including a HBI as a stability constraint in the OPF algorithm to predict both the voltage and oscillatory instabilities in the system. The proposed SSC-OPF is shown to guarantee stable system conditions and adequate market conditions.

- The proposed SSC-OPF and a previously discussed VSC-OPF are compared to show the effect on market and system conditions of the new stability constraint in the SSC-OPF. The results indicate that the SSC-OPF properly

represents voltage and oscillatory instabilities in an OPF-based auction. A VSC-OPF can result in unstable system conditions, since it cannot predict oscillatory instabilities, which can occur before voltage collapse in power systems.

- The comparison between the results obtained from the proposed SSC-OPF and a standard OPF auction, which represents system security via transmitted power limits computed off-line, demonstrates the restrictive nature of the "classical" stability-constrained OPF, as reflected by higher LMPs and lower power transactions.

- The proposed SSC-OPF is used to price the dynamic services provided by PSS, SVC and TCSC controllers. The novel pricing methodology is based on a comparison of the congestion costs of the SSC-OPF with and without the controllers. The methodology shows the benefits of adding the controllers to the system, since they enhance system security, causing the system to become less congested.

- The new pricing methodology reveals the importance of the dynamic modelling of system controllers. A VSC-OPF is used to highlight the difference between the steady state models and the dynamic models used in the proposed SSC-OPF.

- The proposed SSC-OPF is used to devise a novel tuning technique for oscillation damping controllers. The proposed tuning technique enables the ISOs to optimally tune these controllers considering the proper dynamic modelling of these controllers. This tuning technique is shown to decrease system congestion and guarantee that oscillation damping controllers are fully utilized.

6.1 Principal Contributions

The main contributions of this thesis are:

1. A novel SSC-OPF which predicts both voltage and oscillatory instabilities and guarantees secure and stable system conditions is proposed and developed.
2. A methodology for pricing the dynamic services provided by PSS, SVC, and TCSC controllers is devised.
3. The need for the dynamic modelling of power system controllers is exhibited.
4. An optimal tuning technique for oscillation damping controllers is developed.
5. The advantage for market auctions of the proposed techniques are demonstrated.

This thesis has resulted in several papers that have been published or are under review [82, 83, 84].

6.2 Future Work

There are a number of issues that still need to be addressed in the application of the proposed SSC-OPF. Thus;

- The application of the proposed SSC-OPF on larger systems should be considered. The proposed SSC-OPF should also be tested under sever contingencies for these systems.

- The proposed SSC-OPF is significantly expensive from the point of view of computation burden. Hence, there is a need for developing solution techniques to reduce the computation time needed to solve the SSC-OPF problem, especially for large systems.
- The proposed SSC-OPF should be applied to systems with several controllers in order to study the following problems:
  - Optimal tuning of these controllers considering the interactions between them to enhance system stability.
  - Study the effect of interactions among these controllers on market signals.

Appendix A

3-Bus Test System Data

Table A.1: Bus data for 3-bus test system.

	GENCO1	GENCO2	ESCO
P Generated p.u.	4.00	5.00	0.00
Q Generated p.u.	1.5	1.5	0.00
P Load p.u.	0.00	0.00	9.00
Q Load p.u.	0.00	0.00	3.00
V p.u.	1.05	1.00	1.00
Q Generated max. p.u.	10.00	-2.00	0.00
Q Generated min. p.u.	10.00	-10.00	0.00

Table A.2: Line data for 3-bus test system.

From Bus	To Bus	Resist. (p.u.)	React. (p.u.)
GENCO1	ESCO	0.005	0.05
GENCO2	ESCO	0.01	0.0399
GENCO2	ESCO	0.01	0.0399

Table A.3: GENCOS and ESCO bids for 3-bus test system.

Participants	C $/MWh	$P_{bid_{max}}$ MW
GENCO1	9.6	550
GENCO2	9.7	600
ESCO	11	900

Table A.4: Generator data for 3-bus test system.

	GENCO1	GENCO2
MVA	555	700
x_l (p.u.)	0.00	0.00
r_a (p.u.)	0.00	0.00
x_d (p.u.)	1.81	1.81
x'_d (p.u.)	0.3	0.3
T'_{do}	3.8	3.8
x_q (p.u.)	1.76	1.76
x'_q (p.u.)	0.6	0.6
T'_{qo}	0.9	0.9
H	3.53	3.53
D	1	1

Table A.5: Exciter data for 3-bus test system.

	GENCO1	GENCO2
K_A	130	200
T_A	0.02	0.02
T_B	0.00	0.00
T_c	0.00	0.00
V_{Rmax}	7.32	7.32
V_{Rmin}	0.00	0.00
K_E	1.0	1.0
T_E	0.2	0.2
K_F	0.03	0.05
T_F	1.0	1.0

Table A.6: PSS data for GENCO1 for 3-bus test system.

K_{pss}	16
T_W	3
T_1	0.15
T_2	0.05
T_3	0.15
T_4	0.05
V_{smax}	0.05
V_{smin}	-0.05

Appendix B

IEEE 14-BUS Test System

B.1 System data

Table B.1: Exciter data for the IEEE 14-bus test system.

Exciter No.	1	2	3	4	5
K_A	200	20	20	20	20
T_A	0.02	0.02	0.02	0.02	0.02
T_B	0.00	0.00	0.00	0.00	0.00
T_c	0.00	0.00	0.00	0.00	0.00
V_{Rmax}	7.32	4.38	4.38	6.81	6.81
V_{Rmin}	0.00	0.00	0.00	1.395	1.395
K_E	1.00	1.00	1.00	1.00	1.00
T_E	0.19	1.98	1.98	0.70	0.70
K_F	0.0012	0.001	0.001	0.001	0.001
T_F	1.0	1.0	1.0	1.0	1.0

Table B.2: Generator data for the IEEE 14-bus test system.

Generator Bus No.	1	2	3	4	5
MVA	615	60	60	25	25
x_l (p.u.)	0.2396	0.00	0.00	0.134	0.134
r_a (p.u.)	0.00	0.0031	0.0031	0.0014	0.0041
x_d (p.u.)	0.8979	1.05	1.05	1.25	1.25
x'_d (p.u.)	0.2995	0.1850	0.1850	0.232	0.232
x''_d (p.u.)	0.23	0.13	0.13	0.12	0.12
T'_{do}	7.4	6.1	6.1	4.75	4.75
T''_{do}	0.03	0.04	0.04	0.06	0.06
x_q (p.u.)	0.646	0.98	0.98	1.22	1.22
x'_q (p.u.)	0.646	0.36	0.36	0.715	0.715
x''_q (p.u.)	0.4	0.13	0.13	0.12	0.12
T'_{qo}	0.00	0.3	0.3	1.5	1.5
T''_{qo}	0.033	0.099	0.099	0.21	0.21
H	5.148	6.54	6.54	5.06	5.06
D	2	2	2	2	2

Table B.3: Bus data for the IEEE 14-bus test system.

Bus No.	P Generated (p.u.)	Q Generated (p.u.)	P Load (p.u.)	Q Load (p.u.)	Bus Type*	Q Generated max.(p.u.)	Q Generated min.(p.u.)
1	2.32	0.00	0.00	0.00	2	10.0	-10.0
2	0.4	-0.424	0.2170	0.1270	1	0.5	-0.4
3	0.00	0.00	0.9420	0.1900	2	0.4	0.00
4	0.00	0.00	0.4780	0.00	3	0.00	0.00
5	0.00	0.00	0.0760	0.0160	3	0.00	0.00
6	0.00	0.00	0.1120	0.0750	2	0.24	-0.06
7	0.00	0.00	0.00	0.00	3	0.00	0.00
8	0.00	0.00	0.00	0.00	2	0.24	-0.06
9	0.00	0.00	0.2950	0.1660	3	0.00	0.00
10	0.00	0.00	0.0900	0.0580	3	0.00	0.00
11	0.00	0.00	0.0350	0.0180	3	0.00	0.00
12	0.00	0.00	0.0610	0.0160	3	0.00	0.00
13	0.00	0.00	0.1350	0.0580	3	0.00	0.00
14	0.00	0.00	0.1490	0.0500	3	0.00	0.00

*Bus Type: (1) swing bus, (2) generator bus (PV bus), and (3) load bus (PQ bus).

Table B.4: Line data for the IEEE 14-bus test system.

From Bus	To Bus	Resistance (p.u.)	Reactance (p.u)	Line charging (p.u.)	tap ratio
1	2	0.01938	0.05917	0.0528	1
1	5	0.05403	0.22304	0.0492	1
2	3	0.04699	0.19797	0.0438	1
2	4	0.05811	0.17632	0.0374	1
2	5	0.05695	0.17388	0.034	1
3	4	0.06701	0.17103	0.0346	1
4	5	0.01335	0.04211	0.0128	1
4	7	0.00	0.20912	0.00	0.978
4	9	0.00	0.55618	0.00	0.969
5	6	0.00	0.25202	0.00	0.932
6	11	0.09498	0.1989	0.00	1
6	12	0.12291	0.25581	0.00	1
6	13	0.06615	0.13027	0.00	1
7	8	0.00	0.17615	0.00	1
7	9	0.00	0.11001	0.00	1
9	10	0.03181	0.08450	0.00	1
9	14	0.12711	0.27038	0.00	1
10	11	0.08205	0.19207	0.00	1
12	13	0.22092	0.19988	0.00	1
13	14	0.17093	0.34802	0.00	1

Table B.5: GENCOs and ESCOs bidding data for the IEEE 14-bus test system.

	$P_{d_{max_o}}$ / $P_{s_{max}}(MW)$	C_d / $C_s(\$/MWh)$
GENCO1	615	9.50
GENCO2	60	10.20
GENCO3	60	11.30
ESCO2	30.38	13.00
ESCO3	131.9	13.20
ESCO4	66.92	12.10
ESCO5	10.64	12.33
ESCO6	15.68	12.24
ESCO9	41.3	13.55
ESCO10	12.6	14.66
ESCO11	4.9	13.67
ESCO12	8.54	14.62
ESCO13	18.9	14.22
ESCO14	20.86	14.45

B.2 PSS Data

Table B.6: PSS controller parameters for the IEEE 14-bus test system.

K_{pss}	T_W (s)	T_1	T_2	T_3	T_4	V_{smax}	V_{smin}
2.5	5	0.38	0.02	0.38	0.02	0.1	-0.1

B.3 SVC Data

Table B.7: SVC static data for the IEEE 14-bus test system.

X_c (p.u.)	X_l (p.u.)	α_{min} (deg.)	α_{max} (deg.)	Slope (%)	MVA	kV
1.1708	0.4925	90	175	2	200	13.8

Table B.8: SVC controller parameters for the IEEE 14-bus test system.

K	T (s)	B_{max} (p.u.)	B_{min} (p.u.)
25	0.15	2	-2

B.4 TCSC Data

Table B.9: TCSC static data for the IEEE 14-bus test system.

X_c (p.u.)	X_l (p.u.)	α_{min} (deg.)	α_{max} (deg.)	kV
0.00526	0.000526	155	175	69

Table B.10: TCSC controller parameters for the IEEE 14-bus test system.

T	K_w	T_w	T_1	T_2	T_3	T_4	X_{min} (p.u.)	X_{max} (p.u.)
0.015	1.3	5	1.1	0.05	0.08	0.5	0.00527	0.0514

Bibliography

[1] H. G. Kwatny, A. K. Pasrija, and L. Y. Bahar, "Static Bifurcation in Electric Power Networks: Loss of Steady-state Stability and Voltage Collapse," *IEEE Trans. Circuits Systems*, vol. 33, 1986, pp. 981–991.

[2] I. Dobson and H. D. Chiang, "Towards a theory of voltage collapse in electric power systems," *Systems and Control Letters*, vol. 13, 1989, pp. 253–262.

[3] H. D. Chiang, I. Dobson, R. J. Thomas, J. S. Thorp, and L. Fekih-Ahmed, "On Voltage Collapse in Electric Power System," *IEEE Trans. on Power Systems*, vol. 5, March 1990, pp. 601–611.

[4] E. H. Abed, J. C. Alexander, H. Wang, A. M. A. Hamdan, and H-C. Lee, "Dynamic Bifurcation in a Power System Model Exhibiting Voltage Collapse," technical report, Department of Mathematics, University of Maryland, College Park, MD 20742 USA, February 1992.

[5] W. Zhu, R. R. Mohler, R. Spee, W. A. Mittelstadt, and D. Maratukulam, "Hopf bifurcations in a SMIB Power System with SSR," *IEEE Trans. on Power Systems*, vol. 11, no. 3, August 1996, pp. 1579–1584.

[6] A. S. Gui, G. N. Dalakishvili, N. M. Gomareli, and V. M. Kekenadze. "Bifur-

cation and Chaos in Power Systems". In *Proc. of International Conference on Control of Oscillation and Chaos*, pp. 349–353, Russia, 1997.

[7] Y. Mitani and K. Tsuji, "Bifurcations Associated with Sub-Synchronous Resonance," *IEEE Trans. on Power Systems*, vol. 10, no. 4, November 1995, pp. 1471–1478.

[8] J. Li and V. Venkatasubramanian. "Study of Hopf bifurcation in a Simple Power System Model". In *Proc. of the 39th Conference on Decision and Control*, pp. 3075–3079, Sydney, December 2000.

[9] N. Mithulananthan. *Hopf Bifurcation Control and Indices for Power System with Interacting Generator and FACTS Controllers.* PhD thesis, University of Waterloo, Waterloo, ON, Canada, available at http://www.power.uwaterloo.ca, 2002.

[10] IEEE/CIGRE Joint Task Force on Stability Terms and Definitions, "Definitions and Classification of Power System Stability," *IEEE Trans. on Power Systems*, vol. 19, no. 3, August 2004, pp. 1387–1401.

[11] P. Kundur, *Power System Stability and Control.* McGraw-Hill, New York, 1994.

[12] C. A. Cañizares, F. L. Alvarado, C. L. DeMarco, I. Dobson, and W. F. Long, "Point of Collapse Method Applied to AC/DC Power Systems," *IEEE Trans. on Power Systems*, vol. 7, no. 2, May 1992, pp. 673–683.

[13] V. Ajjarapu and B. Lee, "Bifurcation Theory and its Application to Nonlinear Dynamical Phenomena in an Electrical Power System," *IEEE Trans. on Power Systems*, vol. 7, no. 1, February 1992, pp. 424–431.

[14] C. A. Cañizares and S. Hranilovic. "Transcritical and Hopf Bifurcation in AC/DC Systems". In *Proc. of Bulk Power System Voltage Phenomena-III Seminar*, pp. 105–114, Davos, Switzerland, August 1994.

[15] E. H. Abed and P. P. Varaiya, "Nonlinear Oscillations in Power Systems," *International Journal of Electric Power and Energy Systems*, vol. 6, 1984, pp. 37–43.

[16] W. D. Rosehart and C. A. Cañizares, "Bifurcation Analysis of Various Power System Models," *International Journal of Electrical Power and Energy Systems*, vol. 12, 1999, pp. 171–182.

[17] N. Mithulananthan and S. C. Srivastava. "Investigation of a Voltage Collapse Incident in Sri Lankan Power System Network". In *Proc. of EMPD'98*, pp. 47–52, Singapore, March 1998.

[18] C. Alsberg, "WSCC Issues Preliminary Report on August Power Outage: PRESS RELEASE," *WSCC, available at http://www.wscc.com/augdist.htm*, September 1996.

[19] K. Kim, H. Schattler, V. Venkatasubramanin, J. Zaborszky, and P. Hirsch, "Methods for calculating oscillations in large power systems," *IEEE Trans. on Power System*, vol. 12, November 1997, pp. 1639–1648.

[20] C. A. Cañizares, "On Bifurcation Voltage Collapse and Load Modeling," *IEEE Trans. on Power System*, vol. 10, no. 1, February 1995, pp. 512–522.

[21] P. Kundur, M. Klein, G. J. Rogers, and M. S. Zywno, "Application of Power System Stabilizers for Enhancement of Overall System Stability," *IEEE Trans. on Power System*, vol. 4, no. 2, May 1989, pp. 614–626.

[22] G. Hingorani and L. Gyugi, *Understanding FACTS: Concepts and Technology of Flexible AC Transmission Systems*. IEEE Press, New York, 1999.

[23] C. A. Cañizares and Z. T. Faur, "Analysis of SVC and TCSC Controllers in Voltage Collapse," *IEEE Trans. on Power Systems*, vol. 14, no. 1, February 1999, pp. 158–165.

[24] C. A. Cañizares, A. Berizzi, and P. Marannino. "Using FACTS Controllers to Maximize Available Transfer Capability". In *Proc. Bulk Power Systems Dynamics and Control IV-Restructuring*, pp. 633–641, Santorini, Greece, August 1998.

[25] A. Tiranuchit and R. J. Thomas, "A Posturing Strategy Against Voltage Instabilities in Electric Power System," *IEEE Trans. on Power Systems*, vol. 3, no. 1, February 1988, pp. 87–93.

[26] P. A. Lof, T. Smed, G. Andersson, and D. J. Hill, "Fast Calculation of a Voltage Stability Index," *IEEE Trans. on Power Systems*, vol. 7, no. 1, February 1992, pp. 54–64.

[27] C. A. Cañizares, W. Roshart, A. Berizzi, and C. Bovo. "Comparison of Voltage Security Constrained Optimal Power Flow Techniques". In *Proc. of IEEE-PES Summer Meeting*, Vancouver, BC, Canada, July 2001.

[28] F. Milano, C. A. Cañizares, and M. Invernizzi, "Multi-objective Optimization for Pricing System Security in Electricity Markets," *IEEE Trans. on Power Systems*, vol. 18, no. 2, May 2003, pp. 596–604.

[29] C. A. Cañizares, N. Mithulananthan, F. Milano, and J. Reeve, "Linear Performance Indices to Predict Oscillatory Stability Problems in Power System," *IEEE Trans. on Power System*, vol. 19, no. 2, May 2004, pp. 1023–1031.

[30] D. Gan, R. J. Thomas, and R. D. Zimmerman, "Stability-Constrained Optimal Power Flow," *IEEE Trans. on Power Systems*, vol. 15, no. 2, May 2000, pp. 535–540.

[31] *Promoting Wholesale Competition Through Open Access Nondiscriminatory Transmission Services by Public Utilities*. Federal Energy Regulatory Commission of the United States of America, April 1996.

[32] C. A. Cañizares, editor, "Voltage Stability Assessment: Concepts, Practices and Tools," technical report, IEEE/PES Power System Stability Subcommittee Special Publications, SP101PSS, August 2002.

[33] N. Mithulananthan, C. A. Cañizares, J. Reeve, and G. J. Rogers, "Comparison of PSS, SVC and STATCOM Controllers for Damping Power System Oscillations," *IEEE Trans. on Power System*, vol. 18, no. 2, May 2003, pp. 786–792.

[34] A. D. Del Rosso, C. A. Cañizares, and V. M. Doña, "A Study of TCSC Controller Design for Power System Stability Improvement," *IEEE Trans. on Power Systems*, vol. 18, no. 4, November 2004, pp. 1487–1496.

[35] C. Schaffner and G. Andersson. "Valuating Controllable Devices in Congested Networks". In *Proc. of Bulk Power System Dynamics and Control*, Cortina D'Ampezzo, Italy, August 2004.

[36] H. Singh and A. Papalexopoulos, "Competitive Procurement of Ancillary Services by an Independent System Operator," *IEEE Trans. on Power Systems*, vol. 14, no. 2, May 1999, pp. 498–504.

[37] H. F. Wang, "Selection of Operating Conditions for the Co-ordinated Setting of Robust Fixed-Parameter Stabilizers," *IEE Proc. Generation, Transmission and Distribution*, vol. 145, no. 2, March 1998, pp. 111–116.

[38] I. Kamwa, G. Trudel, and D. Lefebvre. "Optimization-Based Tuning and Coordination Flexible Damping Controllers for Bulk Power Systems". In *Proc. of the 1999 IEEE International Conference on Control Applications*, Kohala Cost-Island of Hawaii, Hawaii, August 1999.

[39] X. Lei, E. N. Lerch, and D. Povh, "Optimization and Coordination of Damping Controls for Improving System Dynamic Performance," *IEEE Trans. on Power Systems*, vol. 16, no. 3, August 2001, pp. 473–480.

[40] M. A. Abido, "Robust Design of Multimachine Power System Stabilizers Using Simulated Annealing," *IEEE Trans. on Power Systems*, vol. 15, no. 3, September 2000, pp. 297–304.

[41] Y. L. Abdel-Magid, M. A. Abido, and A. H. Mantawy, "Robust Tuning of Power System Stabilizers in Multimachine Power Systems," *IEEE Trans. on Power Systems*, vol. 15, no. 2, May 2000, pp. 735–740.

[42] Y. L. Abdel-Magid and M. A. Abido, "Optimal Multiobjective Design of Robust Power System Stabilizers Using Genetic Algorithms," *IEEE Trans. on Power Systems*, vol. 18, no. 3, August 2003, pp. 1125–1132.

[43] J. Arrillaga and C. P. Arnold, *Computer Analysis of Power Systems*. John Wiley & Sons, England, 1990.

[44] P. M. Anderson and A. A. Fouad, *Power System Control and Stability*. IEEE Press, Piscataway, NJ, 1994.

[45] P. Sauer and M. Pai, *Power System Dynamics and Stability*. Prentice Hall, Upper Saddle River, NJ, 1998.

[46] R.P. schulz, "Synchronous Machine Modeling. Symposium on Adequency and Philosophy of Modeling System Dynamic Performance," *IEEE Pub. 75 CH O970-PWR*, 1975.

[47] N. Mithulananthan, M. M. A. Salama, C. A. Cañizares, and J. Reeve, "Distribution System Voltage Regulation and Var Compensation for Different Static Load Models," *IJEEE*, vol. 37, no. 4, October 2000, pp. 384–395.

[48] IEEE FACTS working group 15.05.15, *FACTS Application*. IEEE Power Engineering Society, December 1995.

[49] N. Yang, Q. Liu, and J. D. McCalley, "TCSC Controller Design for Damping Interarea Oscillations," *IEEE Trans. on Power Systems*, vol. 13, no. 4, November 1998, pp. 1304–1309.

[50] M. J. Lautenberg, M. A. Pai, and K. R. Padiyar, "Hopf Bifurcation Control in Power Systems with Static Var Compensators," *International Journal of Electric Power and Energy Systems*, vol. 19, no. 5, 1997, pp. 339–347.

[51] N. G. Hingorani, "Flexible AC Transmission Systems," *IEEE Spectrum*, April 1993, pp. 40–45.

[52] L. Gyugyi, "Dynamic Compensation of AC Transmission Lines by Solid State Synchronous Voltage Sources," *IEEE Trans. on Power Systems*, vol. 9, no. 2, April 1994, pp. 904–911.

[53] L. Gyugyi, N. G. Hingorani, P. R. Nannery, and N. Tai, *Advanced Static Var Compensators using Gate Turn-off Thyristors for Utility Application*. CIGRE 23-203, August 1990.

[54] E. Uzunovic, C. A. Cañizares, and J. Reeve. "Fundamental Frequency Model of Static Synchronous Compensator". In *Proc. of the 29th North American Power Symposium*, pp. 49–54, Laramie, Wyoming, October 1997.

[55] C. A. Cañizares. "Power Flow and Transient Stability Models of FACTS Controllers for Voltage and Angle Stability Studies". In *Proc. of IEEE/PES Winter Meeting*, Singapore, January 2000.

[56] N. Martins, H. Pinto, and J. Paserba. "Using a TCSC for Power System Scheduling and System Oscillation Damping-Small Signal and Transient Stability Studies". In *Proc. of IEEE/PES Winter Meeting*, Singapore, January 2000.

[57] *Impact of Interactions Among System Controllers.* CIGRE Task Force 38.02.16, November 1999.

[58] J. Paserba, N. Miller, E. Larsen, and R. Piwko, "A Thyristor Series Controlled Compensation Model for Power System Stability Analysis," *IEEE Trans. on Power Systems*, vol. 10, no. 4, November 1995, pp. 1471–1478.

[59] V. Ajjarapu and B. Lee. "Nonlinear Oscillations and Voltage Collapse Phenomena in an Electrical Power System". In *Proc. of the 22nd North America Power Symposium*, Auburn, Alabama, October 1990.

[60] T. Van Custem and C. Vournas, *Voltage Stability of Electric Power System.* Kluwer Academic Publishers, Boston, 1998.

[61] C. W. Taylor, *Power System Voltage Stability.* McGraw-Hill, New York, 1994.

[62] Task Force 38.02.14, "Analysis and Modeling Needs of Power Systems Under Major Frequency Disturbances," technical report, CIGRE, January 1999.

[63] V. Ajjarapu and C. Christy, "The Continuation Power Flow: a Tool for Steady State Voltage Stability Analysis," *IEEE Trans. on Power System*, vol. 7, 1992, pp. 416–423.

[64] C. A. Cañizares, *UWPFLOW: Continuation and Direct Methods to Locate Fold Bifurcation in AC/DC/FACTS Power Systems*. University of Waterloo, November 1999.

[65] D. J. Hill and I. M. Y. Mareels, "Stability Theory for Differential/Algebraic System with Application to Power Systems," *IEEE Trans. Circuits and Systems*, vol. 37, no. 11, November 1990, pp. 1416–1423.

[66] C. A. Cañizares, N. Mithulananthan, A. Berizzi, and J. Reeve, "On the Linear Profile of Indices for the Prediction of Saddle-node and Limit-induced Bifurcation Points in Power Systems ," *IEEE Transactions on Circuits and Systems-I*, vol. 50, no. 12, December 2003, pp. 1588–1595.

[67] K. Bhattacharya, M. Bollen, and J. Daalder, *Operation of Restructured Power Systems*. Kluwer Academic Publishers, Boston, 2001.

[68] G. B. Sheblé, *Computational Auction Mechanism for Restructured Power Industry Operation*. Kluwer Academic Publishers, Boston, 1998.

[69] K. Xie, Y. H. Song, J. Stonham, E. Yu, and G. Liu, "Decomposition Model and Interior Point Methods for Optimal Spot Pricing of Electricity in Deregulation Environments," *IEEE Trans. on Power System*, vol. 15, no. 1, February 2000, pp. 39–50.

[70] B. S. Gisin, M. V. Obessis, and J. V. Mitsche. "Practical Methods for Transfer Limit Analysis in the Power Industry Deregulated Environment". In *Proc. of PICA IEEE International Conference*, pp. 261–266, 2000.

[71] A. Berizzi, P. Bresesti, P. Marannino, M. Montagna, S. Corsi, and G. Piccini. "Security Enhancement Aspects in Reactive Voltage Control". In *Proc. of IEEE/PES Stockholm Power Tech.*, Stockholm, Sweeden, June 1995.

[72] *Power System Toolbox Version 2.0: Load Flow Tutorial and Functions*. Cherry Tree Scientific Software, RR-5 Colborne, Ontario K0K 1S0, 1991-1999.

[73] G. Rogers, *Power System Oscillations*. Kluwer Academic Publishers, Boston, 2000.

[74] *Power System Toolbox Version 2.0: Dynamic Tutorial and Functions*. Cherry Tree Scientific Software, RR-5 Colborne, Ontario K0K 1S0, 1991-1997.

[75] S. K. M. Kodsi and C. A. Canñizares, "Modeling and Simulation of IEEE 14-bus System with FACTS Controllers," technical report 2003-3, University of Waterloo, Waterloo, Ontario, Canada., March 2003.

[76] G. L. Torres and V. H. Quintana, "An Interior Point Method for Nonlinear Optimal Power Flow Using Voltage Rectangular Coordinates," *IEEE Trans. on Power Systems*, vol. 13, no. 4, November 1998, pp. 1211–1218.

[77] V. H. Quintana and G. L. Torres, "Introduction to Interior-Point Methods," *IEEE PICA*, Santa Clara,CA, May 1999.

[78] E. Castillo, A. J. Conejo, P. Pedregal, R. Garcia, and N. Alguacil, *Building and Solving Mathematical Programming Models in Engineering and Science*. John Willy & Sons, Inc., 2002.

[79] D. H. Wilson, K. Hay, and J. Toal. "Probability of Oscillatory Instability and its Implications". In *Proc. of Bulk Power System Dynamic and Control VI* , Cortina d'Ampezzo, Italy, August 2004.

[80] *Guide for Economic Evaluation of Flexible AC Transmission Systems (FACTS) in open Access Environments*. New York, August 1997.

[81] J. V. Coevering, J. P. Stovall, R. L. Hauth, P. J. Tatto, B. D. Railing, and B. K. Johnson, "The Next Generation of HVDC - needed R&D, Equipment Costs, and Cost Comparisons," *in Proc. of EPRI Conference of Future of Power Delivery*, April 1996.

[82] S. K. M. Kodsi and C. A. Cañizares. "Stability-Constrained Optimal Power Flow and Its Application to Pricing Power System Stabilizers". In *Proc. of the 37th North American Power Symposium*, Iowa, USA, October 2005.

[83] S. K. M. Kodsi and C. A. Cañizares, "Stability-Constrained Optimal Power Flow and Its Application to Pricing Dynamic Services of FACTS Controllers," *Submitted for Publication to IEEE Trans. on Power Systems*, May 2005, no. of pages 13.

[84] S. K. M. Kodsi and C. A. Cañizares, "Optimal Tuning of Oscillation Controls to Improve Electricity Market Operating Conditions," *Submitted for Publication to IEEE Trans. on Power Systems*, September 2005, no. of pages 11.